DESY 10-095
June 2010

ISSN 0418-9833

Measurement of the Diffractive Deep-Inelastic Scattering Cross Section with a Leading Proton at HERA

H1 Collaboration

Abstract

The cross section for the diffractive deep-inelastic scattering process $ep \to eXp$ is measured, with the leading final state proton detected in the H1 Forward Proton Spectrometer. The data sample covers the range $x_{I\!P} < 0.1$ in fractional proton longitudinal momentum loss, $0.1 < |t| < 0.7$ GeV^2 in squared four-momentum transfer at the proton vertex and $4 < Q^2 < 700$ GeV^2 in photon virtuality. The cross section is measured four-fold differentially in $t, x_{I\!P}, Q^2$ and $\beta = x/x_{I\!P}$, where x is the Bjorken scaling variable. The t and $x_{I\!P}$ dependences are interpreted in terms of an effective pomeron trajectory and a sub-leading exchange. The data are compared to perturbative QCD predictions at next-to-leading order based on diffractive parton distribution functions previously extracted from complementary measurements of inclusive diffractive deep-inelastic scattering. The ratio of the diffractive to the inclusive ep cross section is studied as a function of Q^2, β and $x_{I\!P}$.

Submitted to *Eur. Phys. J.* **C**

F.D. Aaron[5,49], C. Alexa[5], V. Andreev[25], S. Backovic[30], A. Baghdasaryan[38], E. Barrelet[29], W. Bartel[11], K. Begzsuren[35], A. Belousov[25], J.C. Bizot[27], V. Boudry[28], I. Bozovic-Jelisavcic[2], J. Bracinik[3], G. Brandt[11], M. Brinkmann[11], V. Brisson[27], D. Britzger[11], D. Bruncko[16], A. Bunyatyan[13,38], G. Buschhorn[26,†], L. Bystritskaya[24], A.J. Campbell[11], K.B. Cantun Avila[22], F. Ceccopieri[4], K. Cerny[32], V. Cerny[16,47], V. Chekelian[26], A. Cholewa[11], J.G. Contreras[22], J.A. Coughlan[6], J. Cvach[31], J.B. Dainton[18], K. Daum[37,43], M. Deák[11], B. Delcourt[27], J. Delvax[4], E.A. De Wolf[4], C. Diaconu[21], M. Dobre[n,12,51], V. Dodonov[13], A. Dossanov[26], A. Dubak[30,46], G. Eckerlin[11], V. Efremenko[24], S. Egli[36], A. Eliseev[25], E. Elsen[11], L. Favart[4], A. Fedotov[24], R. Felst[11], J. Feltesse[10,48], J. Ferencei[16], D.-J. Fischer[11], M. Fleischer[11], A. Fomenko[25], E. Gabathuler[18], J. Gayler[11], S. Ghazaryan[11], A. Glazov[11], L. Goerlich[7], N. Gogitidze[25], M. Gouzevitch[11], C. Grab[40], A. Grebenyuk[11], T. Greenshaw[18], B.R. Grell[11], G. Grindhammer[26], S. Habib[11], D. Haidt[11], C. Helebrant[11], R.C.W. Henderson[17], E. Hennekemper[15], H. Henschel[39], M. Herbst[15], G. Herrera[23], M. Hildebrandt[36], K.H. Hiller[39], D. Hoffmann[21], R. Horisberger[36], T. Hreus[4,44], F. Huber[14], M. Jacquet[27], X. Janssen[4], L. Jönsson[20], A.W. Jung[15], H. Jung[11,4], M. Kapichine[9], J. Katzy[11], I.R. Kenyon[3], C. Kiesling[26], M. Klein[18], C. Kleinwort[11], T. Kluge[18], A. Knutsson[11], R. Kogler[26], P. Kostka[39], M. Kraemer[11], J. Kretzschmar[18], A. Kropivnitskaya[24], K. Krüger[15], K. Kutak[11], M.P.J. Landon[19], W. Lange[39], G. Laštovička-Medin[30], P. Laycock[18], A. Lebedev[25], V. Lendermann[15], S. Levonian[11], K. Lipka[n,11], B. List[12], J. List[11], N. Loktionova[25], R. Lopez-Fernandez[23], V. Lubimov[24], A. Makankine[9], E. Malinovski[25], P. Marage[4], H.-U. Martyn[1], S.J. Maxfield[18], A. Mehta[18], A.B. Meyer[11], H. Meyer[37], J. Meyer[11], S. Mikocki[7], I. Milcewicz-Mika[7], F. Moreau[28], A. Morozov[9], J.V. Morris[6], M.U. Mozer[4], M. Mudrinic[2], K. Müller[41], Th. Naumann[39], P.R. Newman[3], C. Niebuhr[11], A. Nikiforov[11], D. Nikitin[9], G. Nowak[7], K. Nowak[11], J.E. Olsson[11], S. Osman[20], D. Ozerov[24], P. Pahl[11], V. Palichik[9], I. Panagoulias[l,11,42], M. Pandurovic[2], Th. Papadopoulou[l,11,42], C. Pascaud[27], G.D. Patel[18], E. Perez[10,45], A. Petrukhin[11], I. Picuric[30], S. Piec[11], H. Pirumov[14], D. Pitzl[11], R. Plačakytė[11], B. Pokorny[32], R. Polifka[32], B. Povh[13], V. Radescu[14], N. Raicevic[30], T. Ravdandorj[35], P. Reimer[31], E. Rizvi[19], P. Robmann[41], R. Roosen[4], A. Rostovtsev[24], M. Rotaru[5], J.E. Ruiz Tabasco[22], S. Rusakov[25], D. Šálek[32], D.P.C. Sankey[6], M. Sauter[14], E. Sauvan[21], S. Schmitt[11], L. Schoeffel[10], A. Schöning[14], H.-C. Schultz-Coulon[15], F. Sefkow[11], L.N. Shtarkov[25], S. Shushkevich[26], T. Sloan[17], I. Smiljanic[2], Y. Soloviev[25], P. Sopicki[7], D. South[8], V. Spaskov[9], A. Specka[28], Z. Staykova[11], M. Steder[11], B. Stella[33], G. Stoicea[5], U. Straumann[41], D. Sunar[4], T. Sykora[4], G. Thompson[19], P.D. Thompson[3], T. Toll[11], T.H. Tran[27], D. Traynor[19], P. Truöl[41], I. Tsakov[34], B. Tseepeldorj[35,50], J. Turnau[7], K. Urban[15], A. Valkárová[32], C. Vallée[21], P. Van Mechelen[4], A. Vargas Trevino[11], Y. Vazdik[25], M. von den Driesch[11], D. Wegener[8], E. Wünsch[11], J. Žáček[32], J. Zálešák[31], Z. Zhang[27], A. Zhokin[24], H. Zohrabyan[38], and F. Zomer[27]

[1] *I. Physikalisches Institut der RWTH, Aachen, Germany*
[2] *Vinca Institute of Nuclear Sciences, Belgrade, Serbia*
[3] *School of Physics and Astronomy, University of Birmingham, Birmingham, UK[b]*
[4] *Inter-University Institute for High Energies ULB-VUB, Brussels and Universiteit Antwerpen, Antwerpen, Belgium[c]*
[5] *National Institute for Physics and Nuclear Engineering (NIPNE) , Bucharest, Romania[m]*
[6] *Rutherford Appleton Laboratory, Chilton, Didcot, UK[b]*
[7] *Institute for Nuclear Physics, Cracow, Poland[d]*

[8] *Institut für Physik, TU Dortmund, Dortmund, Germany*[a]
[9] *Joint Institute for Nuclear Research, Dubna, Russia*
[10] *CEA, DSM/Irfu, CE-Saclay, Gif-sur-Yvette, France*
[11] *DESY, Hamburg, Germany*
[12] *Institut für Experimentalphysik, Universität Hamburg, Hamburg, Germany*[a]
[13] *Max-Planck-Institut für Kernphysik, Heidelberg, Germany*
[14] *Physikalisches Institut, Universität Heidelberg, Heidelberg, Germany*[a]
[15] *Kirchhoff-Institut für Physik, Universität Heidelberg, Heidelberg, Germany*[a]
[16] *Institute of Experimental Physics, Slovak Academy of Sciences, Košice, Slovak Republic*[f]
[17] *Department of Physics, University of Lancaster, Lancaster, UK*[b]
[18] *Department of Physics, University of Liverpool, Liverpool, UK*[b]
[19] *Queen Mary and Westfield College, London, UK*[b]
[20] *Physics Department, University of Lund, Lund, Sweden*[g]
[21] *CPPM, Aix-Marseille Université, CNRS/IN2P3, Marseille, France*
[22] *Departamento de Fisica Aplicada, CINVESTAV, Mérida, Yucatán, México*[j]
[23] *Departamento de Fisica, CINVESTAV IPN, México City, México*[j]
[24] *Institute for Theoretical and Experimental Physics, Moscow, Russia*[k]
[25] *Lebedev Physical Institute, Moscow, Russia*[e]
[26] *Max-Planck-Institut für Physik, München, Germany*
[27] *LAL, Université Paris-Sud, CNRS/IN2P3, Orsay, France*
[28] *LLR, Ecole Polytechnique, CNRS/IN2P3, Palaiseau, France*
[29] *LPNHE, Université Pierre et Marie Curie Paris 6, Université Denis Diderot Paris 7, CNRS/IN2P3, Paris, France*
[30] *Faculty of Science, University of Montenegro, Podgorica, Montenegro*[e]
[31] *Institute of Physics, Academy of Sciences of the Czech Republic, Praha, Czech Republic*[h]
[32] *Faculty of Mathematics and Physics, Charles University, Praha, Czech Republic*[h]
[33] *Dipartimento di Fisica Università di Roma Tre and INFN Roma 3, Roma, Italy*
[34] *Institute for Nuclear Research and Nuclear Energy, Sofia, Bulgaria*[e]
[35] *Institute of Physics and Technology of the Mongolian Academy of Sciences, Ulaanbaatar, Mongolia*
[36] *Paul Scherrer Institut, Villigen, Switzerland*
[37] *Fachbereich C, Universität Wuppertal, Wuppertal, Germany*
[38] *Yerevan Physics Institute, Yerevan, Armenia*
[39] *DESY, Zeuthen, Germany*
[40] *Institut für Teilchenphysik, ETH, Zürich, Switzerland*[i]
[41] *Physik-Institut der Universität Zürich, Zürich, Switzerland*[i]

[42] *Also at Physics Department, National Technical University, Zografou Campus, GR-15773 Athens, Greece*
[43] *Also at Rechenzentrum, Universität Wuppertal, Wuppertal, Germany*
[44] *Also at University of P.J. Šafárik, Košice, Slovak Republic*
[45] *Also at CERN, Geneva, Switzerland*
[46] *Also at Max-Planck-Institut für Physik, München, Germany*
[47] *Also at Comenius University, Bratislava, Slovak Republic*
[48] *Also at DESY and University Hamburg, Helmholtz Humboldt Research Award*
[49] *Also at Faculty of Physics, University of Bucharest, Bucharest, Romania*

[50] *Also at Ulaanbaatar University, Ulaanbaatar, Mongolia*
[51] *Absent on leave from NIPHE-HH, Bucharest, Romania*
[†] *Deceased*

[a] *Supported by the Bundesministerium für Bildung und Forschung, FRG, under contract numbers 05H09GUF, 05H09VHC, 05H09VHF, 05H16PEA*
[b] *Supported by the UK Science and Technology Facilities Council, and formerly by the UK Particle Physics and Astronomy Research Council*
[c] *Supported by FNRS-FWO-Vlaanderen, IISN-IIKW and IWT and by Interuniversity Attraction Poles Programme, Belgian Science Policy*
[d] *Partially Supported by Polish Ministry of Science and Higher Education, grant DPN/N168/DESY/2009*
[e] *Supported by the Deutsche Forschungsgemeinschaft*
[f] *Supported by VEGA SR grant no. 2/7062/ 27*
[g] *Supported by the Swedish Natural Science Research Council*
[h] *Supported by the Ministry of Education of the Czech Republic under the projects LC527, INGO-1P05LA259 and MSM0021620859*
[i] *Supported by the Swiss National Science Foundation*
[j] *Supported by CONACYT, México, grant 48778-F*
[k] *Russian Foundation for Basic Research (RFBR), grant no 1329.2008.2*
[l] *This project is co-funded by the European Social Fund (75%) and National Resources (25%) - (EPEAEK II) - PYTHAGORAS II*
[m] *Supported by the Romanian National Authority for Scientific Research under the contract PN 09370101*
[n] *Supported by the Initiative and Networking Fund of the Helmholtz Association (HGF) under the contract VH-NG-401*

1 Introduction

Diffractive processes such as $ep \to eXp$ have been studied extensively in deep-inelastic electron[1]-proton scattering (DIS) at the HERA collider [1–17], and provide an essential input for the understanding of quantum chromodynamics (QCD) at high parton densities. The photon virtuality Q^2 supplies a hard scale, which allows the application of perturbative QCD. Diffractive DIS events can be viewed as resulting from processes in which the photon probes a net colour singlet combination of exchanged partons. A hard scattering QCD collinear factorisation theorem [18] allows the definition of 'diffractive parton distribution functions' (DPDFs) for a given scattered proton four-momentum. The dependence of diffractive DIS on x, the Bjorken scaling variable , and Q^2 can thus be treated in a manner similar to inclusive DIS, e.g. through the application of the DGLAP parton evolution equations [19–22].

Within Regge phenomenology, diffractive cross sections are described by the exchange of a pomeron ($I\!P$) trajectory, as illustrated in figure 1. In previous measurements at HERA [5, 6] diffractive DIS cross sections are interpreted in a combined framework, which applies the QCD factorisation theorem to the x and Q^2 dependence and uses a Regge inspired approach to express the dependence on $x_{I\!P}$, the fraction of the incident proton longitudinal momentum carried by the colour singlet exchange. In this framework the data at low $x_{I\!P}$ are well described and DPDFs and a pomeron trajectory intercept are extracted. In order to describe the data at larger $x_{I\!P}$, it is necessary to include a sub-leading exchange trajectory ($I\!R$), with an intercept which is consistent with the approximately degenerate trajectories associated with the exchange of ρ, ω, a_2 and f_2 mesons.

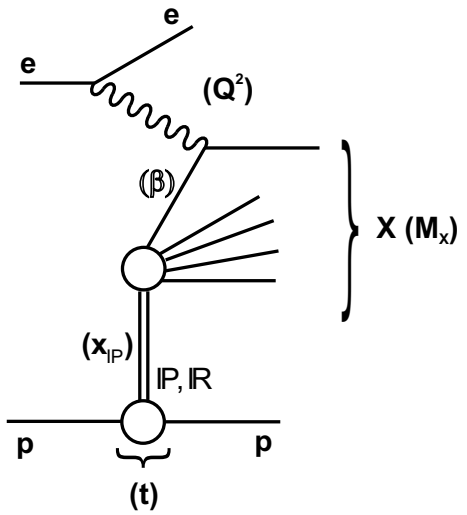

Figure 1: Schematic illustration of the diffractive DIS process $ep \to eXp$ and the kinematic variables used for its description in a model in which the pomeron ($I\!P$) and a sub-leading ($I\!R$) trajectory are exchanged.

In many previous analyses diffractive DIS events are selected on the basis of the presence of a large rapidity gap (LRG) between the leading proton and the remainder of the hadronic final state X [3, 5]. The main advantage of the LRG method is high acceptance for diffractive

[1] In this paper "electron" is used to denote both electron and positron.

processes. A complementary way to study diffractive processes is by direct measurement of the outgoing proton. This is achieved in H1 using the Forward Proton Spectrometer (FPS) [4, 16, 23]. Although the FPS detector has low acceptance, the FPS method of studying diffraction has several advantages. In contrast to the LRG case, the squared four-momentum transfer t at the proton vertex can be reconstructed. The FPS method selects events in which the proton scatters elastically, whereas the LRG method does not distinguish between the case where the scattered proton remains intact or where it dissociates into a system of low mass M_Y. The FPS method also allows measurements up to higher values of $x_{I\!P}$ than is possible with the LRG method, extending into regions where the sub-leading trajectory is the dominant exchange. The FPS and LRG methods provide means to investigate whether the hard scattering process characterised by the variables $\beta = x/x_{I\!P}$ and Q^2 depends also on the variables $x_{I\!P}$, t and M_Y associated with the proton vertex. According to the proton vertex factorisation hypothesis, the cross section can be written as the product of two factors, one characterising the hard interaction depending on β and Q^2, the other characterising the proton vertex depending on $x_{I\!P}$ and t.

In this paper, a measurement of the cross section for the diffractive DIS process $ep \to eXp$ is presented, using H1 FPS data with statistics increased by a factor 20 compared to the previous analysis [4]. In addition the kinematic range of the FPS measurement is extended to higher Q^2. The high statistics of the present data make the FPS results competitive in precision with the results of the LRG method. Reduced diffractive cross sections, $\sigma_r^{D(4)}(\beta, Q^2, x_{I\!P}, t)$ and $\sigma_r^{D(3)}(\beta, Q^2, x_{I\!P})$, are measured. These measurements are used to to extract the parameters of the pomeron trajectory and to quantify the sub-leading exchange contribution. The proton vertex factorisation hypothesis is tested. The cross section dependence on the hard scattering variables, β and Q^2, is further studied. The ratio of diffractive to inclusive ep cross sections is measured as a function of Q^2, β and $x_{I\!P}$. The data are compared with similar measurements of the ZEUS experiment [11, 12]. The data are also compared directly with the LRG measurement [5] in order to test the compatibility between the two measurement techniques and to quantify the proton dissociation contribution in the LRG data.

2 Experimental Technique

The data used in this analysis correspond to an integrated luminosity of $156.6\,\mathrm{pb}^{-1}$ and were collected with the H1 detector in e^-p interactions (luminosity of $77.2\,\mathrm{pb}^{-1}$) and e^+p interactions (luminosity of $79.4\,\mathrm{pb}^{-1}$) during the HERA II running period from 2005 to 2007. During this period the HERA collider was operated at electron and proton beam energies of $E_e = 27.6$ GeV and $E_p = 920$ GeV, respectively, corresponding to an ep centre of mass energy of $\sqrt{s} = 319$ GeV.

2.1 H1 detector

A detailed description of the H1 detector can be found elsewhere [24,25]. Here, the components most relevant for the present measurement are described briefly. A right handed coordinate system is employed with the origin at the position of the nominal interaction point that has its

z-axis pointing in the proton beam, or forward, direction and $x(y)$ pointing in the horizontal (vertical) direction. Transverse momenta are measured with respect to the beam axis.

The Central Tracking Detector (CTD), with a polar angle coverage of $20^\circ < \theta < 160^\circ$, is used to reconstruct the interaction vertex and to measure the momentum of charged particles from the curvature of their trajectories in the $1.16\,\mathrm{T}$ field provided by a superconducting solenoid.

Scattered electrons with polar angles in the range $154^\circ < \theta'_e < 176^\circ$ are measured in a lead / scintillating-fibre calorimeter, the SpaCal [26]. The energy resolution is $\sigma(E)/E \approx 7\%/\sqrt{E[\mathrm{GeV}]}\oplus 1\%$ and the energy scale uncertainty is 1%. A Backward Proportional Chamber (BPC) in front of the SpaCal is used to measure the electron polar angle with a precision of 1 mrad. Hadrons are measured in the Spacal with an energy scale precision of 7%.

The finely segmented Liquid Argon (LAr) sampling calorimeter [27,28] surrounds the tracking system and covers the range in polar angle $4^\circ < \theta < 154^\circ$. The LAr calorimeter is used to reconstruct the scattered electron in DIS processes at high Q^2. The LAr calorimeter consists of an electromagnetic section with lead as absorber, and a hadronic section with steel as absorber. Its total depth varies with θ between 4.5 and 8 interaction lengths. Its energy resolution, determined in test beam measurements, is $\sigma(E)/E \approx 11\%/\sqrt{E[\mathrm{GeV}]} \oplus 1\%$ for electrons and $\sigma(E)/E \approx 50\%/\sqrt{E[\mathrm{GeV}]} \oplus 2\%$ for hadrons. The absolute electromagnetic energy scale is known to 1% precision.

The hadronic final state is reconstructed using an energy flow algorithm which combines charged particles measured in the CTD with information from the SpaCal and LAr calorimeters [29]. The absolute hadronic energy scale is known with a precision of 4% for the measurements presented here.

The luminosity is determined with a precision of 3.7% by detecting photons from the Bethe-Heitler process $ep \to ep\gamma$ in a calorimeter located at $z = -103$ m.

The energy and scattering angle of the leading proton are obtained from track measurements in the FPS [16, 23]. Protons scattered through small angles are deflected by the proton beam-line magnets into a system of detectors placed within the proton beam pipe inside two movable stations, known as Roman Pots. Each Roman Pot station contains four planes of five scintillating fibres, which together measure two orthogonal coordinates in the (x, y) plane. The fibre coordinate planes are sandwiched between planes of scintillator tiles used for the trigger. The stations approach the beam horizontally from outside the proton ring and are positioned at $z = 61$ m and $z = 80$ m. The detectors are sensitive to scattered protons which lose less than 10% of their energy in the ep interaction and which are scattered through angles below 1 mrad.

The leading proton energy resolution is approximately 5 GeV, independent of energy within the measured range. The absolute energy scale uncertainty is 1 GeV. The effective resolution in the reconstruction of the transverse momentum components of the scattered proton with respect to the incident proton is determined to be ~ 50 MeV for p_x and ~ 150 MeV for p_y, dominated by the intrinsic transverse momentum spread of the proton beam at the interaction point. The corresponding t-resolution varies over the measured range from 0.06 GeV^2 at $|t| = 0.1$ GeV^2 to 0.17 GeV^2 at $|t| = 0.7$ GeV^2. The calibration of the FPS is performed using a sample of elastic $ep \to e\rho^0 p$ photoproduction events with $\rho^0 \to \pi^+\pi^-$ decays by comparing the

variables reconstructed in the CTD with the values measured in the FPS. The scale uncertainties in the transverse momentum measurements are 10 MeV for p_x and 30 MeV for p_y. Further details of the analysis of the FPS resolution and scale uncertainties can be found in [4]. For a leading proton which passes through both FPS stations, the average overall track reconstruction efficiency is 48%.

2.2 Event selection and kinematic reconstruction

The events used in this analysis are triggered on the basis of a coincidence between the FPS trigger scintillator tile signals and an electromagnetic cluster signal in the SpaCal or LAr calorimeter. The trigger efficiency is around 99% on average.

Several selection criteria are applied to the data in order to select the DIS event sample and to suppress beam related backgrounds, photoproduction processes and events in which the incoming electron loses significant energy through QED radiation. The DIS selection criteria are summarised below.

- The reconstructed z coordinate of the event vertex is required to lie within 35 cm$(\sim 3\sigma)$ of the mean position. At least one track originating from the interaction vertex and reconstructed in the CTD is required to have a transverse momentum above 0.1 GeV.
- The the energy E'_e and the polar angle θ'_e of the scattered electron are determined from the SpaCal (LAr) cluster, linked to a reconstructed charged particle track in the BPC (CTD), and the interaction vertex reconstructed in the CTD. The electron candidate is required to satisfy either $154^\circ < \theta'_e < 176^\circ$ and $E'_e > 8$ GeV in the Spacal calorimeter or $\theta'_e < 154^\circ$ and $E'_e > 10$ GeV in the LAr calorimeter.
- The quantity $E - p_z$, calculated from the energies and longitudinal momenta of all reconstructed particles including the electron, is required to lie between 35 GeV and 70 GeV. For neutral current DIS events this quantity is expected to be twice the electron beam energy neglecting detector effects and QED radiation.

The following requirements are applied to the leading proton measured in the FPS.

- The measurement is restricted to the region where the FPS acceptance is high by requiring the horizontal and vertical projections of the transverse momentum to lie in the ranges $-0.63 < p_x < -0.27$ GeV and $|p_y| < 0.8$ GeV, respectively, and the energy of the leading proton E'_p to be greater than 90% of the proton beam energy E_p, where E_p is the energy of the proton beam.
- The quantity $E + p_z$, summed over all reconstructed particles including the leading proton, is required to be below 1900 GeV. For neutral current DIS events this quantity is expected to be twice the proton beam energy neglecting detector effects. This requirement is applied to suppress cases where a DIS event reconstructed in the central detector coincides with background in the FPS, for example due to an off-momentum beam proton (beam halo).

The inclusive DIS variables Q^2, x and the inelasticity y are reconstructed by combining information from the scattered electron and the hadronic final state using the method introduced in [3]:

$$y = y_e^2 + y_d(1 - y_d) \quad ; \quad Q^2 = \frac{4E_e^2(1-y)}{\tan^2(\theta_e'/2)} \quad ; \quad x = \frac{Q^2}{sy} \, . \tag{1}$$

Here, y_e and y_d denote the values of y obtained from the scattered electron only ('electron method') and from the angles of the electron and the hadronic final state ('double angle method'), respectively [30].

Variables specific to diffractive DIS are defined as

$$x_{I\!P} = \frac{q \cdot (P - P')}{q \cdot P} \quad ; \quad \beta = \frac{Q^2}{2q \cdot (P - P')} \, , \tag{2}$$

with q, P and P' denoting the four-vectors of the exchanged virtual photon and the incoming and outgoing proton, respectively. The variable β can be interpreted as the fraction of the longitudinal momentum of the colourless exchange which is carried by the struck quark. The variable $x_{I\!P}$ is reconstructed directly from the energy of the leading proton, such that

$$x_{I\!P} = 1 - E_p'/E_p \, . \tag{3}$$

Two methods are used to reconstruct β in order to obtain the optimal resolution across the measured $x_{I\!P}$ range. It is reconstructed as $\beta = x/x_{I\!P}$ in the range $x_{I\!P} \geq 0.012$. For $x_{I\!P} < 0.012$ the hadronic final state is used for the reconstruction according to:

$$\beta = \frac{Q^2}{Q^2 + M_X^2} \quad . \tag{4}$$

The mass M_X of the hadronic system X is obtained from

$$M_X^2 = (E^2 - p_x^2 - p_y^2 - p_z^2)_{\mathrm{had}} \cdot \frac{y}{y_h} \, , \tag{5}$$

where the subscript 'had' represents a sum over all hadronic final state particles excluding the leading proton and y_h is the value of y reconstructed using only the hadronic final state [31]. Including the factor y/y_h leads to cancellations of several measurement inaccuracies.

The squared four-momentum transfer $t = (P - P')^2$ is reconstructed using the transverse momentum p_t of the leading proton measured with the FPS and the value of $x_{I\!P}$ as described above, such that

$$t = t_{\mathrm{min}} - \frac{p_t^2}{1 - x_{I\!P}} \quad ; \quad t_{\mathrm{min}} = -\frac{x_{I\!P}^2 m_p^2}{1 - x_{I\!P}} \, , \tag{6}$$

where $|t_{\mathrm{min}}|$ is the minimum kinematically accessible value of $|t|$ and m_p is the proton mass.

In this measurement, the reconstructed $|t|$ is required to lie in the range $0.1 < |t| < 0.7\,\mathrm{GeV}^2$ and $x_{I\!P}$ in the range $x_{I\!P} < 0.1$. The measurement is restricted to a 'medium' Q^2 region of $4 < Q^2 < 110\,\mathrm{GeV}^2$, $0.03 < y < 0.7$ and a 'high' Q^2 region of $120 < Q^2 < 700\,\mathrm{GeV}^2$, $0.03 < y < 0.8$ for data with electron candidates reconstructed in the Spacal and LAr calorimeters, respectively. The final data sample contains about $68\,200$ events at medium Q^2 and about 400 events at high Q^2.

3 Monte Carlo Simulation and Corrections to the Data

Monte Carlo simulations are used to correct the data for the effects of detector acceptances, inefficiencies, migrations between measurement intervals due to finite resolutions and QED radiation. The reaction $ep \to eXp$ is simulated with the RAPGAP program [32] using the H1 2006 DPDF Fit B set [5]. The H1 2006 DPDF Fit A and H1 2006 DPDF Fit B parameterisations give a consistent description of diffractive inclusive DIS processes [5], but the H1 2006 DPDF Fit B predictions are in better agreement with the diffractive di-jet production cross sections measured in DIS [6]. Contributions from both leading ($I\!P$) and sub-leading ($I\!R$) exchanges are considered. Hadronisation is simulated using the Lund string model [33] implemented within the PYTHIA program [34]. An additional ρ-meson contribution relevant for the low M_X domain is simulated using the DIFFVM generator [35].

The background from photoproduction processes, where the electron is scattered into the backward beam pipe and a particle from the hadronic final state fakes the electron signature, is estimated using the PHOJET Monte Carlo model [36]. This background is negligible except at the highest y values and is 3% at most. The proton dissociation background, where the leading proton originates from the decay of a higher mass state, is estimated using an implementation in RAPGAP of the proton dissociation model originally developed for the DIFFVM Monte Carlo generator. This background is negligible except at the highest $x_{I\!P}$ values, where it reaches 2%.

The response of the H1 detector is simulated in detail using the GEANT3 program [37] and the events are passed through the same analysis chain as is used for the data.

Background mainly arises from random coincidences of DIS events resulting in activity in the central detector with off-momentum beam protons originating from interactions of beam protons with the residual gas in the beam-pipe or with the beam collimators (beam-halo background) giving a signal in the FPS. This contribution is estimated statistically by combining the quantity $E + p_z$ for all reconstructed particles in the central detector in DIS events (without the requirement of a track in the FPS) with the quantity $E + p_z$ for beam-halo protons from randomly triggered events. The resulting background distribution is normalised to the FPS DIS data distribution in the range $E + p_z > 1900$ GeV where beam-halo background dominates. After the selection cut of $E + p_z < 1900$ GeV the background amounts to 13% on average. The $E + p_z$ spectra for leading proton and beam-halo DIS events are shown in figure 2a. The background is determined using the reconstructed $E + p_z$ distribution as a function of the variables x, Q^2 and t. A comparison of the FPS data after background subtraction and the RAPGAP simulation is presented in figure 2b for the energy of the leading proton E'_p and in figure 3 for the variables $x_{I\!P}$, p_x, p_y and $|t|$. The beam-halo background is subtracted from the data. The Monte Carlo simulation reproduces the data within the experimental systematic uncertainties (section 4).

Cross sections are obtained at the Born level by applying corrections for QED radiative effects to the measured values. These corrrections amount to about 10% and are obtained using the HERACLES [38] program within the RAPGAP event generator. The measured cross sections are quoted at the bin centres in $Q^2, \beta, x_{I\!P}$ and $|t|$. Bin centre corrections are applied for the influence of the finite bin sizes using pomeron and sub-leading exchange parameterisations in the framework of the H1 2006 DPDF Fit B [5] for the Q^2, β and $x_{I\!P}$ dependences and the measured t dependences at each (Q^2, β, $x_{I\!P}$) value (section 5.1).

4 Systematic Uncertainties on the Measured Cross Sections

Systematic uncertainties are considered from the following sources.

- The uncertainties in the leading proton energy and in the horizontal and vertical projections of the proton transverse momentum are 1 GeV, 10 MeV and 30 MeV, respectively (section 2.1). The corresponding average uncertainties on the $\sigma_r^{D(3)}$ and $\sigma_r^{D(4)}$ measurements are 2.5%, 4.8% and 1.8%. The dominant uncertainty originates from the FPS acceptance variation as a function of the leading proton transverse momentum in the horizontal projection.

- The electromagnetic energy scale uncertainty implies an error of 1% on the E'_e measurement, which leads to an average systematic error of 1.2% on the σ_r^D measurements. Possible biases in the θ'_e measurement in the SpaCal (LAr) calorimeter at the level of $\pm 1\,\mathrm{mrad}$ ($\pm 3\,\mathrm{mrad}$) lead to an average systematic error of 2.5%.

- The systematic uncertainties arising from the hadronic final state reconstruction are determined by varying the hadronic energy scale of the LAr calorimeter by $\pm 4\%$ and that of the Spacal calorimeter by $\pm 7\%$. These sources lead to an uncertainty in the σ_r^D measurements of around 1%.

- The model dependence of the acceptance and migration corrections is estimated by varying the shapes of the distributions in the kinematic variables $x_{I\!P}$, β, Q^2 and t in the RAPGAP simulation within the constraints imposed on those distributions to describe the present data. The $x_{I\!P}$ distribution is reweighted by $(1/x_{I\!P})^{\pm 0.05}$, the β distribution by $\beta^{\pm 0.05}$ and $(1-\beta)^{\mp 0.05}$, the Q^2 distribution by $\log(Q^2)^{\pm 0.2}$. These sources result in an uncertainty in the σ_r^D measurements of 1%. Reweighting the t distribution by $e^{\pm t}$ results in an uncertainty of 1.4% for the measured range of $0.1 < |t| < 0.7\ \mathrm{GeV}^2$.

- The model dependence of the bin centre corrections for the reduced cross section is estimated by comparing the results obtained in the framework of the H1 2006 DPDF Fit B and H1 2006 DPDF Fit A parameterisations [5] for the kinematic variables β and Q^2. The $x_{I\!P}$ parameterisation is reweighted by $(1/x_{I\!P})^{\pm 0.05}$. The average uncertainty for the reduced cross section is around 1%. Reweighting the t distribution by $e^{\pm t}$ results in bin centre correction uncertainties of 1.6% for the $\sigma_r^{D(4)}$ measurements.

- The uncertainties related to the subtraction of background are at most 2% for proton dissociation, 3% for photoproduction and 3% for the proton beam-halo contribution (section 3).

- The systematic error related to the reconstruction of the event vertex is on average 1%, as evaluated by comparing the reconstruction efficiencies for the data and Monte Carlo simulation.

- A normalisation uncertainty of 1% is attributed to the trigger efficiencies (section 2.2), evaluated using event samples obtained with independent triggers.

- The uncertainty in the FPS track reconstruction efficiency results in the normalisation uncertainty of 2%.
- A further normalisation uncertainty of 3.7% arises from the luminosity measurement.
- The extrapolation in t from the measured FPS range of $0.1 < |t| < 0.7\ \mathrm{GeV}^2$ to the region $|t_{\min}| < |t| < 1\ \mathrm{GeV}^2$ covered by the LRG data [5] results in an additional normalisation error of 4% for the $\sigma_r^{D(3)}$ data (section 5.5).

The systematic errors shown in the figures are obtained by adding in quadrature all contributions except the normalisation uncertainty, leading to an average uncertainty of 8% for the data. The overall normalisation uncertainties are of 4.3% and 6% for the $\sigma_r^{D(4)}$ and $\sigma_r^{D(3)}$ measurements, respectively.

5 Results

5.1 The reduced cross section $\sigma_r^{D(4)}$

The dependence of diffractive DIS on $\beta, Q^2, x_{I\!P}$ and t is studied in terms of the reduced diffractive cross section $\sigma_r^{D(4)}$. This observable is related to the measured differential cross section by

$$\frac{\mathrm{d}^4\sigma^{ep\to eXp}}{\mathrm{d}\beta \mathrm{d}Q^2 \mathrm{d}x_{I\!P} \mathrm{d}t} = \frac{4\pi\alpha^2}{\beta Q^4} \cdot \left(1 - y + \frac{y^2}{2}\right) \cdot \sigma_r^{D(4)}(\beta, Q^2, x_{I\!P}, t)\ . \tag{7}$$

The reduced cross section depends on the diffractive structure functions $F_2^{D(4)}$ and $F_L^{D(4)}$ according to

$$\sigma_r^{D(4)} = F_2^{D(4)} - \frac{y^2}{1 + (1-y)^2}\, F_L^{D(4)}\ . \tag{8}$$

To a good approximation the reduced cross section is equal to the diffractive structure function $F_2^{D(4)}(\beta, Q^2, x_{I\!P}, t)$ in the region of relatively low y values covered by the current analysis. Results for $\sigma_r^{D(4)}$ are obtained in three t ranges, $0.1 \le |t| < 0.3\ \mathrm{GeV}^2, 0.3 \le |t| < 0.5\ \mathrm{GeV}^2$ and $0.5 \le |t| < 0.7\ \mathrm{GeV}^2$, and are interpolated to the values $|t| = 0.2,\ 0.4,\ 0.6\ \mathrm{GeV}^2$ using the measured t dependence at each $x_{I\!P}$, β and Q^2 value. Only the high statistics medium Q^2 data are used to evaluate the four-dimensional distributions $\sigma_r^{D(4)}$.

The reduced cross section $x_{I\!P}\,\sigma_r^{D(4)}$ is presented in table 3. Figure 4 shows $x_{I\!P}\,\sigma_r^{D(4)}$ as a function of $x_{I\!P}$ for different $|t|$, β and Q^2 values. At medium and large β values, $x_{I\!P}\,\sigma_r^{D(4)}$ falls or is flat as a function of $x_{I\!P}$. Qualitatively this behaviour is consistent with a dominant contribution of the pomeron exchange described in the Regge framework by a linear trajectory $\alpha_{I\!P}(t) = \alpha_{I\!P}(0) + \alpha'_{I\!P} t$ with an intercept $\alpha_{I\!P}(0) \gtrsim 1$ [39]. At low β values $x_{I\!P}\sigma_r^{D(4)}$ rises with $x_{I\!P}$ at the highest $x_{I\!P}$, which can be interpreted as a contribution from a sub-leading exchange ($I\!R$) with an intercept $\alpha_{I\!R}(0) < 1$. This observation is consistent with the previous H1 FPS analysis [4].

5.2 Cross section dependence on $x_{I\!P}$ and t and extraction of the pomeron trajectory

The structure function $F_2^{D(4)}$ is obtained by correcting $\sigma_r^{D(4)}$ for the small $F_L^{D(4)}$ contribution using the prediction of H1 2006 DPDF Fit B given in [5]. To describe the $x_{I\!P}$ and t dependence quantitatively, the structure function $F_2^{D(4)}$ is parameterised by the form

$$F_2^{D(4)} = f_{I\!P}(x_{I\!P}, t) F_{I\!P}(\beta, Q^2) + n_{I\!R} \cdot f_{I\!R}(x_{I\!P}, t) F_{I\!R}(\beta, Q^2) \,, \tag{9}$$

which assumes proton vertex factorisation of the $x_{I\!P}$ and t dependences from those on β and Q^2 for both the pomeron and any sub-leading exchange, with no interference between the two contributions. The $x_{I\!P}$ and t dependences are parameterised using flux factors $f_{I\!P}$ and $f_{I\!R}$ motivated by Regge phenomenology,

$$f_{I\!P}(x_{I\!P}, t) = A_{I\!P} \cdot \frac{e^{B_{I\!P}\, t}}{(x_{I\!P})^{2\alpha_{I\!P}(t)-1}} \;\; ; \;\; f_{I\!R}(x_{I\!P}, t) = A_{I\!R} \cdot \frac{e^{B_{I\!R}\, t}}{(x_{I\!P})^{2\alpha_{I\!R}(t)-1}} \,, \tag{10}$$

assuming that the sub-leading exchanges have a linear trajectory, $\alpha_{I\!R}(t) = \alpha_{I\!R}(0) + \alpha'_{I\!R} t$, as is also assumed for the pomeron. Following the convention of [3], the values of $A_{I\!P}$ and $A_{I\!R}$ are chosen such that $x_{I\!P} \cdot \int_{t_{cut}}^{t_{\min}} f_{I\!P,I\!R}(x_{I\!P}, t)\, \mathrm{d}t = 1$ at $x_{I\!P} = 0.003$ with $t_{cut} = -1$ GeV^2. Fitting the form of equation 9 to the experimental $F_2^{D(4)}$ data, the free parameters in the fit are the intercept and slope of the pomeron trajectory, $\alpha_{I\!P}(t) = \alpha_{I\!P}(0) + \alpha'_{I\!P} t$, the exponential t-slope parameter $B_{I\!P}$ for $x_{I\!P} \to 1$, the pomeron structure function $F_{I\!P}(\beta, Q^2)$ at each of the (β, Q^2) values considered, and the single parameter $n_{I\!R}$ describing the normalisation of the sub-leading exchange contribution. As in [3–5], the structure function $F_{I\!R}(\beta, Q^2)$ for the sub-leading exchange in each β and Q^2 bin are taken from a parameterisation of the pion structure function [40].

The behaviour of $F_2^{D(4)}$ at large $x_{I\!P}$ and low β is sensitive to the parameters of the sub-leading exchange $\alpha_{I\!R}(0)$, $\alpha'_{I\!R}$ and $B_{I\!R}$. They are taken to be the same as in the previous fits to the H1 F_2^D data [4, 5] in order to compare the normalisation parameters for the the sub-leading exchange contribution between the measurements. The intercept $\alpha_{I\!R}(0) = 0.50$ of the sub-leading exchange is taken from [3]. The parameters $\alpha'_{I\!R} = 0.3$ GeV^{-2} and $B_{I\!R} = 1.6$ GeV^{-2} are obtained from a parameterisation of the previously published H1 FPS data [4]. The model dependent uncertainty is determined by repeating the fit with the fixed parameters made free one after another in the fit. The fitted parameters of the sub-leading exchange are consistent with the values given above. The influence of neglecting the $F_L^{D(4)}$ contribution to $\sigma_r^{D(4)}$ is also included in the model dependent uncertainty. The experimental systematic uncertainties on the free parameters are evaluated by repeating the fit after shifting the data points according to each individual uncertainty listed in section 4.

The fit to equation 9 provides a good description of the $x_{I\!P}$ and t dependences of the data, with a minimum $\chi^2 = 273$ for 289 degrees of freedom, combining statistical and uncorrelated systematic errors. The data hence support the proton vertex factorisation hypothesis for both the pomeron and the sub-leading contribution as given by the fit.

The results for the free parameters of the fit are summarised in table 1. The experimental uncertainty of the fit parameters is defined as the quadratic sum of the statistical and systematic

Parameter	Value
$\alpha_{I\!P}(0)$	$1.10 \pm 0.02\,(\text{exp.}) \pm 0.03\,(\text{model})$
$\alpha'_{I\!P}$	$0.04 \pm 0.02\,(\text{exp.})\,^{+\,0.08}_{-\,0.06}\,(\text{model})\ \text{GeV}^{-2}$
$B_{I\!P}$	$5.73 \pm 0.25\,(\text{exp.})\,^{+\,0.80}_{-\,0.90}\,(\text{model})\ \text{GeV}^{-2}$
$n_{I\!R}$	$[0.87 \pm 0.10\,(\text{exp.})\,^{+\,0.60}_{-\,0.40}\,(\text{model})] \cdot 10^{-3}$

Table 1: The central values of the Regge model parameters extracted from a fit to $F_2^{D(4)}$ and their experimental and model uncertainties. The experimental uncertainty is defined as the quadratic sum of the statistical and systematic uncertainties. The model uncertainty is determined by varying the fixed parameters in the fit as explained in the text.

uncertainties. The overall normalisation uncertainty of $\sigma_r^{D(4)}$ contributes only to the experimental uncertainty of the sub-leading exchange normalisation parameter $n_{I\!R}$. The result for $\alpha_{I\!P}(0)$ is compatible with that obtained from H1 data previously measured using the LRG and FPS methods [4,5] and with the ZEUS measurements [12,13]. It is also consistent with the pomeron intercept describing soft hadronic scattering, $\alpha_{I\!P}(0) \simeq 1.08$ [39,41,42].

In a Regge approach with a single linear exchanged pomeron trajectory, $\alpha_{I\!P}(t) = \alpha_{I\!P}(0) + \alpha'_{I\!P} t$, the exponential t-slope parameter B of the diffractive cross section is expected to decrease logarithmically with increasing $x_{I\!P}$ according to

$$B = B_{I\!P} - 2\alpha'_{I\!P} \ln x_{I\!P}\ , \tag{11}$$

an effect which is often referred to as 'shrinkage' of the diffractive peak. The degree of shrinkage depends on the slope of the pomeron trajectory, $\alpha'_{I\!P}$. The present FPS data favour a small value of $\alpha'_{I\!P}$, as expected in perturbative models of the pomeron [43,44]. This result is incompatible with the value of $\alpha'_{I\!P} \simeq 0.25\ \text{GeV}^{-2}$ obtained from soft hadron-hadron scattering at high energies [39,41,42]. Vector meson measurements at HERA have also resulted in smaller values of $\alpha'_{I\!P}$, whether a hard scale is present [45–47] or not [48]. The present FPS results for $\alpha'_{I\!P}$ and $B_{I\!P}$ are compatible with those obtained previously from the H1 / ZEUS data using the FPS / LPS detectors [4,12]. Although the value of $B_{I\!P}$ measured in the H1 experiment is lower than that from the ZEUS data ($7.1 \pm 0.7\,(\text{stat.}) \pm^{1.4}_{0.7}\,(\text{syst.})\ \text{GeV}^{-2}$), the results are consistent within uncertainties.

The result for the sub-leading exchange normalisation parameter is slightly smaller but agrees within experimental uncertainties with $n_{I\!R} = [1.0 \pm 0.2\,(\text{exp.})] \cdot 10^{-3}$ extracted from the previously published H1 FPS data [4] and $n_{I\!R} = [1.4 \pm 0.4\,(\text{exp.})] \cdot 10^{-3}$ obtained from the H1 2006 DPDF Fit B to the H1 LRG data [5]. The FPS and LRG measurements give consistent results as expected for a dominantly isosinglet sub-leading trajectory (ω or f_2, rather than ρ or a_2 exchanges). The sub-leading exchange is important at low β and high $x_{I\!P}$, contributing up to 50% of the cross section at the highest bin centre value of $x_{I\!P} = 0.075$.

5.3 Test of proton vertex factorisation

To test in more detail a possible breakdown of proton vertex factorisation the dependence of $\alpha_{I\!P}(0)$, $\alpha'_{I\!P}$ and $B_{I\!P}$ on Q^2 is studied by repeating the fit described above in three different ranges

of Q^2. The results of the fits, shown in figure 5 and table 2, indicate no strong dependence on Q^2. The experimental uncertainty is defined as the quadratic sum of the statistical and uncorrelated systematic uncertainties. In the fit procedure, the normalisation factor $n_{I\!R}$ for the sub-leading exchange contribution is fixed to the central value, presented in table 1, as it is found to be insensitive to Q^2.

Q^2 range of Fit (GeV^2)	$\alpha_{I\!P}(0)$	$\alpha'_{I\!P}$ (GeV^{-2})	$B_{I\!P}$ (GeV^{-2})
$4 < Q^2 < 12$	1.088 ± 0.012 (exp.)	0.009 ± 0.031 (exp.)	5.78 ± 0.20 (exp.)
$12 < Q^2 < 36$	1.102 ± 0.016 (exp.)	0.063 ± 0.041 (exp.)	5.75 ± 0.30 (exp.)
$36 < Q^2 < 110$	1.139 ± 0.022 (exp.)	0.023 ± 0.026 (exp.)	5.17 ± 0.40 (exp.)

Table 2: The central values of $\alpha'_{I\!P}$ and $B_{I\!P}$ and their experimental uncertainties extracted from fits to $F_2^{D(4)}$ performed in three different ranges of Q^2.

In order to quantify a possible breakdown of proton vertex factorization, the data are fitted using parameterisations of the form $A + D \cdot \ln(Q^2/1\ \mathrm{GeV}^2)$ for $\alpha_{I\!P}(0)$ and $B_{I\!P}$. The logarithmic derivatives of $\alpha_{I\!P}(0)$ and $B_{I\!P}$ are found to be $D(\alpha_{I\!P}(0)) = 0.018 \pm 0.013$ (exp.) and $D(B_{I\!P}) = -0.20 \pm 0.14$ (exp.) GeV^{-2}, respectively. Given the experimental uncertainties, the values of the logarithmic derivatives are within 1.5σ from zero and hence do not contradict to proton vertex factorisation.

Assuming an exponential t-dependence of the cross section, $\mathrm{d}\sigma/\mathrm{d}t \propto e^{Bt}$, the slope parameter B is measured as function of $x_{I\!P}$ at fixed values of Q^2 and β. The results are presented in figure 6. The results for B are compared with a parameterisation of the t-dependence from the fit to $F_2^{D(4)}$ (section 5.2) as shown in figure 6. The fit results are shown as curves of the form:

$$B(x_{I\!P}, \beta, Q^2) = [1 - w_{I\!R}(x_{I\!P}, \beta, Q^2)][B_{I\!P} - 2\alpha'_{I\!P} \ln x_{I\!P}] + w_{I\!R}(x_{I\!P}, \beta, Q^2)[B_{I\!R} - 2\alpha'_{I\!R} \ln x_{I\!P}]\ ,$$

$w_{I\!R}(x_{I\!P}, \beta, Q^2)$ being the fraction of $F_2^{D(4)}$ which is due to the sub-leading exchange A good description of the data over the full $x_{I\!P}$, Q^2 and β range is obtained. At low $x_{I\!P}$, the data are compatible with a constant slope parameter, $B \simeq 6\ \mathrm{GeV}^{-2}$. No significant Q^2 or β dependence of the slope parameter B is observed for data points with $x_{I\!P} \leq 0.025$. The sub-leading exchange contribution integrated over this kinematic range is 5%. A parameterisation of the data in this $x_{I\!P}$ range with a constant slope parameter B gives $\chi^2 = 89$ for 75 data points, where the errors include the combined statistical and uncorrelated systematic uncertainties. Within uncertainties, the t dependence of the cross section in the pomeron dominated low $x_{I\!P}$ region can therefore be factorised from the Q^2 and β dependences.

Since no significant Q^2 or β dependence is observed, the slope parameter B is obtained by averaging over the Q^2 and β and compared with the result of a parameterisation of the t-dependence from the fit to $F_2^{D(4)}$. The result is shown as a function of $x_{I\!P}$ in figure 7. The previously published H1 FPS results [4] are also shown. A weak decrease of the B parameter value from $6\ \mathrm{GeV}^{-2}$ to less than $5\ \mathrm{GeV}^{-2}$ is observed towards larger values of $x_{I\!P} \gtrsim 0.05$, where the contribution from the sub-leading exchange is significant. This reduction of the slope parameter indicates that the size of the interaction region is reduced for $I\!R$ exchange, as compared to $I\!P$ exchange.

5.4 The reduced cross section $\sigma_r^{D(3)}$ and comparison with other measurements

The reduced cross section $\sigma_r^{D(3)}(\beta, Q^2, x_{I\!P})$, defined as the integral of $\sigma_r^{D(4)}(\beta, Q^2, x_{I\!P}, t)$ over t in the range $|t_{\min}| < |t| < 1\ \mathrm{GeV}^2$, is obtained by extrapolating the FPS data from the measured range $0.1 < |t| < 0.7\ \mathrm{GeV}^2$ using the t-dependence at each $(x_{I\!P}, \beta, Q^2)$ value (section 5.3). This extrapolation factor, which amounts to a value of 1.8 with an uncertainty of 4%, depends only weakly on $x_{I\!P}$.

In figure 8 the H1 FPS measurements of $x_{I\!P}\,\sigma_r^{D(3)}$ are presented. They are compared with those of the ZEUS collaboration, measured using their Leading Proton Spectrometer (LPS) [12]. The ZEUS data points are interpolated to the β, Q^2 and $x_{I\!P}$ values of this measurement using a parameterisation of the ZEUS DPDF SJ fit [15]. The ratio of the H1 FPS to ZEUS LPS data averaged over the measured kinematic range is $0.85 \pm 0.01(\mathrm{stat.}) \pm 0.03(\mathrm{syst.})^{+0.09}_{-0.12}(\mathrm{norm.})$, which is consistent with unity taking into account the normalisation uncertainties of 6% and $^{+11}_{-\ 7}\%$ for the H1 FPS and ZEUS LPS data, respectively. Within the errors, there is no strong $x_{I\!P}$, β or Q^2 dependence of the ratio. The FPS data extend the kinematic range of the cross section measurement to higher Q^2 and low β.

The reduced cross section $\sigma_r^{D(3)}$ can be compared with H1 measurements obtained using the LRG technique [5] after taking into account the slightly different cross section definitions in the two cases. The cross section $ep \to eXY$ measured with the LRG data is defined to include proton dissociation to any system Y with a mass in the range $M_Y < 1.6\ \mathrm{GeV}$, whereas Y is defined to be a proton in the cross section measured with the FPS. The results on $x_{I\!P}\,\sigma_r^{D(3)}$ measured using the FPS and LRG methods are shown in figure 9 as a function Q^2 in bins of β and $x_{I\!P}$, and in figure 10 as a function of β in selected bins of Q^2 and $x_{I\!P}$. The kinematic range of the measurements is extended to higher $x_{I\!P}$. The experimental uncertainties of the two measurements are defined as the quadratic sum of the statistical and uncorrelated systematic uncertainties. As can be seen in figure 10, the present FPS measurement has a precision comparable to the measurement [5] obtained using the LRG method. The LRG results are interpolated to the Q^2, β and $x_{I\!P}$ bin centre values of the FPS data using the parameterisation H1 2006 DPDF Fit B [5].

Since the two data sets are statistically independent and the dominant sources of systematic errors are different, correlations between the uncertainties of the FPS and LRG data are negligible. The ratio of the two measurements is formed for each (Q^2, β, $x_{I\!P}$) point in the range $x_{I\!P} < 0.04$, where LRG data are available. The dependence of this ratio on each kinematic variable is studied by taking statistically weighted averages over the other two variables.

The ratio of the LRG to the FPS cross section is shown in figure 11 as a function of Q^2, β and $x_{I\!P}$. Within the uncorrelated uncertainties of typically 6% per data point, there is no significant dependence on β, Q^2 or $x_{I\!P}$. The ratio of overall normalisations, LRG / FPS, is $1.18 \pm 0.01(\mathrm{stat.}) \pm 0.06(\mathrm{uncor.syst.}) \pm 0.10(\mathrm{norm.})$, the dominant uncertainties arising from the normalisations of the FPS and LRG data. This result is in agreement within uncertainties with the value of $1.23 \pm 0.03(\mathrm{stat.}) \pm 0.16(\mathrm{syst.})$ obtained from the previously published H1 LRG and FPS data [4]. Combining the result of [4] with the present measurement leads to a more precise value of the cross section ratio:

$$\frac{\sigma(M_Y < 1.6\ \mathrm{GeV})}{\sigma(M_Y = m_p)} = 1.20\ \pm\ 0.11\ (\mathrm{exp.})\ . \tag{12}$$

where the experimental uncertainty is a combination of the statistical, uncorrelated systematic and normalisation uncertainties of the measurements. The result is consistent with the prediction of $1.15^{+0.15}_{-0.08}$ from the DIFFVM generator, where the total proton elastic and proton dissociation cross sections are taken to be equal for the central value and their ratio is varied in the range $1:2$ to $2:1$ for the uncertainties [5, 35].

The good agreement, after accounting for proton dissociation, between the LRG and the FPS data confirms that the two measurement methods lead to compatible results, despite their very different systematics. The lack of any kinematic dependence of the ratio of the two cross sections shows, within the uncertainties, that proton dissociation with $M_Y < 1.6$ GeV can be treated in a similar way to the elastic proton case. The result confirms that contributions from proton dissociation in the LRG measurement do not significantly alter the measured β, Q^2 or $x_{I\!P}$ dependences and hence cannot have a large influence on the diffractive parton densities extracted from the LRG data up to the normalisation difference.

5.5 Cross section dependence on Q^2 and β

The measured reduced cross sections $x_{I\!P}\,\sigma_r^{D(3)}$ are presented in figures 12-14 and in table 4 as a function of $x_{I\!P}$, β and Q^2. The FPS data are compared with QCD predictions at next-to-leading order derived from the H1 2006 DPDF Fit B to the H1 LRG cross sections [5], which include both the pomeron and a sub-leading exchange. The normalisation of the H1 2006 DPDF Fit B predictions is reduced by a global factor 1.20 to correct for the contributions of proton dissociation processes to the LRG cross sections, as evaluated in section 5.4.

As can be seen in figure 12, the rise of the data at large $x_{I\!P}$ is in agreement with a significant contribution from a sub-leading exchange. The reduced cross section $\sigma_r^{D(3)}$ shown in figure 13 decreases with β over most of the kinematic range. However, it clearly rises as $\beta \to 1$ at low Q^2 and $x_{I\!P}$. Within the framework of DPDFs, this can be explained in terms of diffractive quark densities peaking at high fractional momentum at low Q^2 [3, 5].

The figure 14 shows the Q^2 dependence of $\sigma_r^{D(3)}$ at fixed $x_{I\!P}$ and β. Positive scaling violations ($\partial\,\sigma_r^{D(3)}/\partial \ln\,Q^2 > 0$) are observed throughout the kinematic range, except at the highest $\beta = 0.56$. This observation is consistent with previous H1 measurements using the LRG method [3, 5] and implies a large gluonic component in the DPDFs. As can be seen from QCD predictions, the positive scaling violations may be attributed to the pomeron contribution even at the highest $x_{I\!P}$ values, where the sub-leading exchange is largest. The Q^2 dependence is quantified by fitting the data at fixed $x_{I\!P}$ and β to the form

$$x_{I\!P}\sigma_r^{D(3)}(\beta, x_{I\!P}, Q^2) = a_D(\beta, x_{I\!P}) + b_D(\beta, x_{I\!P}) \ln(Q^2/1\ \mathrm{GeV}^2) \qquad (13)$$

such that $b_D(\beta, x_{I\!P})$ is the derivative of the reduced cross section with respect to $\ln Q^2$ multiplied by $x_{I\!P}$. This form is fitted to data points for which the $x_{I\!P}$ bin centre values satisfy $x_{I\!P} \leq 0.035$ and for which the β bin contains at least 3 data points. The sub-leading exchange contribution at $x_{I\!P} = 0.035$ is below 15%. The resulting logarithmic derivatives are shown in figure 15. Although the logarithmic derivatives at different $x_{I\!P}$ values cover different Q^2 regions, they are similar when viewed as a function of β. This confirms the applicability of the proton vertex factorisation framework to the description of the current data. The FPS results are consistent with predictions derived from the H1 2006 DPDF Fit B to the H1 LRG data also shown in figure 15.

5.6 Comparison of the diffractive and inclusive DIS cross sections

By analogy with hadronic scattering, the diffractive and the total cross sections in DIS can be related via the generalisation of the optical theorem to virtual photon scattering [49]. Many models of low x DIS [50–55] assume links between these quantities. Comparing the Q^2 and x dynamics of the diffractive with the inclusive cross section is therefore a powerful means of testing models and of comparing the properties of the DPDFs with their inclusive counterparts. A detailed comparison of the diffractive and inclusive cross section is performed in [5]. Following [5], the evolution of the reduced diffractive cross section with Q^2 is compared with that of the reduced inclusive DIS cross section σ_r by forming the quantity $(1-\beta)\frac{x_{I\!P}\sigma_r^{D(3)}(x_{I\!P},\beta,Q^2)}{\sigma_r(x=\beta x_{I\!P},Q^2)}$ at fixed Q^2, β and $x_{I\!P}$, using a parameterisation of the σ_r data from [56]. This quantity is equivalent to the ratio of diffractive to inclusive DIS cross section $M_X^2\frac{\mathrm{d}\sigma^{D(3)}(M_X,W,Q^2)}{\mathrm{d}M_X^2}/\sigma_{incl}^{\gamma^*p\to X}(W,Q^2)$ studied in [11, 13, 14] as a function of the γ^*p centre of mass energy W and Q^2 in ranges of M_X. The ratio is shown in figure 16 as a function of β at fixed $x_{I\!P}$ and Q^2.

The ratio of the diffractive to the inclusive cross section is approximately constant as a function of β at fixed Q^2 and $x_{I\!P}$ except at high β. As can be seen in figure 16, the decrease of the ratio towards high β is reproduced by QCD predictions based on diffractive and inclusive proton PDFs [5, 56]. The ratio also rises towards larger values of $x_{I\!P}$ where the sub-leading exchange contribution to the diffractive cross section is not negligible.

The ratio, shown in figure 17 as a function of Q^2 at fixed $x_{I\!P}$ and β, depends only weakly on Q^2 for most β and $x_{I\!P}$ values. In order to compare the Q^2 dependences of the diffractive and the inclusive cross sections quantitatively, the derivative b_r of the ratio with respect to $\ln Q^2$ is extracted through fits of the form $a_r(\beta,x_{I\!P})+b_r(\beta,x_{I\!P})\cdot\ln(Q^2/1\ \mathrm{GeV}^2)$. To reduce the influence of the sub-leading exchange contribution, only data points with bin centres at $x_{I\!P}\leq 0.035$ are included in the analysis of b_r. The resulting values of b_r are shown in figure 18. They are consistent with zero within 3σ. At fixed β, there is no significant dependence of the logarithmic derivative on $x_{I\!P}$. Whereas the reduced diffractive and inclusive cross sections are closely related to their respective quark densities, the logarithmic derivatives are approximately proportional to the relevant gluon densities in regions where the Q^2 evolution is dominated by the $g\to\bar{q}q$ splitting [57]. The compatibility of b_r with zero thus implies that the ratio of the quark to the gluon density is similar in the diffractive and inclusive DIS when considered at the same low x value. As can be seen in figure 18, QCD predictions based on proton PDFs extracted in diffractive and inclusive DIS [5, 56] reproduce a weak decrease of the logarithmic derivative towards larger β.

6 Summary

A cross section measurement is presented for the diffractive deep-inelastic scattering process $ep\to eXp$. The results are obtained using high statistics data taken with the H1 detector at HERA. In the process studied, the scattered proton carries at least 90% of the incoming proton momentum and is measured in the Forward Proton Spectrometer (FPS). The data cover the range $x_{I\!P}<0.1$ in fractional proton longitudinal momentum loss, $0.1<|t|<0.7\ \mathrm{GeV}^2$ in

squared four-momentum transfer at the proton vertex, $4 < Q^2 < 700\ \mathrm{GeV}^2$ in photon virtuality and $0.001 < \beta = x/x_{I\!P} < 1$. The measurement is performed in the range of the inelasticity variable $0.03 < y < 0.7$ for $4 < Q^2 < 110\ \mathrm{GeV}^2$ and in the range $0.03 < y < 0.8$ for $120 < Q^2 < 700\ \mathrm{GeV}^2$. The new H1 FPS data are in good agreement with the previously published H1 FPS results and are consistent within uncertainties with results of the ZEUS collaboration obtained with their Leading Proton Spectrometer. The new measurements extend the kinematic range to higher Q^2 values.

The reduced diffractive cross section $\sigma_r^{D(4)}(\beta, Q^2, x_{I\!P}, t)$ is measured. The $x_{I\!P}$ and t dependences are described using a model which is motivated by Regge phenomenology, in which a leading pomeron and a sub-leading exchange contribute. The effective pomeron intercept describing the data is $\alpha_{I\!P}(0) = 1.10 \pm 0.02\ (\mathrm{exp.}) \pm 0.03\ (\mathrm{model})$, which is compatible within uncertainties with the pomeron intercept measured in soft hadron-hadron scattering. The slope of the pomeron trajectory $\alpha'_{I\!P}$ is consistent with zero and smaller than the value $\sim 0.25\ \mathrm{GeV}^{-2}$ obtained from soft hadron-hadron scattering data. The t-dependence of the pomeron exchange is described by an exponential function with constant slope parameter $B_{I\!P} = 5.73 \pm 0.25\ (\mathrm{exp.})\ ^{+0.80}_{-0.90}\ (\mathrm{model})\ \mathrm{GeV}^{-2}$. The measured values of the slope of the pomeron trajectory and the t-dependences are characteristic of diffractive hard scattering processes. The Q^2 dependence of the parameters $\alpha_{I\!P}(0), \alpha'_{I\!P}$ and $B_{I\!P}$ is studied. The logarithmic derivatives are consistent with zero within 1.5σ of the experimental uncertainties thereby supporting the proton vertex factorisation hypothesis.

The data are also analysed in terms of the reduced diffractive cross section $\sigma_r^{D(3)}$, obtained by integrating $\sigma_r^{D(4)}$ over the range $|t_{\mathrm{min}}| < |t| < 1\ \mathrm{GeV}^2$. At fixed $x_{I\!P}$, a decrease of $\sigma_r^{D(3)}$ with β is observed over most of the kinematic range, except at the lowest values of Q^2 and $x_{I\!P}$. The data display positive scaling violations except at the highest β value of 0.56. The size of the measured scaling violations implies a large gluonic component in the diffractive parton distributions, in agreement with previous observations.

The FPS results are compared with those obtained from an earlier H1 measurement using events selected on the basis of a large rapidity gap rather than a leading proton. This LRG measurement includes proton dissociation to states Y with masses $M_Y < 1.6\ \mathrm{GeV}$. The FPS data extend the kinematic range to higher $x_{I\!P}$ and thus constrain the sub-leading exchange contribution. The ratio of the LRG to the FPS cross section is $1.20 \pm 0.11\ (\mathrm{exp.})$. It is independent of Q^2, β and $x_{I\!P}$ within uncertainties, confirming that contributions from proton dissociation in the LRG measurement do not significantly alter the measured Q^2, β or $x_{I\!P}$ dependences.

The ratio of the diffractive to the inclusive ep cross sections is measured as a function of Q^2, β and $x_{I\!P}$. At fixed $x_{I\!P}$ the ratio depends only weakly on Q^2 or on β except at the highest β. QCD predictions based on diffractive and inclusive proton PDFs reproduce the behaviour of the ratio. This result implies that the ratio of quark to gluon distributions at low x is similar in the diffractive and inclusive processes.

Acknowledgements

We are grateful to the HERA machine group whose outstanding efforts have made this experiment possible. We thank the engineers and technicians for their work in constructing and

maintaining the H1 detector, our funding agencies for financial support, the DESY technical staff for continual assistance and the DESY directorate for support and for the hospitality which they extend to the non-DESY members of the collaboration.

References

[1] T. Ahmed *et al.* [H1 Collaboration], Nucl. Phys. B **429** (1994) 477.

[2] T. Ahmed *et al.* [H1 Collaboration], Phys. Lett. B **348** (1995) 681 [hep-ex/9503005].

[3] C. Adloff *et al.* [H1 Collaboration], Z. Phys. C **76** (1997) 613 [hep-ex/9708016].

[4] A. Aktas *et al.* [H1 Collaboration], Eur. Phys. J. C **48** (2006) 749 [hep-ex/0606003].

[5] A. Aktas *et al.* [H1 Collaboration], Eur. Phys. J. C **48** (2006) 715 [hep-ex/0606004].

[6] A. Aktas *et al.* [H1 Collaboration], JHEP 0710:042 (2007) [arXiv:0708.3217].

[7] M. Derrick *et al.* [ZEUS Collaboration], Phys. Lett. B **315** (1993) 481.

[8] M. Derrick *et al.* [ZEUS Collaboration], Z. Phys. C **68** (1995) 569 [hep-ex/9505010].

[9] J. Breitweg *et al.* [ZEUS Collaboration], Eur. Phys. J. C **6** (1999) 43 [hep-ex/9807010].

[10] S. Chekanov *et al.* [ZEUS Collaboration], Eur. Phys. J. C **25** (2002) 169 [hep-ex/0203039].

[11] S. Chekanov *et al.* [ZEUS Collaboration], Eur. Phys. J. C **38** (2004) 43 [hep-ex/0408009].

[12] S. Chekanov *et al.* [ZEUS Collaboration], Nucl. Phys. B **816** (2009) 1 [arXiv:0812.2003].

[13] S. Chekanov *et al.* [ZEUS Collaboration], Nucl. Phys. B **713** (2005) 3 [hep-ex/0501060].

[14] S. Chekanov *et al.* [ZEUS Collaboration], Nucl. Phys. B **800** (2008) 1 [arXiv:0802.3017].

[15] S. Chekanov *et al.* [ZEUS Collaboration], Nucl. Phys. B **831** (2010) 1 [arXiv:0911.4119].

[16] C. Adloff *et al.* [H1 Collaboration], Eur. Phys. J. C **6** (1999) 587 [hep-ex/9811013].

[17] C. Adloff *et al.* [H1 Collaboration], Nucl. Phys. B **619** (2001) 3 [hep-ex/0106070].

[18] J. Collins, Phys. Rev. D **57** (1998) 3051 [Erratum-ibid. D **61** (2000) 019902] [hep-ph/9709499].

[19] V. Gribov and L. Lipatov, Sov. J. Nucl. Phys. **15** (1972) 438 [Yad. Fiz. **15** (1972) 781].

[20] V. Gribov and L. Lipatov, Sov. J. Nucl. Phys. **15** (1972) 675 [Yad. Fiz. **15** (1972) 1218].

[21] Y. Dokshitzer, Sov. Phys. JETP **46** (1977) 641 [Zh. Eksp. Teor. Fiz. **73** (1977) 1216].

[22] G. Altarelli and G. Parisi, Nucl. Phys. B **126** (1977) 298.

[23] P. Van Esch *et al.*, Nucl. Instrum. Meth. A **446** (2000) 409 [hep-ex/0001046].

[24] I. Abt *et al.* [H1 Collaboration], Nucl. Instrum. Meth. A **386** (1997) 310.

[25] I. Abt *et al.* [H1 Collaboration], Nucl. Instrum. Meth. A **386** (1997) 348.

[26] R. Appuhn *et al.* [H1 SPACAL Group], Nucl. Instrum. Meth. A **386** (1997) 397.

[27] B. Andrieu *et al.* [H1 Calorimeter Group], Nucl. Instrum. Meth. A **336** (1993) 499.

[28] B. Andrieu *et al.* [H1 Calorimeter Group], Nucl. Instrum. Meth. A **350** (1994) 57.

[29] M. Peez, "Search for Deviations from the Standard Model in High Transverse Energy Processes at the Electron-Proton Collider HERA," Ph.D. thesis (in French), University of Lyon (2003), H1 thesis 317, available from http://www-h1.desy.de/publications/theses list.html.

[30] S. Bentvelsen *et al.*, Proceedings of the Workshop "Physics at HERA", eds. W. Buchmüller, G. Ingelman, DESY (1992), 23;// C. Hoeger, ibid. 43.

[31] A. Blondel and F. Jacquet, Proceedings of the Study of an ep Facility for Europe, ed. U. Amaldi, DESY 79/48 (1979) 391.

[32] H. Jung, Comput. Phys. Commun. **86** (1995) 147 (see also http://www.desy.de/∼jung/rapgap.html).

[33] B. Andersson, G. Gustafson, G. Ingelman and T. Sjöstrand, Phys. Rept. **97** (1983) 31.

[34] T. Sjöstrand, Comput. Phys. Commun. **135** (2001) 74;// T. Sjöstrand, S. Mrenna and P. Skands, JHEP 0605:026 (2006) [hep-ph/0603175].

[35] B. List and A. Mastroberardino, Proc. of the Workshop on Monte Carlo Generators for HERA Physics, eds. A. Doyle, G. Grindhammer, G. Ingelman, H. Jung, DESY-PROC-1999-02 (1999) 396.

[36] R. Engel and J. Ranft, Phys. Rev. D **54** (1996) 4244 [hep-ph/9509373].

[37] R. Brun, R. Hagelberg, M. Hansroul and J. C. Lassalle, CERN-DD-78-2-REV.

[38] A. Kwiatkowski, H. Spiesberger and H. J. Möhring, Comput. Phys. Commun. **69** (1992) 155.

[39] A. Donnachie and P. Landshoff, Phys. Lett. B **296** (1992) 227 [hep-ph/9209205].

[40] J. Owens, Phys. Rev. D **30** (1984) 943.

[41] G. Jaroszkiewicz and P. Landshoff, Phys. Rev. D **10** (1974) 170.

[42] J. Cudell, K. Kang and S. Kim, Phys. Lett. B **395** (1997) 311 [hep-ph/9601336].

[43] J. Bartels and H. Kowalski, Eur. Phys. J. C **19** (2001) 693 [hep-ph/0010345].

[44] I. Ivanov, N. Nikolaev and A. Savin, hep-ph/0501034.

[45] S. Chekanov *et al.* [ZEUS Collaboration], Eur. Phys. J. C **24** (2002) 345 [hep-ex/0201043].

[46] A. Aktas *et al.* [H1 Collaboration], Eur. Phys. J. C **46** (2006) 585 [hep-ex/0510016].

[47] F.D. Aron *et al.* [H1 Collaboration], JHEP 1005:032 (2010) [arXiv:0910.5831].

[48] J. Breitweg *et al.* [ZEUS Collaboration], Eur. Phys. J. C **14** (2000) 213 [hep-ex/9910038].

[49] A. Mueller, Phys. Rev. D **2** (1970) 2963.

[50] W. Buchmüller and A. Hebecker, Phys. Lett. B**355** (1995) 573 [hep-ph/9504374].

[51] W. Buchmüller, T. Gehrmann and A Hebecker, Nucl. Phys. B**537** (1999) 477 [hep-ph9808454].

[52] A. Edin, G. Ingelman and J. Rathsman, Phys. Lett. B **366** (1996) 371 [hep-ph/9508386].

[53] A. Edin, G. Ingelman and J. Rathsman, Z. Phys. C **75** (1997) 57 [hep-ph/9605281].

[54] J. Rathsman, Phys. Lett. B **452** (1999) 364 [hep-ph/9812423].

[55] S. Brodsky, R. Enberg, P. Hoyer and G. Ingelman, Phys. Rev. D **71** (2005) 074020 [hep-ph/0409119].

[56] F.D. Aaron *et al.* [H1 Collaboration], Eur. Phys. J. C **64** (2009) 561 [arXiv:0904.3513].

[57] K. Prytz, Phys. Lett. B **311** (1993) 286.

Q^2 [GeV^2]	β	$x_{I\!P}$	$-t$ [GeV^2]	$x_{I\!P}\sigma_r^{D(4)}$ [GeV^{-2}]	δ_{stat} [%]	δ_{sys} [%]	δ_{tot} [%]	δ_{had} [%]	δ_{ele} [%]	δ_{θ} [%]	δ_{β} [%]	$\delta_{x_{I\!P}}$ [%]	δ_t [%]	δ_{E_p} [%]	δ_{p_x} [%]	δ_{p_y} [%]	δ_{Q^2} [%]	δ_{vtx} [%]	δ_{bgn} [%]	δ_{bcc} [%]
5.1	0.0018	0.0500	0.2	0.0689	7.6	8.7	11.5	−0.1	2.7	1.8	−1.2	0.0	−3.9	0.8	5.2	0.0	1.6	−3.5	−1.5	1.9
5.1	0.0018	0.0500	0.4	0.0204	10.2	8.7	13.4	−0.6	1.3	0.8	−1.0	0.0	0.8	0.2	6.6	4.4	1.0	−1.7	−0.8	1.9
5.1	0.0018	0.0500	0.6	0.0080	15.1	8.7	17.4	0.0	4.2	−4.2	−0.4	−0.1	0.3	2.5	−0.4	−3.6	3.3	−2.1	−0.9	1.9
5.1	0.0018	0.0750	0.2	0.0786	11.3	7.3	13.5	−0.2	0.7	2.1	−0.3	0.1	−1.8	0.5	6.2	0.8	1.1	−0.9	−1.6	1.6
5.1	0.0018	0.0750	0.4	0.0297	11.4	7.3	13.6	−0.1	0.6	4.2	−0.7	0.2	1.4	1.2	1.7	0.8	2.0	−2.4	−3.9	1.6
5.1	0.0018	0.0750	0.6	0.0078	17.7	7.3	19.2	0.0	0.8	4.4	−0.9	0.1	0.2	1.5	4.1	1.2	1.5	−1.2	−2.6	1.6
5.1	0.0056	0.0160	0.2	0.0433	4.9	9.5	10.7	−0.3	1.7	3.2	−1.1	−0.1	−2.5	2.0	6.3	0.8	2.2	−3.6	−1.9	2.0
5.1	0.0056	0.0160	0.4	0.0152	6.1	9.5	11.3	−0.9	0.0	4.2	−0.6	−0.1	1.7	2.4	6.3	−1.6	2.2	−3.1	−1.6	2.0
5.1	0.0056	0.0160	0.6	0.0050	13.1	9.5	16.2	0.0	4.8	−5.8	−0.9	0.0	0.1	3.4	2.8	2.9	0.0	−1.0	−0.5	2.0
5.1	0.0056	0.0250	0.2	0.0376	4.7	8.4	9.6	0.0	2.0	2.9	−0.5	−0.1	−2.5	1.5	6.2	−0.3	2.0	−1.9	−0.7	1.7
5.1	0.0056	0.0250	0.4	0.0129	6.3	8.4	10.5	0.0	−0.8	3.9	−0.2	0.0	1.0	0.6	6.4	2.4	1.3	−1.1	−0.5	1.7
5.1	0.0056	0.0250	0.6	0.0036	13.6	8.4	15.9	0.0	5.2	1.9	−1.5	−0.3	−0.8	−1.1	4.1	1.1	3.1	−1.7	−1.5	1.7
5.1	0.0056	0.0350	0.2	0.0449	5.8	7.4	9.4	−0.3	0.8	3.2	0.0	0.1	−1.9	2.1	5.4	−0.1	1.3	−1.0	−0.3	1.6
5.1	0.0056	0.0350	0.4	0.0123	8.1	7.4	10.9	−0.3	1.1	5.1	0.1	0.0	1.4	−0.1	2.5	3.8	0.9	−0.8	−0.3	1.6
5.1	0.0056	0.0350	0.6	0.0051	12.9	7.4	14.8	0.0	−1.8	−4.2	0.4	0.1	1.2	2.3	4.2	−1.8	1.4	−0.7	−0.3	1.6
5.1	0.0056	0.0500	0.2	0.0473	6.3	9.0	11.0	0.0	0.3	6.2	−0.4	0.2	−3.6	0.3	4.4	0.9	1.9	−1.3	−0.5	1.6
5.1	0.0056	0.0500	0.4	0.0151	7.5	9.0	11.7	0.0	−1.5	7.9	0.0	0.1	0.2	1.1	2.6	1.1	1.8	−0.8	−0.4	1.6
5.1	0.0056	0.0500	0.6	0.0054	12.9	9.0	15.7	0.0	−2.0	4.7	−0.4	0.0	−0.3	−1.7	6.7	1.5	0.3	−0.5	−0.3	1.6
5.1	0.0056	0.0750	0.2	0.0544	11.6	10.3	15.5	0.0	0.2	6.9	−0.6	0.2	−2.6	−0.3	6.2	1.5	1.3	−1.1	−2.5	1.6
5.1	0.0056	0.0750	0.4	0.0255	10.2	10.3	14.5	0.0	−0.6	7.7	−0.8	0.2	0.7	0.0	5.0	1.5	2.3	−1.3	−3.1	1.6
5.1	0.0056	0.0750	0.6	0.0094	17.1	10.3	20.0	0.0	−2.0	9.4	−1.2	0.2	−0.7	0.3	0.6	1.7	1.3	−0.9	−2.2	1.6
5.1	0.0178	0.0085	0.2	0.0345	4.3	10.6	11.4	−7.0	1.2	3.6	−0.8	−0.2	−1.7	0.5	5.4	0.1	1.7	−1.6	−2.6	2.0
5.1	0.0178	0.0085	0.4	0.0119	5.5	10.6	11.9	−6.2	1.0	4.6	−0.8	−0.2	1.3	2.2	5.1	0.6	1.1	−1.4	−3.1	2.0
5.1	0.0178	0.0085	0.6	0.0039	11.2	10.6	15.4	−8.6	1.2	2.9	−0.5	−0.2	0.6	−0.2	4.1	1.6	0.7	−0.6	−1.8	2.0
5.1	0.0178	0.0160	0.2	0.0366	3.6	9.2	9.9	0.0	0.5	4.8	−0.1	0.2	−2.3	4.9	4.8	−0.3	1.3	−1.2	−1.4	1.6
5.1	0.0178	0.0160	0.4	0.0110	5.1	9.2	10.5	0.5	−0.4	5.6	0.3	0.0	1.2	0.9	6.6	1.1	1.1	−0.7	−1.0	1.6
5.1	0.0178	0.0160	0.6	0.0032	10.2	9.2	13.7	0.0	−0.3	6.7	−0.2	0.2	0.1	1.3	2.8	4.6	1.9	−0.7	−1.2	1.6
5.1	0.0178	0.0250	0.2	0.0333	4.7	8.9	10.1	0.0	0.3	6.0	−0.2	0.0	−2.0	0.7	5.6	0.1	1.6	−1.5	−0.6	1.6
5.1	0.0178	0.0250	0.4	0.0113	6.4	8.9	10.9	0.0	1.7	5.8	−0.3	0.1	1.4	0.4	5.2	2.4	1.4	−1.4	−0.6	1.6
5.1	0.0178	0.0250	0.6	0.0038	13.3	8.9	16.0	0.0	−2.4	7.1	1.2	0.0	0.1	−0.1	4.4	0.0	−0.2	−0.6	−0.4	1.6
5.1	0.0178	0.0350	0.2	0.0303	7.1	8.7	11.2	0.0	0.6	6.7	−0.3	0.1	−1.9	1.4	4.4	0.2	0.9	−1.4	−0.4	1.6
5.1	0.0178	0.0350	0.4	0.0122	9.0	8.7	12.5	0.0	−0.7	7.8	−1.0	0.1	1.2	0.7	1.7	1.9	0.5	−1.2	−0.4	1.6
5.1	0.0178	0.0350	0.6	0.0039	13.9	8.7	16.4	0.0	1.6	−0.8	0.0	0.0	0.5	−2.3	7.7	1.9	0.2	−0.8	−0.3	1.6
5.1	0.0178	0.0500	0.2	0.0449	7.1	8.8	11.3	0.0	0.4	6.0	−1.1	0.1	−2.3	0.8	5.2	1.2	0.2	−1.5	−0.3	1.6
5.1	0.0178	0.0500	0.4	0.0133	9.0	8.8	12.6	0.4	1.2	3.0	−0.7	0.2	1.2	1.6	5.0	4.9	0.6	−3.1	−0.7	1.6
5.1	0.0178	0.0500	0.6	0.0050	15.2	8.8	17.6	0.0	0.4	8.4	0.2	0.2	−0.5	1.5	−0.3	−1.2	0.2	−0.7	−0.2	1.6

Table 3: The reduced diffractive cross sections $x_{I\!P}\sigma_r^{D(4)}$ as a function of Q^2, β, $x_{I\!P}$ and t values (columns $1-5$). The statistical (δ_{stat}), systematic (δ_{sys}) and total (δ_{tot}) uncertainties are given in columns 6 to 8. The remaining columns give the changes of the cross sections due to a $+1\sigma$ variation of the various systematic error sources described in section 4: the hadronic energy scale (δ_{had}); the electromagnetic energy scale (δ_{ele}); the scattering angle of the electron (δ_{θ}); the reweighting of the simulation in β (δ_{β}), $x_{I\!P}$ ($\delta_{x_{I\!P}}$) and t (δ_t); the leading proton energy E_p (δ_{E_p}), the proton transverse momentum components p_x (δ_{p_x}) and p_y (δ_{p_y}); the reweighting of the simulation in Q^2 (δ_{Q^2}); the background from beam halo, photoproduction and proton dissociation processes (δ_{bgn}); the vertex reconstruction efficiency (δ_{vtx}) and the bin centre corrections (δ_{bcc}). All uncertainties are given in per cent. The normalisation uncertainty of 4.3% is not included. The table continues on the next pages.

Q^2 [GeV^2]	β	$x_{I\!P}$	$-t$ [GeV^2]	$x_{I\!P}\sigma_r^{D(4)}$ [GeV^{-2}]	δ_{stat} [%]	δ_{sys} [%]	δ_{tot} [%]	δ_{had} [%]	δ_{ele} [%]	δ_{θ} [%]	δ_{β} [%]	$\delta_{x_{I\!P}}$ [%]	δ_t [%]	δ_{E_p} [%]	δ_{p_x} [%]	δ_{p_y} [%]	δ_{Q^2} [%]	δ_{vtx} [%]	δ_{bgn} [%]	δ_{bcc} [%]
5.1	0.0178	0.0750	0.2	0.0508	12.7	8.2	15.1	0.0	−0.5	3.4	−0.5	0.2	−2.8	0.7	6.0	0.3	−0.3	−1.3	−2.6	1.6
5.1	0.0178	0.0750	0.4	0.0208	15.2	8.2	17.3	0.0	1.2	6.4	−0.8	0.4	0.6	0.8	−1.2	0.9	−0.7	−1.8	−3.8	1.6
5.1	0.0178	0.0750	0.6	0.0093	20.3	8.2	21.9	0.0	0.9	2.8	−0.1	0.0	−0.3	−1.2	7.2	0.9	0.2	−0.6	−1.3	1.6
5.1	0.0562	0.0025	0.2	0.0345	3.4	10.1	10.7	−4.9	0.6	2.8	−1.5	0.1	−1.9	−5.8	3.5	−0.1	1.3	−1.5	−2.9	2.6
5.1	0.0562	0.0025	0.4	0.0102	4.5	10.1	11.1	−4.7	0.3	2.5	−1.2	0.1	0.8	−4.4	6.0	1.1	1.0	−1.0	−2.7	2.6
5.1	0.0562	0.0025	0.6	0.0030	9.1	10.1	13.7	−1.8	−1.2	5.8	−1.4	0.3	0.2	−4.9	3.6	2.3	1.6	−0.9	−3.2	2.6
5.1	0.0562	0.0085	0.2	0.0301	3.6	9.7	10.3	3.2	−0.3	3.6	0.6	0.0	−1.7	6.7	4.1	0.2	0.9	−1.1	−0.8	1.7
5.1	0.0562	0.0085	0.4	0.0097	4.7	9.7	10.8	1.5	−0.3	6.7	0.3	0.1	0.9	5.5	3.2	−0.2	0.9	−0.9	−0.9	1.7
5.1	0.0562	0.0085	0.6	0.0029	9.9	9.7	13.9	5.4	−0.9	4.1	0.7	−0.1	0.3	2.9	5.2	2.4	1.1	−0.6	−0.7	1.7
5.1	0.0562	0.0160	0.2	0.0279	4.3	8.8	9.8	0.0	−0.6	5.4	−1.1	0.1	−1.5	3.5	5.1	−0.2	0.6	−1.5	−1.2	1.6
5.1	0.0562	0.0160	0.4	0.0093	6.1	8.8	10.7	0.0	1.1	2.4	−0.5	−0.1	2.0	1.6	6.3	3.7	0.8	−1.9	−1.9	1.6
5.1	0.0562	0.0160	0.6	0.0037	13.0	8.8	15.7	0.0	0.9	1.3	−0.5	0.0	0.7	1.7	8.2	−0.9	0.0	−0.8	−0.9	1.6
5.1	0.0562	0.0250	0.2	0.0267	6.3	7.3	9.6	0.0	−0.9	2.2	0.6	0.2	−2.1	1.5	6.0	−0.3	−0.3	−1.4	−0.5	1.6
5.1	0.0562	0.0250	0.4	0.0095	8.5	7.3	11.2	0.0	−3.2	0.2	0.7	0.3	0.8	2.5	−1.9	4.8	0.1	−2.4	−1.0	1.6
5.1	0.0562	0.0250	0.6	0.0028	17.1	7.3	18.6	0.0	1.6	1.8	−0.1	0.4	−1.2	4.6	3.4	3.0	−0.9	−0.8	−0.4	1.6
5.1	0.1780	0.0025	0.2	0.0383	2.4	10.9	11.1	−2.6	0.2	5.9	−0.5	−0.1	−2.4	−1.0	7.3	0.1	1.5	−1.7	−1.9	2.8
5.1	0.1780	0.0025	0.4	0.0108	3.2	10.9	11.3	−1.6	0.0	6.7	0.5	0.2	1.4	−1.6	6.6	1.7	1.6	−1.8	−2.5	2.8
5.1	0.1780	0.0025	0.6	0.0029	7.4	10.9	13.1	−1.3	0.7	4.2	0.4	−0.2	0.4	−0.7	7.1	5.4	1.7	−1.4	−2.4	2.8
5.1	0.1780	0.0085	0.2	0.0346	3.3	10.5	11.0	4.4	0.5	2.5	1.9	0.2	−1.2	8.2	2.7	−0.2	0.3	−0.8	0.0	2.2
5.1	0.1780	0.0085	0.4	0.0104	4.4	10.5	11.4	5.3	0.5	3.0	1.2	0.3	0.5	6.8	4.4	0.7	0.2	−0.7	0.0	2.2
5.1	0.1780	0.0085	0.6	0.0037	9.1	10.5	13.9	5.1	0.9	1.5	2.5	0.0	0.1	7.1	0.5	4.3	0.0	−0.8	0.0	2.2
5.1	0.5620	0.0025	0.2	0.0576	1.9	10.5	10.6	5.4	−0.8	5.6	0.8	0.0	−1.7	0.8	4.4	0.1	0.9	−0.9	−0.9	4.8
5.1	0.5620	0.0025	0.4	0.0162	2.6	10.5	10.8	5.0	−1.1	5.6	0.6	0.0	0.8	0.4	4.8	1.2	0.8	−0.8	−1.0	4.8
5.1	0.5620	0.0025	0.6	0.0043	5.7	10.5	11.9	4.5	−1.4	5.3	0.9	0.3	−0.2	0.4	3.6	4.4	0.5	−0.9	−1.3	4.8
8.8	0.0018	0.0750	0.2	0.0924	19.6	7.6	21.0	−0.2	0.2	1.2	−1.3	0.1	−2.7	0.9	4.7	0.9	0.7	−2.9	−3.2	2.2
8.8	0.0018	0.0750	0.4	0.0328	19.4	7.6	20.8	0.1	0.1	1.9	−2.8	−0.1	−0.7	−0.3	4.1	2.7	1.1	−2.5	−3.3	2.2
8.8	0.0018	0.0750	0.6	0.0250	29.5	7.6	30.4	0.0	4.8	−1.9	−1.6	−0.1	−0.2	2.6	−3.6	0.9	−0.2	−1.1	−1.7	2.2
8.8	0.0056	0.0250	0.2	0.0494	7.9	8.4	11.6	−0.3	−0.1	4.5	−1.4	−0.1	−2.3	−0.7	4.2	−0.6	1.0	−3.5	−2.7	2.1
8.8	0.0056	0.0250	0.4	0.0171	9.8	8.4	13.0	−0.1	1.7	−0.2	−0.3	0.0	0.8	−0.2	7.2	2.2	0.9	−1.8	−1.5	2.1
8.8	0.0056	0.0250	0.6	0.0043	19.8	8.4	21.5	0.0	1.6	0.5	−0.2	−0.1	−0.5	2.9	7.2	0.6	0.5	−1.2	−0.9	2.1
8.8	0.0056	0.0350	0.2	0.0575	7.8	8.2	11.3	0.0	−0.1	3.8	−1.0	0.1	−2.2	1.0	6.0	0.1	1.1	−2.5	−0.5	1.7
8.8	0.0056	0.0350	0.4	0.0155	11.5	8.2	14.2	−0.1	1.0	0.7	−0.8	0.0	0.4	1.5	6.9	2.6	0.6	−2.1	−0.6	1.7
8.8	0.0056	0.0350	0.6	0.0068	17.0	8.2	18.9	0.0	0.7	7.4	−0.8	0.0	0.0	2.0	−1.2	1.7	0.1	−1.1	−0.4	1.7
8.8	0.0056	0.0500	0.2	0.0647	7.3	7.2	10.2	−0.1	0.1	3.3	−0.5	0.1	−1.7	1.4	5.4	1.2	0.8	−1.4	−0.2	1.6
8.8	0.0056	0.0500	0.4	0.0192	9.5	7.2	11.9	−0.1	−2.7	3.0	0.1	0.2	1.0	−1.3	5.0	1.2	0.7	−1.7	−0.4	1.6
8.8	0.0056	0.0500	0.6	0.0095	13.2	7.2	15.0	0.0	0.1	1.9	−0.7	0.0	0.4	−1.3	6.2	1.9	0.1	−1.2	−0.3	1.6
8.8	0.0056	0.0750	0.2	0.0784	11.8	7.3	13.8	0.0	−0.8	3.7	−0.4	0.2	−3.9	−0.4	3.0	0.4	0.6	−1.2	−3.1	1.6
8.8	0.0056	0.0750	0.4	0.0260	13.3	7.3	15.2	0.0	−0.8	2.4	−0.9	0.1	0.3	0.2	5.9	0.9	0.5	−0.9	−2.6	1.6
8.8	0.0056	0.0750	0.6	0.0091	21.5	7.3	22.7	0.0	−2.6	4.8	−2.1	0.1	−0.2	−0.4	0.2	1.6	0.1	−1.3	−3.3	1.6
8.8	0.0178	0.0085	0.2	0.0394	6.5	8.4	10.6	−6.8	0.0	0.8	−0.9	−0.1	−0.9	−1.6	2.2	0.0	0.4	−1.3	−2.7	2.0
8.8	0.0178	0.0085	0.4	0.0123	9.0	8.4	12.3	−6.2	−0.1	2.1	−0.9	0.0	0.7	−1.1	3.0	0.4	0.3	−1.3	−3.1	2.0
8.8	0.0178	0.0085	0.6	0.0037	16.8	8.4	18.7	−6.7	1.0	1.2	−0.9	0.0	0.3	−0.1	−1.3	1.3	0.0	−1.1	−3.5	2.0
8.8	0.0178	0.0160	0.2	0.0409	4.7	7.9	9.2	−0.3	1.2	2.6	−0.2	0.0	−2.0	1.9	6.1	0.1	0.8	−1.9	−1.4	1.6
8.8	0.0178	0.0160	0.4	0.0132	6.1	7.9	10.0	0.0	0.9	2.1	−0.5	0.0	2.3	0.8	6.2	1.9	0.5	−1.7	−1.5	1.6
8.8	0.0178	0.0160	0.6	0.0036	13.1	7.9	15.3	0.0	−0.6	2.2	−0.7	−0.1	0.2	3.9	4.0	−4.5	0.2	−1.0	−1.1	1.6
8.8	0.0178	0.0250	0.2	0.0437	5.1	7.8	9.3	0.0	0.5	2.2	−0.1	0.0	−2.4	2.2	6.3	0.6	0.7	−1.3	−0.7	1.6
8.8	0.0178	0.0250	0.4	0.0139	6.9	7.8	10.4	−0.4	0.1	3.9	−0.3	0.1	2.2	2.7	5.2	0.2	0.2	−1.4	−1.0	1.6
8.8	0.0178	0.0250	0.6	0.0036	14.6	7.8	16.5	0.0	1.3	−2.2	0.3	−0.4	1.4	−5.5	−2.8	−0.1	2.2	−1.8	−1.5	1.6

Q^2 [GeV^2]	β	$x_{I\!P}$	$-t$ [GeV^2]	$x_{I\!P}\sigma_r^{D(4)}$ [GeV^{-2}]	δ_{stat} [%]	δ_{sys} [%]	δ_{tot} [%]	δ_{had} [%]	δ_{ele} [%]	δ_{θ} [%]	δ_{β} [%]	$\delta_{x_{I\!P}}$ [%]	δ_t [%]	δ_{E_p} [%]	δ_{p_x} [%]	δ_{p_y} [%]	δ_{Q2} [%]	δ_{vtx} [%]	δ_{bgn} [%]	δ_{bcc} [%]
8.8	0.0178	0.0350	0.2	0.0432	6.3	7.4	9.7	0.1	0.7	1.9	−0.4	0.1	−2.8	1.2	5.8	−0.6	1.3	−1.7	−0.6	1.6
8.8	0.0178	0.0350	0.4	0.0128	9.5	7.4	12.0	0.0	−0.7	2.8	−0.4	0.1	0.4	0.0	5.3	3.6	0.7	−1.2	−0.5	1.6
8.8	0.0178	0.0350	0.6	0.0059	14.3	7.4	16.1	0.0	0.1	2.1	0.7	−0.1	0.9	0.0	5.5	3.9	0.5	−0.7	−0.3	1.6
8.8	0.0178	0.0500	0.2	0.0484	7.0	6.8	9.8	0.5	−0.3	2.5	−1.0	0.1	−2.4	0.2	5.4	0.0	0.7	−1.2	−0.2	1.6
8.8	0.0178	0.0500	0.4	0.0192	8.1	6.8	10.6	0.0	0.7	0.7	−0.3	0.0	0.5	0.9	5.6	3.1	0.4	−0.7	−0.2	1.6
8.8	0.0178	0.0500	0.6	0.0057	13.9	6.8	15.5	0.0	2.4	1.2	−1.3	−0.2	0.5	1.6	5.3	0.5	1.0	−1.7	−0.5	1.6
8.8	0.0178	0.0750	0.2	0.0489	13.3	7.1	15.1	0.0	0.8	1.9	−0.6	0.2	−2.7	1.4	5.1	1.5	0.4	−0.6	−2.3	1.6
8.8	0.0178	0.0750	0.4	0.0235	12.4	7.1	14.3	0.0	1.1	1.7	−1.7	0.2	−0.5	1.5	3.9	−3.5	0.1	−0.9	−3.2	1.6
8.8	0.0178	0.0750	0.6	0.0070	21.0	7.1	22.2	0.0	−0.1	4.7	−1.7	0.1	0.0	−0.2	3.3	1.9	0.0	−0.8	−2.8	1.6
8.8	0.0562	0.0025	0.2	0.0418	4.6	10.0	11.0	−5.5	0.0	0.9	−1.4	0.1	−0.9	−6.0	3.6	0.1	0.3	−1.2	−3.2	2.1
8.8	0.0562	0.0025	0.4	0.0113	6.3	10.0	11.8	−5.0	−0.6	1.4	−1.0	0.1	0.4	−6.9	0.3	0.5	0.3	−1.4	−4.1	2.1
8.8	0.0562	0.0025	0.6	0.0039	12.8	10.0	16.2	−6.1	1.2	−0.6	−1.7	0.2	0.0	−4.2	2.9	3.5	0.0	−0.8	−3.8	2.1
8.8	0.0562	0.0085	0.2	0.0362	4.3	8.8	9.8	0.7	0.3	2.8	−0.2	−0.2	−2.0	5.5	4.8	0.1	0.7	−1.4	−2.4	1.7
8.8	0.0562	0.0085	0.4	0.0105	6.1	8.8	10.7	0.5	0.5	1.7	−0.1	−0.1	0.8	3.9	7.1	0.0	0.5	−0.9	−2.0	1.7
8.8	0.0562	0.0085	0.6	0.0032	13.2	8.8	15.8	0.4	1.4	1.8	0.3	−0.3	−0.3	2.5	7.1	2.6	0.5	−0.9	−2.3	1.7
8.8	0.0562	0.0160	0.2	0.0353	4.3	8.5	9.5	0.0	−0.5	3.8	−0.1	0.0	−1.7	2.4	6.5	0.1	0.9	−1.1	−1.0	1.6
8.8	0.0562	0.0160	0.4	0.0115	5.8	8.5	10.3	0.0	−1.1	3.0	−0.5	0.1	1.6	4.0	5.4	2.4	0.9	−1.4	−1.6	1.6
8.8	0.0562	0.0160	0.6	0.0038	12.3	8.5	14.9	0.0	0.8	3.1	−0.6	0.0	−0.4	6.7	3.0	0.6	0.6	−1.1	−1.5	1.6
8.8	0.0562	0.0250	0.2	0.0290	5.6	8.8	10.4	0.0	−0.5	5.5	−0.3	0.1	−1.7	2.0	5.8	0.2	0.7	−0.7	−0.9	1.6
8.8	0.0562	0.0250	0.4	0.0108	7.3	8.8	11.4	0.0	−0.9	5.7	−0.3	0.1	1.1	1.0	5.9	1.2	0.6	−0.6	−1.0	1.6
8.8	0.0562	0.0250	0.6	0.0039	13.9	8.8	16.4	0.0	−0.4	5.9	−0.1	0.0	−0.3	2.5	4.4	3.5	0.4	−0.6	−1.3	1.6
8.8	0.0562	0.0350	0.2	0.0341	7.7	8.0	11.1	0.0	−0.6	5.3	−1.0	0.1	−3.0	−0.2	4.7	0.0	0.3	−0.5	−0.6	1.6
8.8	0.0562	0.0350	0.4	0.0129	9.5	8.0	12.4	0.0	0.2	1.2	0.1	0.1	0.7	0.5	6.6	3.9	0.5	−0.3	−0.5	1.6
8.8	0.0562	0.0350	0.6	0.0044	19.0	8.0	20.7	0.0	0.6	4.9	−0.2	−0.1	0.9	−3.2	−0.2	−5.0	−0.2	−0.2	−0.7	1.6
8.8	0.0562	0.0500	0.2	0.0460	8.6	9.0	12.4	0.0	−0.9	5.8	1.3	0.3	−2.0	0.3	6.0	1.2	−0.1	−0.1	−0.4	1.6
8.8	0.0562	0.0500	0.4	0.0170	10.9	9.0	14.1	0.0	−0.1	5.9	2.7	0.4	2.6	−2.1	4.6	1.7	0.0	−0.3	−0.9	1.6
8.8	0.0562	0.0500	0.6	0.0051	18.4	9.0	20.4	0.0	2.5	7.7	1.0	0.2	−0.9	−0.5	3.1	−1.0	0.3	−0.2	−0.5	1.6
8.8	0.1780	0.0025	0.2	0.0427	3.1	9.7	10.2	−3.1	−0.2	3.5	−0.4	−0.9	−2.2	−3.2	6.3	0.4	1.0	−1.6	−2.6	2.4
8.8	0.1780	0.0025	0.4	0.0110	4.4	9.7	10.6	−2.7	−0.1	3.1	−0.3	−0.8	1.3	−3.5	6.6	0.8	0.8	−1.5	−3.1	2.4
8.8	0.1780	0.0025	0.6	0.0042	8.4	9.7	12.8	−2.5	0.5	3.4	−0.4	−0.9	−0.1	−2.8	5.3	4.3	0.9	−1.3	−3.4	2.4
8.8	0.1780	0.0085	0.2	0.0379	3.6	8.9	9.6	3.1	0.0	1.9	1.4	0.1	−1.2	6.9	3.5	−0.1	0.3	−0.4	−0.3	1.7
8.8	0.1780	0.0085	0.4	0.0107	4.9	8.9	10.2	3.1	−0.4	3.1	1.4	0.2	0.6	6.8	2.7	0.8	0.4	−0.4	−0.3	1.7
8.8	0.1780	0.0085	0.6	0.0039	9.9	8.9	13.3	3.6	−0.3	1.6	1.5	0.1	−0.1	6.3	3.1	3.0	0.1	−0.4	−0.3	1.7
8.8	0.1780	0.0160	0.2	0.0284	6.1	8.6	10.6	0.0	0.3	2.3	3.6	0.3	−1.8	4.0	5.6	0.0	0.1	−0.2	−0.8	1.7
8.8	0.1780	0.0160	0.4	0.0105	7.6	8.6	11.5	0.0	0.8	3.8	3.2	0.1	0.7	3.0	5.6	2.1	0.1	−0.1	−0.9	1.7
8.8	0.1780	0.0160	0.6	0.0029	16.5	8.6	18.6	0.0	−0.2	−2.6	4.7	0.3	−1.5	−3.5	3.1	−3.9	−0.5	−0.2	−1.5	1.7
8.8	0.5620	0.0025	0.2	0.0633	2.2	11.0	11.2	6.9	−0.8	4.0	1.0	−1.5	−1.9	0.4	5.3	0.2	0.5	−0.9	−1.3	4.2
8.8	0.5620	0.0025	0.4	0.0182	2.9	11.0	11.4	6.2	−0.7	3.8	0.9	−0.9	1.0	−0.2	6.5	0.9	0.4	−0.9	−1.5	4.2
8.8	0.5620	0.0025	0.6	0.0053	6.6	11.0	12.8	6.6	−1.1	3.8	1.0	−0.9	0.2	0.1	3.2	5.3	0.4	−0.8	−1.7	4.2
15.3	0.0056	0.0500	0.2	0.0751	12.3	7.2	14.2	0.0	0.7	1.4	−1.5	0.0	−2.1	0.7	6.0	0.8	0.9	−1.1	−0.7	1.8
15.3	0.0056	0.0500	0.4	0.0318	13.8	7.2	15.6	−0.3	2.5	3.4	−3.9	0.2	0.3	1.7	−2.6	0.5	0.2	−2.1	−1.2	1.8
15.3	0.0056	0.0500	0.6	0.0082	20.0	7.2	21.3	−0.2	0.5	0.2	−1.3	0.0	0.5	0.6	5.5	4.0	0.7	−0.4	−0.3	1.8
15.3	0.0056	0.0750	0.2	0.1073	19.1	6.8	20.3	0.0	0.5	1.4	−1.4	0.2	−4.1	1.5	1.8	1.9	1.0	−1.2	−3.4	1.6
15.3	0.0056	0.0750	0.4	0.0317	15.6	6.8	17.1	0.0	2.7	−1.6	−0.4	0.0	−0.3	0.7	4.4	2.5	0.4	−1.0	−2.5	1.6
15.3	0.0056	0.0750	0.6	0.0137	25.7	6.8	26.6	0.0	1.1	−1.1	−0.6	0.0	−0.6	−1.7	5.6	−1.8	0.0	−0.5	−1.8	1.6
15.3	0.0178	0.0160	0.2	0.0609	6.8	8.1	10.6	−0.2	−0.8	3.5	−1.7	−0.1	−1.3	1.7	6.3	0.0	0.7	−1.2	−0.9	1.8
15.3	0.0178	0.0160	0.4	0.0176	9.5	8.1	12.5	0.0	0.3	1.4	−1.8	−0.2	3.7	4.3	−1.2	2.8	0.8	−3.1	−2.4	1.8
15.3	0.0178	0.0160	0.6	0.0055	16.9	8.1	18.7	0.0	2.1	2.4	−1.2	−0.6	0.4	3.1	−6.1	−0.3	0.7	−1.1	−1.3	1.8

Q^2 [GeV^2]	β	$x_{I\!P}$	$-t$ [GeV^2]	$x_{I\!P}\sigma_r^{D(4)}$ [GeV^{-2}]	δ_{stat} [%]	δ_{sys} [%]	δ_{tot} [%]	δ_{had} [%]	δ_{ele} [%]	δ_{θ} [%]	δ_{β} [%]	$\delta_{x_{I\!P}}$ [%]	δ_t [%]	δ_{E_p} [%]	δ_{p_x} [%]	δ_{p_y} [%]	δ_{Q^2} [%]	δ_{vtx} [%]	δ_{bgn} [%]	δ_{bcc} [%]
15.3	0.0178	0.0250	0.2	0.0549	6.6	7.5	10.0	0.0	−1.0	3.2	−0.7	0.0	−1.8	0.3	5.8	0.4	1.9	−0.9	−0.7	1.6
15.3	0.0178	0.0250	0.4	0.0164	9.0	7.5	11.7	0.4	0.2	−0.1	−0.5	0.0	2.4	1.5	4.3	4.2	1.1	−2.2	−1.9	1.6
15.3	0.0178	0.0250	0.6	0.0053	18.3	7.5	19.8	−1.2	1.0	0.3	−0.1	0.0	−0.3	4.3	5.3	−1.9	0.2	−0.4	−0.5	1.6
15.3	0.0178	0.0350	0.2	0.0488	9.2	7.3	11.8	0.0	0.6	3.0	−0.3	0.0	−2.4	0.3	5.8	0.6	0.5	−1.3	−0.5	1.6
15.3	0.0178	0.0350	0.4	0.0199	11.3	7.3	13.4	0.0	−0.9	2.7	0.1	0.0	0.5	2.8	4.9	3.1	0.4	−1.0	−0.6	1.6
15.3	0.0178	0.0350	0.6	0.0076	20.6	7.3	21.9	0.7	−0.6	−3.3	0.1	−0.2	0.4	−5.1	−1.2	−3.2	0.3	−0.9	−0.6	1.6
15.3	0.0178	0.0500	0.2	0.0534	9.5	7.4	12.1	0.0	−0.2	2.2	−0.5	0.2	−3.1	1.8	5.7	0.1	0.5	−1.4	−0.4	1.6
15.3	0.0178	0.0500	0.4	0.0206	10.3	7.4	12.6	0.1	−0.9	2.6	−1.5	0.0	0.4	−0.7	5.6	3.0	0.2	−1.0	−0.4	1.6
15.3	0.0178	0.0500	0.6	0.0089	16.3	7.4	17.9	0.0	0.2	−1.1	1.2	−0.1	1.1	−4.1	−3.6	1.6	2.9	−2.5	−1.1	1.6
15.3	0.0178	0.0750	0.2	0.0758	15.7	6.6	17.0	0.0	0.4	−0.6	−0.3	0.2	−2.3	1.0	5.0	1.9	0.3	−1.0	−2.3	1.6
15.3	0.0178	0.0750	0.4	0.0323	14.3	6.6	15.7	0.0	0.0	0.2	−1.5	0.3	0.4	0.5	4.5	0.7	0.0	−1.5	−3.9	1.6
15.3	0.0178	0.0750	0.6	0.0109	21.2	6.6	22.2	0.0	3.5	−0.3	−0.1	0.4	0.7	3.2	3.0	0.2	0.1	−1.2	−2.8	1.6
15.3	0.0562	0.0085	0.2	0.0420	6.2	9.6	11.4	−4.0	0.1	2.9	−0.7	−0.3	−2.0	2.8	6.1	0.6	0.8	−1.4	−3.5	1.7
15.3	0.0562	0.0085	0.4	0.0132	8.1	9.6	12.5	−4.2	−0.5	2.0	−0.4	−0.1	1.4	1.3	6.2	−1.2	0.8	−1.3	−4.6	1.7
15.3	0.0562	0.0085	0.6	0.0049	15.0	9.6	17.8	−1.2	0.4	2.9	−0.6	−0.2	0.4	−1.3	6.4	4.8	0.5	−0.8	−3.5	1.7
15.3	0.0562	0.0160	0.2	0.0406	5.8	8.3	10.2	0.0	0.0	3.1	−0.6	0.0	−2.9	5.1	4.1	0.3	0.7	−1.6	−1.6	1.6
15.3	0.0562	0.0160	0.4	0.0137	7.5	8.3	11.2	0.0	0.5	0.5	−0.1	0.2	1.4	1.9	7.6	0.4	0.2	−1.0	−1.3	1.6
15.3	0.0562	0.0160	0.6	0.0038	16.3	8.3	18.3	0.0	0.5	5.7	−0.4	−0.5	−0.9	−1.2	−2.1	−1.7	0.7	−2.7	−4.0	1.6
15.3	0.0562	0.0250	0.2	0.0377	7.0	7.5	10.3	0.0	0.3	1.8	−0.4	0.0	−2.0	0.8	6.5	0.3	0.5	−1.2	−0.8	1.6
15.3	0.0562	0.0250	0.4	0.0108	9.5	7.5	12.1	0.0	0.9	1.3	−0.5	0.1	1.1	1.9	6.6	1.3	0.3	−0.9	−0.8	1.6
15.3	0.0562	0.0250	0.6	0.0035	17.4	7.5	18.9	0.0	−3.3	0.1	0.1	−0.1	−1.0	6.3	0.3	−0.7	0.3	−0.9	−1.0	1.6
15.3	0.0562	0.0350	0.2	0.0392	9.6	6.9	11.8	0.0	−1.1	2.1	−0.3	0.0	−2.7	0.4	5.4	0.9	0.3	−1.0	−0.7	1.6
15.3	0.0562	0.0350	0.4	0.0142	11.9	6.9	13.7	0.0	2.3	1.4	−0.6	0.1	2.5	4.5	0.6	2.2	1.3	−1.7	−1.3	1.6
15.3	0.0562	0.0350	0.6	0.0047	21.5	6.9	22.6	0.0	−2.8	−0.1	−0.8	0.2	1.9	0.0	4.9	2.6	0.9	−0.8	−0.8	1.6
15.3	0.0562	0.0500	0.2	0.0464	9.2	6.8	11.5	0.0	−0.8	2.1	−0.2	0.2	−1.9	1.1	5.7	1.1	0.2	−0.7	−0.3	1.6
15.3	0.0562	0.0500	0.4	0.0128	12.5	6.8	14.3	0.0	0.3	−1.2	−0.9	0.4	1.2	−3.4	4.3	2.2	−0.2	−2.2	−0.9	1.6
15.3	0.0562	0.0500	0.6	0.0076	18.6	6.8	19.9	0.0	2.4	−0.1	−0.3	−0.2	−0.1	−1.2	5.6	2.1	0.3	−0.7	−0.3	1.6
15.3	0.0562	0.0750	0.2	0.0656	18.5	7.6	20.0	0.0	−0.8	3.8	1.2	0.4	−4.3	−0.3	1.8	−0.4	0.0	−1.3	−4.0	1.6
15.3	0.0562	0.0750	0.4	0.0156	24.1	7.6	25.2	0.0	−0.3	2.4	0.4	0.0	0.4	0.1	6.3	2.7	−0.1	−0.5	−1.5	1.6
15.3	0.0562	0.0750	0.6	0.0072	27.6	7.6	28.7	0.0	−2.7	4.8	0.5	0.0	−0.7	−2.3	3.1	2.9	0.0	−0.4	−1.3	1.6
15.3	0.1780	0.0025	0.2	0.0461	4.7	9.5	10.6	−3.1	−0.4	1.9	−0.4	−0.9	−2.1	−4.5	5.5	−0.2	0.5	−1.2	−3.8	2.0
15.3	0.1780	0.0025	0.4	0.0127	6.5	9.5	11.5	−3.0	−0.1	2.0	−0.3	−0.7	0.9	−4.7	5.6	1.5	0.3	−1.0	−3.9	2.0
15.3	0.1780	0.0025	0.6	0.0030	14.4	9.5	17.2	−1.9	−0.7	2.2	0.5	−0.5	0.0	−3.9	5.0	4.4	0.4	−0.8	−4.0	2.0
15.3	0.1780	0.0085	0.2	0.0381	4.9	9.0	10.2	2.7	−0.2	1.4	0.7	0.0	−1.4	6.5	4.8	0.2	0.3	−0.8	−0.7	1.7
15.3	0.1780	0.0085	0.4	0.0124	6.3	9.0	11.0	1.6	0.3	0.9	0.5	0.1	1.2	6.6	5.2	0.1	0.4	−0.8	−0.9	1.7
15.3	0.1780	0.0085	0.6	0.0041	13.2	9.0	15.9	3.7	−1.0	2.2	0.5	0.1	0.2	6.3	2.8	2.9	0.0	−0.7	−0.9	1.7
15.3	0.1780	0.0160	0.2	0.0312	6.2	8.3	10.4	0.0	0.4	1.8	3.1	0.1	−2.2	4.4	5.0	0.6	0.3	−1.1	−1.7	1.6
15.3	0.1780	0.0160	0.4	0.0101	8.4	8.3	11.8	0.0	0.3	3.7	2.6	0.2	1.1	3.2	5.2	−1.9	0.2	−1.0	−1.9	1.6
15.3	0.1780	0.0160	0.6	0.0036	16.2	8.3	18.2	0.0	−0.8	2.3	0.8	0.1	0.6	0.8	7.6	0.7	0.1	−0.4	−0.8	1.6
15.3	0.1780	0.0250	0.2	0.0320	8.6	7.8	11.6	0.0	−0.3	2.5	2.9	0.2	−1.6	1.9	5.9	0.6	0.0	−0.8	−0.8	1.6
15.3	0.1780	0.0250	0.4	0.0094	11.7	7.8	14.1	0.0	−0.8	4.7	4.7	0.1	2.0	−0.7	−1.4	1.4	0.0	−1.5	−1.5	1.6
15.3	0.1780	0.0250	0.6	0.0034	26.0	7.8	27.2	0.0	−2.2	3.9	3.1	0.2	1.2	−0.1	2.6	−4.1	0.6	−0.9	−1.2	1.6
15.3	0.5620	0.0025	0.2	0.0682	3.0	10.3	10.7	6.5	−1.3	3.2	0.8	−1.7	−1.9	−2.0	4.7	−0.1	0.4	−0.9	−1.6	3.8
15.3	0.5620	0.0025	0.4	0.0184	4.2	10.3	11.1	5.2	−1.2	1.3	0.9	−1.0	1.0	−2.0	6.9	1.8	0.2	−0.8	−1.7	3.8
15.3	0.5620	0.0025	0.6	0.0051	9.7	10.3	14.1	4.5	−1.2	1.0	1.1	−2.0	0.3	−2.9	5.2	4.8	0.2	−0.8	−2.3	3.8
15.3	0.5620	0.0085	0.2	0.0609	4.0	10.2	10.9	3.8	1.1	1.0	1.4	0.5	−0.7	8.4	2.2	0.0	−0.1	−0.5	0.0	2.7
15.3	0.5620	0.0085	0.4	0.0188	5.3	10.2	11.4	6.3	−1.3	0.0	1.2	0.5	0.4	6.8	2.4	0.2	−0.2	−0.5	0.0	2.7
15.3	0.5620	0.0085	0.6	0.0062	11.1	10.2	15.0	3.1	2.0	1.2	−0.7	0.7	0.7	6.4	1.8	5.8	−0.4	−0.5	0.0	2.7

Q^2 [GeV^2]	β	$x_{I\!P}$	$-t$ [GeV^2]	$x_{I\!P}\sigma_r^{D(4)}$ [GeV^{-2}]	δ_{stat} [%]	δ_{sys} [%]	δ_{tot} [%]	δ_{had} [%]	δ_{ele} [%]	δ_{θ} [%]	δ_{β} [%]	$\delta_{x_{I\!P}}$ [%]	δ_t [%]	δ_{E_p} [%]	δ_{p_x} [%]	δ_{p_y} [%]	δ_{Q^2} [%]	δ_{vtx} [%]	δ_{bgn} [%]	δ_{bcc} [%]
26.5	0.0056	0.0750	0.2	0.1363	29.5	7.3	30.4	0.0	−0.4	2.1	−1.5	0.3	−2.5	0.6	5.3	−0.2	0.5	−0.6	−2.6	2.1
26.5	0.0056	0.0750	0.4	0.0307	33.9	7.3	34.7	0.0	−2.0	5.4	−1.0	0.1	0.9	0.4	0.9	1.6	0.7	−0.9	−3.1	2.1
26.5	0.0056	0.0750	0.6	0.0188	39.8	7.3	40.5	0.0	−0.1	0.8	−0.8	0.1	0.0	1.2	6.3	1.8	0.3	−0.6	−1.9	2.1
26.5	0.0178	0.0250	0.2	0.0574	12.4	7.6	14.6	0.5	0.1	2.5	−1.4	−0.1	−2.6	4.1	3.9	0.6	1.3	−1.1	−1.9	1.9
26.5	0.0178	0.0250	0.4	0.0200	15.1	7.6	16.9	0.2	−0.9	2.7	−1.3	0.0	1.3	1.7	6.0	0.9	0.6	−0.9	−1.5	1.9
26.5	0.0178	0.0250	0.6	0.0074	29.9	7.6	30.9	0.0	3.1	0.3	−1.1	−0.1	−0.2	2.9	5.8	−1.1	0.5	−0.4	−0.8	1.9
26.5	0.0178	0.0350	0.2	0.0709	11.9	7.1	13.8	0.0	1.9	0.7	−1.2	−0.1	−1.9	0.8	5.9	0.7	0.5	−1.0	−0.4	1.6
26.5	0.0178	0.0350	0.4	0.0195	17.8	7.1	19.2	0.1	0.3	0.2	−0.9	0.0	0.9	0.9	5.6	3.4	0.6	−0.7	−0.4	1.6
26.5	0.0178	0.0350	0.6	0.0052	31.8	7.1	32.5	0.0	1.1	3.7	0.0	0.1	−0.4	−0.6	−5.4	−1.1	0.7	−0.6	−0.4	1.6
26.5	0.0178	0.0500	0.2	0.0758	11.4	7.4	13.6	0.0	−0.8	2.2	−1.1	0.1	−1.8	0.1	6.2	1.4	0.1	−0.8	−0.3	1.6
26.5	0.0178	0.0500	0.4	0.0307	13.4	7.4	15.3	0.1	1.0	5.9	−1.1	0.0	1.1	0.5	3.3	−0.4	0.6	−0.9	−0.4	1.6
26.5	0.0178	0.0500	0.6	0.0133	19.9	7.4	21.2	0.0	0.2	2.0	−0.2	0.0	−0.8	2.6	−5.7	2.6	0.3	−0.6	−0.3	1.6
26.5	0.0178	0.0750	0.2	0.0810	19.3	8.1	20.9	0.0	−0.9	4.0	−0.9	0.2	−2.6	1.4	5.4	1.5	0.2	−0.9	−2.2	1.6
26.5	0.0178	0.0750	0.4	0.0295	22.6	8.1	24.0	0.0	−0.4	0.4	−1.2	−0.1	−0.4	−1.2	6.6	0.5	0.8	−1.5	−3.5	1.6
26.5	0.0178	0.0750	0.6	0.0132	33.4	8.1	34.4	0.0	2.5	−0.1	−0.4	0.5	0.0	1.2	6.8	0.6	0.8	−1.1	−2.7	1.6
26.5	0.0562	0.0085	0.2	0.0503	9.7	8.6	13.0	−6.7	−0.6	0.9	−1.4	0.0	−1.1	−1.4	2.6	0.2	0.3	−0.7	−3.5	1.9
26.5	0.0562	0.0085	0.4	0.0157	13.0	8.6	15.6	−4.1	0.0	0.1	−0.9	−0.1	0.5	−2.4	6.1	−0.3	0.4	−0.4	−2.9	1.9
26.5	0.0562	0.0085	0.6	0.0058	33.8	8.6	34.9	−4.5	−1.0	2.0	−0.8	0.1	1.2	0.5	−3.8	−0.2	0.2	−0.6	−5.2	1.9
26.5	0.0562	0.0160	0.2	0.0505	7.0	8.2	10.7	0.2	0.3	1.5	−0.4	0.0	−1.7	2.8	6.9	0.4	0.3	−1.0	−1.2	1.6
26.5	0.0562	0.0160	0.4	0.0144	9.9	8.2	12.9	0.0	−0.4	5.5	−0.4	0.0	2.1	1.6	4.6	0.6	0.8	−1.2	−1.8	1.6
26.5	0.0562	0.0160	0.6	0.0046	18.6	8.2	20.3	0.0	0.7	0.2	0.5	−0.2	0.6	−1.4	−5.1	−5.7	0.2	−0.7	−1.3	1.6
26.5	0.0562	0.0250	0.2	0.0428	9.0	7.4	11.7	0.2	0.3	2.4	−0.6	0.0	−1.4	0.7	6.5	0.2	0.4	−1.1	−0.9	1.6
26.5	0.0562	0.0250	0.4	0.0142	12.0	7.4	14.1	0.0	−0.2	2.8	−0.7	0.1	1.0	5.8	0.6	−0.9	0.5	−2.0	−2.2	1.6
26.5	0.0562	0.0250	0.6	0.0048	24.2	7.4	25.4	0.0	−4.9	0.5	−1.1	−0.2	0.6	−0.5	3.9	3.2	0.5	−0.6	−0.8	1.6
26.5	0.0562	0.0350	0.2	0.0523	10.4	7.2	12.6	0.9	−1.6	3.0	−0.3	0.0	−4.4	0.7	3.2	1.0	0.7	−2.0	−0.3	1.6
26.5	0.0562	0.0350	0.4	0.0165	14.0	7.2	15.8	0.0	1.1	2.1	−0.1	0.0	0.4	0.4	6.4	0.9	0.0	−0.3	−0.1	1.6
26.5	0.0562	0.0350	0.6	0.0052	24.9	7.2	26.0	0.0	−0.2	4.1	−3.3	0.1	−1.1	−2.9	2.8	0.4	−1.2	−1.3	−0.3	1.6
26.5	0.0562	0.0500	0.2	0.0622	10.6	7.4	12.9	0.0	2.1	−1.4	−0.5	0.1	−2.3	1.6	6.1	0.9	0.1	−0.9	−0.5	1.6
26.5	0.0562	0.0500	0.4	0.0174	15.1	7.4	16.8	0.0	−0.9	6.6	−0.5	0.1	1.3	1.0	1.6	1.3	0.4	−1.0	−0.6	1.6
26.5	0.0562	0.0500	0.6	0.0077	28.9	7.4	29.8	0.0	0.3	−1.4	0.2	−0.2	1.0	1.2	4.7	5.0	0.5	−0.7	−0.5	1.6
26.5	0.0562	0.0750	0.2	0.0821	19.0	6.8	20.1	0.0	−0.7	−0.4	−1.0	0.2	−3.4	−0.3	4.5	1.0	0.3	−0.8	−2.8	1.6
26.5	0.0562	0.0750	0.4	0.0225	21.8	6.8	22.8	0.0	0.1	−1.1	−0.9	0.0	0.5	0.6	2.3	4.0	0.2	−1.4	−4.2	1.6
26.5	0.0562	0.0750	0.6	0.0063	40.5	6.8	41.1	0.0	−2.6	0.9	−1.1	0.4	−0.9	−2.1	3.7	−1.7	0.6	−1.1	−3.2	1.6
26.5	0.1780	0.0025	0.2	0.0485	7.5	9.3	12.0	−1.9	−0.3	1.6	−0.4	−0.6	−1.6	−6.0	4.3	0.1	0.3	−0.8	−4.2	2.2
26.5	0.1780	0.0025	0.4	0.0115	11.3	9.3	14.7	−2.5	−0.2	1.4	−0.6	−0.5	0.9	−5.1	4.4	0.6	0.1	−0.8	−5.0	2.2
26.5	0.1780	0.0025	0.6	0.0059	17.1	9.3	19.4	−0.1	−0.6	−0.6	−0.1	−0.5	−0.2	−5.1	4.7	3.2	0.2	−0.6	−4.7	2.2
26.5	0.1780	0.0085	0.2	0.0448	6.6	8.5	10.8	1.9	−0.3	1.6	0.1	−0.1	−1.4	6.0	4.7	−0.1	0.4	−0.8	−1.3	1.7
26.5	0.1780	0.0085	0.4	0.0128	9.3	8.5	12.6	−0.3	0.0	1.7	0.5	−0.2	1.4	5.4	5.3	1.3	0.6	−1.1	−2.0	1.7
26.5	0.1780	0.0085	0.6	0.0047	18.8	8.5	20.6	1.4	1.3	−1.5	−0.2	−0.1	−1.3	7.4	1.2	0.4	−0.3	−0.9	−2.0	1.7
26.5	0.1780	0.0160	0.2	0.0379	7.4	8.1	11.0	0.0	−0.1	1.4	0.6	0.0	−2.6	3.3	6.2	−0.8	0.3	−1.3	−1.3	1.6
26.5	0.1780	0.0160	0.4	0.0121	10.0	8.1	12.8	0.0	−0.4	1.3	0.3	0.1	1.4	3.1	5.0	4.5	0.2	−1.1	−1.4	1.6
26.5	0.1780	0.0160	0.6	0.0037	19.0	8.1	20.7	0.0	3.0	−4.5	0.6	0.0	−0.1	3.9	3.2	−2.2	−0.1	−0.9	−1.3	1.6
26.5	0.1780	0.0250	0.2	0.0298	10.1	7.0	12.3	0.0	0.2	0.4	1.6	0.1	−2.0	1.6	6.0	0.1	0.2	−0.9	−1.0	1.6
26.5	0.1780	0.0250	0.4	0.0092	13.4	7.0	15.2	0.0	−0.6	1.2	0.8	−0.1	0.5	1.1	6.4	0.9	0.1	−0.5	−0.6	1.6
26.5	0.1780	0.0250	0.6	0.0034	25.8	7.0	26.8	0.0	−1.1	2.2	0.9	0.0	−0.2	−1.7	−3.7	4.8	0.2	−0.4	−0.6	1.6
26.5	0.1780	0.0350	0.2	0.0287	15.4	7.8	17.3	0.0	−1.7	3.0	3.6	0.2	−3.1	3.0	3.2	0.9	0.1	−1.7	−0.9	1.6
26.5	0.1780	0.0350	0.4	0.0110	16.5	7.8	18.2	0.0	−2.8	0.9	1.6	0.1	0.5	−0.3	6.8	0.1	0.5	−0.5	−0.4	1.6
26.5	0.1780	0.0350	0.6	0.0083	28.1	7.8	29.1	0.0	1.8	4.8	2.2	0.1	−0.9	4.7	1.2	−1.6	−0.1	−0.7	−0.5	1.6

Q^2 [GeV^2]	β	$x_{I\!P}$	$-t$ [GeV^2]	$x_{I\!P}\sigma_r^{D(4)}$ [GeV^{-2}]	δ_{stat} [%]	δ_{sys} [%]	δ_{tot} [%]	δ_{had} [%]	δ_{ele} [%]	δ_{θ} [%]	δ_{β} [%]	$\delta_{x_{I\!P}}$ [%]	δ_t [%]	δ_{E_p} [%]	δ_{p_x} [%]	δ_{p_y} [%]	δ_{Q^2} [%]	δ_{vtx} [%]	δ_{bgn} [%]	δ_{bcc} [%]
26.5	0.5620	0.0025	0.2	0.0711	4.6	10.4	11.3	5.4	−1.5	2.4	0.5	−1.3	−1.9	−3.3	6.0	0.2	0.3	−0.9	−2.2	3.4
26.5	0.5620	0.0025	0.4	0.0215	6.2	10.4	12.1	6.0	−0.8	1.0	1.2	−1.2	1.0	−4.7	4.4	1.5	0.4	−1.0	−3.0	3.4
26.5	0.5620	0.0025	0.6	0.0059	13.1	10.4	16.7	4.6	−1.1	2.4	0.6	−0.6	0.0	−1.8	7.2	2.2	0.2	−0.7	−2.6	3.4
26.5	0.5620	0.0085	0.2	0.0534	5.2	9.5	10.9	5.7	−0.5	1.4	0.9	0.0	−1.3	6.1	2.9	−0.1	0.1	−0.7	−0.3	2.8
26.5	0.5620	0.0085	0.4	0.0144	7.4	9.5	12.1	5.6	−0.6	1.3	0.7	0.1	0.6	4.9	5.0	0.2	0.0	−0.5	−0.3	2.8
26.5	0.5620	0.0085	0.6	0.0062	13.3	9.5	16.4	0.2	0.0	0.1	1.0	−0.4	−0.3	5.2	−5.1	5.3	0.1	−0.9	−0.5	2.8
46.0	0.0178	0.0500	0.2	0.0962	19.3	7.5	20.7	−0.6	−0.3	2.6	−2.0	0.1	−2.8	1.3	5.3	0.4	1.4	−1.3	−0.3	1.7
46.0	0.0178	0.0500	0.4	0.0481	20.4	7.5	21.7	0.0	0.2	0.2	−1.0	0.0	0.6	1.0	6.9	1.8	−0.3	−0.5	−0.1	1.7
46.0	0.0178	0.0500	0.6	0.0132	41.9	7.5	42.5	0.0	0.3	6.3	−0.2	−0.1	0.3	2.0	0.5	2.5	1.2	−0.8	−0.2	1.7
46.0	0.0178	0.0750	0.2	0.0611	36.1	7.2	36.8	0.3	0.5	3.2	−1.0	0.2	−2.7	−0.8	4.8	1.0	0.3	−0.7	−2.2	1.6
46.0	0.0178	0.0750	0.4	0.0282	32.8	7.2	33.6	0.5	0.7	0.9	−2.9	−0.2	−0.3	−1.8	1.3	5.0	0.8	−0.8	−2.7	1.6
46.0	0.0178	0.0750	0.6	0.0206	51.8	7.2	52.3	0.1	−0.3	−0.3	−0.1	0.0	−0.5	−1.8	5.8	−3.0	0.4	−0.4	−1.5	1.6
46.0	0.0562	0.0160	0.2	0.0493	14.5	8.2	16.6	0.1	−0.8	2.1	−1.2	0.0	−2.7	3.4	6.1	0.6	0.6	−0.9	−0.8	1.7
46.0	0.0562	0.0160	0.4	0.0193	17.6	8.2	19.4	0.0	1.6	0.9	−1.1	0.0	0.9	3.3	6.7	1.2	0.3	−0.6	−0.6	1.7
46.0	0.0562	0.0160	0.6	0.0085	29.5	8.2	30.6	−0.1	−2.4	3.0	−3.5	0.1	0.7	−0.7	0.2	−5.6	1.1	−1.0	−1.4	1.7
46.0	0.0562	0.0250	0.2	0.0581	11.7	7.7	14.0	0.1	0.8	1.0	−1.3	−0.1	−1.1	−0.9	7.1	0.5	0.1	−0.8	−0.5	1.6
46.0	0.0562	0.0250	0.4	0.0178	16.8	7.7	18.5	0.0	−1.1	3.8	−1.5	0.1	2.0	−0.7	5.7	0.7	0.9	−0.9	−0.6	1.6
46.0	0.0562	0.0250	0.6	0.0042	39.1	7.7	39.8	0.0	−0.1	0.1	−1.2	0.0	−0.1	−2.3	5.4	−3.9	0.0	−1.9	−1.5	1.6
46.0	0.0562	0.0350	0.2	0.0576	14.9	7.2	16.6	0.3	−0.3	1.7	−0.1	0.1	−1.1	3.2	5.8	0.8	0.2	−0.7	−0.7	1.6
46.0	0.0562	0.0350	0.4	0.0159	21.2	7.2	22.4	0.1	−3.9	1.3	−0.6	−0.2	0.9	−3.2	2.9	0.8	0.6	−2.2	−2.7	1.6
46.0	0.0562	0.0350	0.6	0.0057	31.9	7.2	32.7	0.0	1.7	−1.8	1.1	0.2	0.9	5.1	3.3	0.6	0.7	−1.0	−1.8	1.6
46.0	0.0562	0.0500	0.2	0.0605	14.6	7.1	16.2	0.0	−1.3	3.3	−1.0	0.0	−2.4	−0.2	5.1	0.2	0.3	−1.3	−0.3	1.6
46.0	0.0562	0.0500	0.4	0.0234	17.3	7.1	18.7	0.0	0.9	−0.7	−0.2	0.1	1.2	−0.3	5.5	3.8	0.0	−1.0	−0.3	1.6
46.0	0.0562	0.0500	0.6	0.0134	24.4	7.1	25.4	0.0	−0.6	0.4	0.1	0.0	−0.1	−1.6	5.9	−3.0	0.3	−0.8	−0.2	1.6
46.0	0.0562	0.0750	0.2	0.0792	25.1	6.9	26.0	0.0	−0.5	2.6	−1.3	0.2	−3.1	0.5	4.4	0.0	0.5	−0.8	−2.3	1.6
46.0	0.0562	0.0750	0.4	0.0396	24.2	6.9	25.1	0.0	−0.9	3.9	−0.3	0.1	−0.5	0.4	3.4	3.6	0.1	−0.7	−1.9	1.6
46.0	0.0562	0.0750	0.6	0.0162	49.1	6.9	49.6	0.0	−1.4	−4.0	−0.3	−0.1	−1.5	−1.4	4.1	−2.1	0.0	−0.5	−1.3	1.6
46.0	0.1780	0.0085	0.2	0.0447	11.1	9.4	14.5	0.0	−1.2	3.0	−1.0	−0.2	−2.5	5.3	5.1	0.2	0.4	−1.3	−3.4	1.7
46.0	0.1780	0.0085	0.4	0.0127	14.7	9.4	17.4	0.2	−0.8	1.7	−0.3	0.2	0.9	5.4	6.5	0.2	0.5	−0.9	−2.8	1.7
46.0	0.1780	0.0085	0.6	0.0047	32.0	9.4	33.4	1.2	−1.8	2.6	−0.7	−0.1	0.8	0.6	7.7	2.6	0.1	−0.6	−2.3	1.7
46.0	0.1780	0.0160	0.2	0.0409	10.0	7.9	12.7	0.4	0.1	0.2	−0.3	0.0	−1.9	4.2	5.9	0.2	0.2	−1.0	−1.3	1.6
46.0	0.1780	0.0160	0.4	0.0146	12.7	7.9	14.9	0.6	−1.2	2.6	0.2	−0.1	1.6	1.1	6.2	1.8	0.0	−1.2	−2.0	1.6
46.0	0.1780	0.0160	0.6	0.0068	24.5	7.9	25.8	0.0	−2.7	5.7	−0.4	−0.4	0.0	−1.3	1.9	−3.1	0.4	−0.8	−1.9	1.6
46.0	0.1780	0.0250	0.2	0.0492	11.7	7.6	14.0	0.0	−0.5	1.9	−0.5	0.1	−1.9	2.2	6.3	0.4	0.2	−1.0	−1.1	1.6
46.0	0.1780	0.0250	0.4	0.0116	16.7	7.6	18.3	0.0	1.2	−1.7	0.4	0.0	1.2	5.5	2.7	−1.9	0.2	−1.8	−2.2	1.6
46.0	0.1780	0.0250	0.6	0.0031	36.6	7.6	37.4	0.0	0.0	0.0	0.1	−0.2	−0.6	5.4	2.9	3.7	−0.4	−0.9	−1.6	1.6
46.0	0.1780	0.0350	0.2	0.0445	14.4	7.3	16.2	0.0	−0.8	1.9	−0.1	0.2	−1.7	2.5	6.1	0.6	0.1	−0.9	−0.3	1.6
46.0	0.1780	0.0350	0.4	0.0121	22.1	7.3	23.2	0.0	3.5	4.8	0.3	0.2	1.1	−1.5	3.0	0.9	0.6	−1.4	−0.5	1.6
46.0	0.1780	0.0350	0.6	0.0070	40.9	7.3	41.5	0.0	0.0	0.0	1.9	0.1	0.4	−5.8	2.2	2.9	−0.1	−0.7	−0.4	1.6
46.0	0.1780	0.0500	0.2	0.0407	16.8	8.2	18.7	0.0	−0.7	6.0	1.0	0.3	−4.3	−0.1	2.8	0.2	0.2	−1.4	−0.4	1.6
46.0	0.1780	0.0500	0.4	0.0167	20.9	8.2	22.4	0.0	3.2	4.1	0.9	0.1	0.7	0.2	5.4	2.4	−0.2	−1.5	−0.4	1.6
46.0	0.1780	0.0500	0.6	0.0116	31.0	8.2	32.0	0.0	1.9	0.0	1.3	0.4	0.5	6.3	3.5	2.4	0.2	−0.9	−0.4	1.6
46.0	0.1780	0.0750	0.2	0.0903	37.8	7.3	38.4	0.0	−2.6	0.9	−2.4	0.1	−3.3	−1.8	−3.7	−0.9	−0.1	−1.4	−2.5	1.6
46.0	0.1780	0.0750	0.4	0.0254	40.7	7.3	41.3	0.0	0.1	−0.3	1.0	0.1	−0.2	−0.1	6.7	1.4	−0.1	−0.5	−1.2	1.6
46.0	0.1780	0.0750	0.6	0.0288	39.7	7.3	40.3	0.0	−1.3	−0.1	2.0	−0.2	−1.2	0.7	4.9	3.7	−0.5	−0.7	−2.1	1.6
46.0	0.5620	0.0025	0.2	0.0777	7.6	10.9	13.3	6.0	−1.6	1.8	0.4	−1.3	−1.6	−4.9	5.0	0.4	0.3	−0.9	−2.8	3.9
46.0	0.5620	0.0025	0.4	0.0230	10.5	10.9	15.1	4.3	−2.6	3.7	0.5	−0.7	0.9	−5.7	4.6	0.0	0.4	−0.8	−2.9	3.9
46.0	0.5620	0.0025	0.6	0.0089	19.6	10.9	22.5	6.6	−0.7	0.0	−0.2	−1.5	0.3	−6.3	−1.1	2.9	−0.1	−0.6	−2.7	3.9

Q^2 [GeV^2]	β	$x_{I\!P}$	$-t$ [GeV^2]	$x_{I\!P}\sigma_r^{D(4)}$ [GeV^{-2}]	δ_{stat} [%]	δ_{sys} [%]	δ_{tot} [%]	δ_{had} [%]	δ_{ele} [%]	δ_θ [%]	δ_β [%]	$\delta_{x_{I\!P}}$ [%]	δ_t [%]	δ_{E_p} [%]	δ_{p_x} [%]	δ_{p_y} [%]	δ_{Q^2} [%]	δ_{vtx} [%]	δ_{bgn} [%]	δ_{bcc} [%]
46.0	0.5620	0.0085	0.2	0.0490	7.9	9.8	12.6	6.2	−0.8	1.3	0.6	−0.2	−1.7	4.9	4.0	0.5	0.1	−0.7	−0.9	3.3
46.0	0.5620	0.0085	0.4	0.0160	10.3	9.8	14.2	6.7	−1.1	2.6	0.6	−0.1	0.8	5.0	1.8	−1.3	0.1	−0.6	−0.9	3.3
46.0	0.5620	0.0085	0.6	0.0066	17.8	9.8	20.3	1.9	−1.1	1.6	0.8	0.0	1.4	5.9	4.9	3.8	0.0	−0.4	−1.0	3.3
46.0	0.5620	0.0160	0.2	0.0384	12.5	8.6	15.2	0.0	−1.0	6.0	1.1	0.2	−1.9	−2.3	3.3	0.1	0.0	−1.4	−1.9	3.2
46.0	0.5620	0.0160	0.4	0.0177	14.6	8.6	17.0	0.0	−3.2	1.9	2.4	0.4	2.3	0.8	5.6	−0.4	0.2	−1.1	−2.3	3.2
46.0	0.5620	0.0160	0.6	0.0036	39.6	8.6	40.5	0.0	−4.1	0.0	2.2	0.1	−0.3	2.1	4.7	2.6	0.6	−1.3	−2.5	3.2
46.0	0.5620	0.0250	0.2	0.0343	20.0	7.7	21.5	0.0	−2.1	−3.9	2.9	0.0	−1.3	−0.5	3.2	2.7	−0.9	−1.1	−0.5	3.1
46.0	0.5620	0.0250	0.4	0.0102	26.8	7.7	27.9	0.0	3.0	5.6	0.6	0.1	0.9	−1.4	1.9	−1.4	−0.2	−0.7	−0.3	3.1
46.0	0.5620	0.0250	0.6	0.0066	48.3	7.7	48.9	0.0	0.0	0.0	1.7	0.5	0.7	5.9	−3.0	−1.1	−0.4	−0.7	−0.5	3.1
80.0	0.0562	0.0350	0.2	0.0660	29.0	8.1	30.1	0.1	−0.5	0.7	−3.1	0.0	−3.3	0.1	5.6	2.2	1.7	−0.8	−1.7	1.6
80.0	0.0562	0.0350	0.4	0.0258	36.9	8.1	37.8	0.8	1.7	0.1	−0.1	−0.2	1.4	1.3	6.3	−3.4	1.0	−0.5	−1.6	1.6
80.0	0.0562	0.0350	0.6	0.0182	71.6	8.1	72.0	0.0	−3.8	3.6	−0.3	0.0	0.1	3.9	−3.5	−2.8	0.0	−0.1	−0.4	1.6
80.0	0.0562	0.0500	0.2	0.0613	22.2	7.1	23.3	0.0	−0.7	2.6	−0.8	0.0	−1.9	−0.4	5.9	−0.2	1.0	−0.8	0.0	1.6
80.0	0.0562	0.0500	0.4	0.0339	27.4	7.1	28.3	0.0	−0.2	1.0	−2.0	0.0	0.6	1.5	−4.1	4.7	0.9	−0.8	0.0	1.6
80.0	0.0562	0.0500	0.6	0.0164	59.0	7.1	59.4	0.0	−0.1	0.0	−1.5	0.0	0.8	1.2	6.6	0.2	0.1	−0.4	0.0	1.6
80.0	0.0562	0.0750	0.2	0.0668	40.2	7.6	40.9	0.0	0.3	−0.2	−0.5	0.2	−1.3	1.0	6.8	1.7	0.2	−0.7	−1.5	1.6
80.0	0.0562	0.0750	0.4	0.0269	37.4	7.6	38.2	0.0	2.0	0.0	−3.5	−0.1	2.5	−2.0	1.0	2.1	0.2	−1.8	−4.3	1.6
80.0	0.0562	0.0750	0.6	0.0159	68.9	7.6	69.3	0.0	−0.5	4.9	0.0	−0.1	0.4	−0.2	−5.3	1.1	0.1	−0.5	−1.0	1.6
80.0	0.1780	0.0085	0.2	0.0642	20.7	8.8	22.5	−2.9	−1.6	2.8	−2.5	0.0	−1.7	−1.9	3.3	−1.2	0.6	−1.1	−5.3	1.9
80.0	0.1780	0.0085	0.4	0.0252	23.1	8.8	24.8	−0.9	−0.1	0.9	−0.9	−0.2	0.6	−0.3	7.7	0.3	0.3	−0.5	−3.3	1.9
80.0	0.1780	0.0085	0.6	0.0098	54.3	8.8	55.0	0.0	0.0	0.0	0.1	0.4	0.7	4.7	2.1	6.3	0.2	−0.1	−2.6	1.9
80.0	0.1780	0.0160	0.2	0.0352	17.4	8.1	19.2	0.0	−0.1	3.9	−0.9	0.0	−2.8	5.2	2.8	0.3	0.5	−1.3	−1.7	1.6
80.0	0.1780	0.0160	0.4	0.0120	22.1	8.1	23.5	0.0	0.7	0.2	0.1	0.0	0.6	2.2	7.6	0.0	0.1	−0.4	−0.6	1.6
80.0	0.1780	0.0160	0.6	0.0156	42.5	8.1	43.2	0.0	0.0	0.0	−0.1	−0.1	−2.2	3.6	4.8	4.4	0.5	−0.8	−1.4	1.6
80.0	0.1780	0.0250	0.2	0.0402	16.6	7.9	18.4	0.0	−0.1	2.2	−0.6	0.1	−2.7	0.6	6.6	−0.2	0.5	−1.6	−1.1	1.6
80.0	0.1780	0.0250	0.4	0.0159	20.7	7.9	22.2	0.0	0.4	0.3	−1.5	0.0	0.1	−0.1	5.6	4.7	0.5	−1.6	−1.5	1.6
80.0	0.1780	0.0250	0.6	0.0121	42.2	7.9	42.9	0.0	3.9	−5.9	−2.2	−0.3	−0.4	0.6	−1.9	−0.1	0.4	−0.6	−0.8	1.6
80.0	0.1780	0.0350	0.2	0.0608	20.3	7.2	21.6	0.0	0.2	−0.3	−4.0	0.1	−1.4	3.2	4.3	0.3	0.2	−0.6	−0.5	1.6
80.0	0.1780	0.0350	0.4	0.0122	30.9	7.2	31.8	0.0	0.2	0.0	−1.7	0.1	−0.1	5.8	−2.4	1.1	0.4	−1.4	−1.7	1.6
80.0	0.1780	0.0350	0.6	0.0065	39.5	7.2	40.1	0.0	2.8	0.0	−0.1	0.0	−0.2	−4.8	2.6	−3.3	0.3	−0.5	−0.5	1.6
80.0	0.1780	0.0500	0.2	0.0440	24.9	7.0	25.9	0.0	−1.1	1.0	−0.4	−0.2	−4.2	−0.4	4.6	0.1	0.4	−1.8	−1.0	1.6
80.0	0.1780	0.0500	0.4	0.0226	24.4	7.0	25.4	0.0	−0.2	0.2	−0.2	0.1	0.2	−3.1	1.1	5.7	0.3	−1.0	−0.9	1.6
80.0	0.1780	0.0500	0.6	0.0058	44.6	7.0	45.2	0.0	0.0	−0.1	−0.5	0.1	0.6	5.8	−1.3	−3.0	−0.2	−0.3	−0.4	1.6
80.0	0.1780	0.0750	0.2	0.0570	44.2	7.1	44.7	0.0	−1.1	2.1	0.2	0.2	−3.6	−2.2	3.0	0.6	−0.2	−1.4	−3.5	1.6
80.0	0.1780	0.0750	0.4	0.0134	49.7	7.1	50.2	0.0	−1.9	1.6	1.9	0.2	0.0	4.4	3.1	−1.0	0.2	−0.9	−2.7	1.6
80.0	0.1780	0.0750	0.6	0.0231	51.1	7.1	51.6	0.0	0.3	0.1	0.8	0.0	−0.1	−2.0	5.4	3.5	0.2	−0.2	−0.9	1.6
80.0	0.5620	0.0085	0.2	0.0464	13.4	10.6	17.1	5.2	−1.0	0.8	0.5	−0.3	−2.0	4.2	6.3	−0.2	0.3	−1.2	−2.9	3.4
80.0	0.5620	0.0085	0.4	0.0111	19.7	10.6	22.4	6.4	−0.6	2.9	−0.2	0.3	0.8	2.8	−0.8	2.8	1.0	−1.8	−5.5	3.4
80.0	0.5620	0.0085	0.6	0.0040	42.8	10.6	44.1	0.0	0.0	0.0	0.8	0.0	−0.3	6.3	6.7	3.6	0.4	−0.5	−1.4	3.4
80.0	0.5620	0.0160	0.2	0.0290	18.4	9.5	20.7	0.0	−3.7	1.8	0.4	0.2	−2.8	−2.4	3.8	1.2	0.2	−0.7	−5.7	3.3
80.0	0.5620	0.0160	0.4	0.0094	24.9	9.5	26.6	0.0	−3.4	−2.5	1.0	0.2	0.4	−1.6	6.0	−3.7	0.2	−0.3	−2.8	3.3
80.0	0.5620	0.0160	0.6	0.0088	35.3	9.5	36.6	0.0	0.0	0.0	−0.7	0.1	0.1	−3.5	6.4	4.5	0.0	−0.2	−2.4	3.3
80.0	0.5620	0.0250	0.2	0.0362	26.1	8.3	27.4	0.0	−3.5	3.6	1.8	0.1	−2.1	−0.5	4.4	−1.9	0.3	−1.2	−1.2	3.1
80.0	0.5620	0.0250	0.4	0.0133	21.1	8.3	22.7	0.0	−3.5	0.0	0.9	0.5	1.7	−3.9	−0.7	4.2	0.7	−2.1	−2.3	3.1
80.0	0.5620	0.0350	0.2	0.0332	49.6	10.1	50.6	0.0	−1.0	1.0	3.9	0.3	−1.4	−1.9	8.2	−0.6	0.0	−1.6	−0.3	3.0
80.0	0.5620	0.0350	0.4	0.0163	28.6	10.1	30.4	0.0	−4.9	−1.0	1.0	−0.1	1.1	−4.6	5.1	4.3	−0.5	−0.2	−0.1	3.0

Q^2 [GeV^2]	β	$x_{I\!P}$	$x_{I\!P}\sigma_r^{D(3)}$	δ_{stat} [%]	δ_{sys} [%]	δ_{tot} [%]	δ_{had} [%]	δ_{ele} [%]	δ_θ [%]	δ_β [%]	$\delta_{x_{I\!P}}$ [%]	δ_t [%]	δ_{E_p} [%]	δ_{p_x} [%]	δ_{p_y} [%]	δ_{Q^2} [%]	δ_{vtx} [%]	δ_{bgn} [%]	δ_{bcc} [%]
5.1	0.0018	0.0500	0.0340	5.9	8.5	10.3	−0.2	4.2	0.7	−0.9	0.0	−2.8	1.1	5.0	2.9	1.5	−2.4	−1.1	1.0
5.1	0.0018	0.0750	0.0352	6.7	7.1	9.8	−0.1	1.1	2.7	−0.4	0.1	−3.1	0.8	4.7	2.1	1.0	−0.9	−1.7	0.3
5.1	0.0056	0.0160	0.0217	4.1	9.4	10.2	−0.5	2.8	3.1	−0.9	−0.1	1.1	3.0	6.4	1.3	1.9	−3.0	−1.6	1.2
5.1	0.0056	0.0250	0.0220	3.6	8.2	9.0	0.0	2.2	3.5	−0.4	0.0	0.2	1.5	6.3	1.5	1.7	−1.5	−0.7	0.5
5.1	0.0056	0.0350	0.0237	4.2	7.2	8.3	−0.3	1.2	3.7	0.0	0.1	0.1	2.2	5.0	2.2	1.2	−0.8	−0.3	0.3
5.1	0.0056	0.0500	0.0253	4.3	8.8	9.8	0.0	−1.0	6.9	−0.2	0.1	−1.1	0.3	4.1	2.9	1.4	−0.8	−0.4	0.2
5.1	0.0056	0.0750	0.0312	6.4	10.2	12.0	0.0	−0.6	7.3	−0.6	0.2	−3.7	−0.1	4.1	3.7	1.2	−0.8	−2.0	0.2
5.1	0.0178	0.0085	0.0174	2.9	10.4	10.8	−6.7	2.0	4.2	−0.7	−0.1	0.6	1.1	5.2	0.9	1.3	−1.3	−2.7	1.1
5.1	0.0178	0.0160	0.0188	2.7	9.0	9.4	0.2	0.2	5.6	0.1	0.1	0.8	4.3	5.1	1.3	1.1	−0.9	−1.2	0.3
5.1	0.0178	0.0250	0.0182	3.3	8.7	9.3	0.0	0.7	6.4	−0.1	0.0	1.3	0.7	5.2	1.7	1.1	−1.2	−0.5	0.3
5.1	0.0178	0.0350	0.0174	4.6	8.5	9.7	0.0	0.5	7.0	−0.4	0.1	0.6	1.2	3.9	2.1	0.6	−1.1	−0.4	0.3
5.1	0.0178	0.0500	0.0221	5.0	8.6	10.0	0.0	0.8	6.5	−0.6	0.1	−1.7	1.3	3.8	3.1	0.2	−1.3	−0.3	0.2
5.1	0.0178	0.0750	0.0252	8.3	8.0	11.6	0.0	0.4	4.3	−0.4	0.2	−3.4	0.2	5.0	1.7	−0.2	−1.1	−2.2	0.2
5.1	0.0562	0.0025	0.0163	2.5	10.0	10.3	−4.3	0.7	2.9	−1.1	0.1	−0.2	−6.4	4.0	0.9	1.0	−1.1	−2.7	2.0
5.1	0.0562	0.0085	0.0145	2.8	9.5	9.9	2.5	−0.5	4.4	0.4	0.0	0.0	7.0	3.5	0.7	0.7	−0.8	−0.7	0.5
5.1	0.0562	0.0160	0.0147	3.4	8.7	9.3	0.0	−0.2	4.8	−0.8	0.0	0.8	3.8	5.5	1.3	0.5	−1.3	−1.3	0.3
5.1	0.0562	0.0250	0.0149	4.7	7.1	8.5	0.0	−1.7	2.3	0.5	0.2	−0.6	2.8	5.1	2.4	−0.3	−1.5	−0.6	0.3
5.1	0.1780	0.0025	0.0172	1.7	10.7	10.9	−2.3	0.2	6.5	−0.4	0.0	−0.8	−1.4	7.0	1.8	1.3	−1.4	−2.0	2.2
5.1	0.1780	0.0085	0.0145	2.8	10.3	10.7	3.9	0.7	2.5	1.3	0.2	0.1	8.6	2.6	0.4	0.2	−0.6	0.0	1.4
5.1	0.5620	0.0025	0.0301	1.3	10.3	10.4	5.0	−1.4	6.0	0.7	0.0	−0.5	0.9	4.4	1.3	0.7	−0.8	−0.9	4.5
8.8	0.0018	0.0750	0.0543	11.6	7.4	13.7	−0.1	1.6	0.9	−1.5	0.0	−3.3	1.0	3.0	3.9	0.6	−2.1	−2.5	1.5
8.8	0.0056	0.0250	0.0300	5.7	8.3	10.0	−0.2	1.2	3.1	−0.9	−0.1	0.1	−0.3	6.3	1.4	0.9	−2.6	−2.1	1.4
8.8	0.0056	0.0350	0.0317	5.7	8.0	9.8	0.0	0.3	4.4	−0.8	0.1	0.1	1.6	5.6	2.1	0.8	−2.1	−0.5	0.5
8.8	0.0056	0.0500	0.0365	4.9	7.0	8.5	−0.1	−0.7	3.2	−0.3	0.1	−0.2	0.8	5.0	3.2	0.6	−1.2	−0.3	0.3
8.8	0.0056	0.0750	0.0410	7.5	7.1	10.3	0.0	−1.3	2.9	−0.5	0.1	−4.7	−0.2	3.0	1.7	0.3	−0.8	−2.0	0.2
8.8	0.0178	0.0085	0.0210	4.8	8.2	9.5	−6.6	0.0	1.2	−0.8	−0.1	0.3	−1.9	2.3	0.4	0.3	−1.2	−2.9	1.2
8.8	0.0178	0.0160	0.0234	3.4	7.7	8.4	−0.2	1.7	2.8	−0.3	0.0	1.0	2.4	6.0	0.2	0.6	−1.6	−1.4	0.3
8.8	0.0178	0.0250	0.0238	3.8	7.6	8.5	−0.1	0.8	2.7	−0.1	0.0	0.6	2.7	6.1	1.5	0.6	−1.2	−0.8	0.3
8.8	0.0178	0.0350	0.0236	4.7	7.2	8.6	0.0	0.4	2.4	−0.2	0.1	0.1	0.9	5.7	3.0	0.9	−1.3	−0.5	0.3
8.8	0.0178	0.0500	0.0289	4.5	6.6	8.0	0.3	0.2	2.0	−0.6	0.1	0.0	0.6	5.3	3.1	0.5	−0.9	−0.2	0.3
8.8	0.0178	0.0750	0.0278	7.5	6.9	10.2	0.0	1.0	2.3	−0.8	0.1	−4.2	1.3	4.0	0.9	0.2	−0.5	−2.0	0.3
8.8	0.0562	0.0025	0.0196	3.6	9.9	10.5	−4.8	−0.1	0.9	−1.1	0.1	−0.1	−7.2	2.7	0.9	0.2	−1.0	−3.1	1.4
8.8	0.0562	0.0085	0.0172	3.5	8.6	9.3	0.6	0.6	2.5	−0.1	−0.1	0.3	5.9	5.2	0.4	0.5	−1.0	−2.1	0.5
8.8	0.0562	0.0160	0.0192	3.1	8.3	8.9	0.0	−0.8	3.9	−0.2	0.0	0.6	3.5	6.0	1.3	0.7	−1.0	−1.1	0.3
8.8	0.0562	0.0250	0.0173	4.0	8.6	9.5	0.0	−0.9	5.8	−0.2	0.0	0.8	2.2	5.4	1.6	0.5	−0.5	−0.9	0.3
8.8	0.0562	0.0350	0.0190	5.3	7.8	9.4	0.0	−0.5	4.9	−0.6	0.1	−0.1	−0.3	5.4	2.6	0.3	−0.4	−0.7	0.3

Table 4: The reduced diffractive cross sections $x_{I\!P}\sigma_r^{D(3)}$ as a function of Q^2, β and $x_{I\!P}$ values (columns $1-4$). The statistical (δ_{stat}), systematic (δ_{sys}) and total (δ_{tot}) uncertainties are given in columns 6 to 8. The remaining columns give the changes of the cross sections due to a $+1\sigma$ variation of the various systematic error sources described in section 4: the hadronic energy scale (δ_{had}); the electromagnetic energy scale (δ_{ele}); the scattering angle of the electron (δ_θ); the reweighting of the simulation in β (δ_β), $x_{I\!P}$ ($\delta_{x_{I\!P}}$) and t (δ_t); the leading proton energy E_p (δ_{E_p}), the proton transverse momentum components p_x (δ_{p_x}) and p_y (δ_{p_y}); the reweighting of the simulation in Q^2 (δ_{Q^2}); the background from beam halo, photoproduction and proton dissociation processes (δ_{bgn}); the vertex reconstruction efficiency (δ_{vtx}) and the bin centre corrections (δ_{bcc}). All uncertainties are given in per cent. The normalisation uncertainty of 6% is not included. The table continues on the next pages.

Q^2 [GeV^2]	β	$x_{I\!P}$	$x_{I\!P}\sigma_r^{D(3)}$	δ_{stat} [%]	δ_{sys} [%]	δ_{tot} [%]	δ_{had} [%]	δ_{ele} [%]	δ_θ [%]	δ_β [%]	$\delta_{x_{I\!P}}$ [%]	δ_t [%]	δ_{E_p} [%]	δ_{p_x} [%]	δ_{p_y} [%]	δ_{Q^2} [%]	δ_{vtx} [%]	δ_{bgn} [%]	δ_{bcc} [%]
8.8	0.0562	0.0500	0.0252	6.0	8.8	10.7	0.0	−0.3	6.5	1.2	0.2	−1.3	−0.3	5.1	2.4	0.0	−0.1	−0.5	0.3
8.8	0.1780	0.0025	0.0204	2.5	9.5	9.9	−2.8	−0.2	3.6	−0.3	−0.7	−0.6	−4.0	6.1	1.6	0.8	−1.3	−2.7	1.8
8.8	0.1780	0.0085	0.0182	2.7	8.8	9.2	2.6	−0.2	2.0	1.1	0.1	−0.1	7.5	2.8	0.5	0.2	−0.3	−0.2	0.6
8.8	0.1780	0.0160	0.0164	4.3	8.4	9.5	0.0	0.6	2.8	3.1	0.2	−0.2	4.5	5.5	1.2	0.0	−0.1	−0.9	0.7
8.8	0.5620	0.0025	0.0328	1.5	10.8	10.9	6.6	−1.3	4.4	0.9	−1.2	−0.6	0.3	5.5	1.5	0.4	−0.8	−1.4	3.9
15.3	0.0056	0.0500	0.0456	8.1	7.0	10.7	−0.1	1.6	1.7	−1.6	0.1	−1.5	1.1	4.8	3.5	0.7	−1.0	−0.6	0.9
15.3	0.0056	0.0750	0.0498	10.2	6.6	12.2	0.0	1.9	0.0	−0.7	0.1	−3.7	0.7	3.0	3.3	0.5	−0.8	−2.2	0.3
15.3	0.0178	0.0160	0.0335	5.1	8.0	9.4	−0.2	−0.9	4.0	−1.5	−0.2	0.8	2.9	5.5	0.8	0.7	−1.3	−1.2	0.8
15.3	0.0178	0.0250	0.0318	4.7	7.3	8.7	−0.1	−1.2	3.1	−0.5	0.0	−0.1	1.1	5.9	1.6	1.5	−0.9	−0.8	0.2
15.3	0.0178	0.0350	0.0313	6.1	7.1	9.4	0.0	0.4	3.1	−0.2	0.0	1.1	0.7	5.5	2.6	0.5	−1.1	−0.6	0.1
15.3	0.0178	0.0500	0.0338	5.9	7.2	9.3	0.0	−0.7	2.5	−0.6	0.1	−1.4	0.9	5.5	3.2	0.5	−1.2	−0.4	0.2
15.3	0.0178	0.0750	0.0407	8.9	6.4	11.0	0.0	0.9	−0.3	−0.4	0.2	−2.3	1.2	4.0	3.4	0.1	−0.8	−2.1	0.2
15.3	0.0562	0.0085	0.0214	4.7	9.4	10.5	−3.8	0.0	3.0	−0.6	−0.2	0.2	2.9	6.2	1.4	0.7	−1.2	−3.8	0.4
15.3	0.0562	0.0160	0.0221	4.1	8.2	9.1	0.0	0.4	2.7	−0.4	0.0	−0.8	5.1	5.2	0.8	0.5	−1.3	−1.6	0.2
15.3	0.0562	0.0250	0.0203	4.9	7.3	8.8	0.0	0.5	1.8	−0.3	0.0	0.8	1.8	6.5	1.4	0.4	−1.0	−0.9	0.2
15.3	0.0562	0.0350	0.0221	6.3	6.7	9.2	0.0	−1.3	2.1	−0.3	0.0	0.6	1.3	4.8	3.5	0.4	−1.0	−0.8	0.3
15.3	0.0562	0.0500	0.0240	6.2	6.6	9.1	0.0	−0.3	1.5	−0.3	0.1	−1.6	0.3	5.1	3.5	0.1	−0.7	−0.3	0.3
15.3	0.0562	0.0750	0.0259	11.6	7.4	13.8	0.0	−1.3	3.3	0.5	0.1	−1.9	−0.6	3.9	4.4	0.0	−0.6	−1.8	0.3
15.3	0.1780	0.0025	0.0218	3.7	9.3	10.0	−2.8	−0.5	2.0	−0.3	−0.7	−0.4	−5.5	5.2	1.0	0.4	−0.9	−3.7	1.2
15.3	0.1780	0.0085	0.0193	3.6	8.8	9.5	2.1	−0.2	1.3	0.5	0.0	0.1	7.2	4.1	0.7	0.2	−0.6	−0.7	0.5
15.3	0.1780	0.0160	0.0182	4.4	8.2	9.3	0.0	0.3	2.5	2.2	0.1	0.0	4.5	5.6	0.2	0.2	−0.9	−1.6	0.3
15.3	0.1780	0.0250	0.0182	6.6	7.6	10.0	0.0	−0.8	3.4	3.0	0.2	0.5	2.0	5.3	1.5	0.0	−0.9	−1.0	0.3
15.3	0.5620	0.0025	0.0335	2.4	10.2	10.4	6.0	−2.1	3.0	0.8	−1.3	−0.2	−2.6	5.3	1.3	0.3	−0.8	−1.7	3.4
15.3	0.5620	0.0085	0.0294	3.4	10.0	10.6	4.9	1.1	0.9	1.3	0.5	0.0	7.7	2.6	0.7	−0.1	−0.5	0.0	2.2
26.5	0.0056	0.0750	0.0554	16.9	7.1	18.3	0.0	−1.2	2.9	−1.0	0.2	−3.5	0.8	4.1	1.8	0.4	−0.6	−2.1	1.3
26.5	0.0178	0.0250	0.0346	8.7	7.4	11.4	0.3	0.4	2.5	−1.1	−0.1	−1.0	4.3	4.6	1.2	0.9	−0.9	−1.5	1.1
26.5	0.0178	0.0350	0.0341	8.8	6.8	11.1	0.0	2.6	1.1	−1.0	0.0	0.1	0.9	5.1	3.1	0.5	−0.9	−0.5	0.3
26.5	0.0178	0.0500	0.0489	7.4	7.2	10.3	0.0	−0.7	3.2	−0.9	0.1	−0.1	0.6	4.9	3.7	0.2	−0.7	−0.3	0.1
26.5	0.0178	0.0750	0.0414	11.9	7.9	14.3	0.0	−0.5	2.7	−0.7	0.1	−3.6	0.9	5.3	2.8	0.3	−0.8	−2.0	0.2
26.5	0.0562	0.0085	0.0266	7.1	8.4	11.1	−6.1	−0.8	0.8	−1.1	0.0	0.6	−2.2	3.5	0.3	0.3	−0.6	−3.6	1.0
26.5	0.0562	0.0160	0.0266	5.3	8.0	9.6	0.2	0.3	2.7	−0.3	0.0	0.7	3.3	6.4	0.3	0.3	−1.0	−1.5	0.2
26.5	0.0562	0.0250	0.0249	6.4	7.2	9.7	0.2	−0.3	2.8	−0.6	0.0	0.3	1.8	6.1	0.8	0.4	−1.1	−1.2	0.2
26.5	0.0562	0.0350	0.0290	7.6	6.9	10.3	0.4	−0.1	3.1	−0.3	0.0	0.1	0.6	5.4	2.9	0.2	−1.0	−0.2	0.2
26.5	0.0562	0.0500	0.0293	7.5	7.2	10.4	0.0	1.9	0.8	−0.4	0.1	−1.3	1.8	4.9	4.2	0.2	−0.8	−0.5	0.3
26.5	0.0562	0.0750	0.0325	12.3	6.5	14.0	0.0	−1.2	−0.2	−0.6	0.1	−4.6	−0.5	3.0	2.3	0.2	−0.7	−2.2	0.3
26.5	0.1780	0.0025	0.0235	5.5	9.2	10.7	−1.7	−0.5	1.4	−0.4	−0.4	−0.4	−6.6	3.9	0.8	0.2	−0.6	−4.0	1.5
26.5	0.1780	0.0085	0.0217	5.1	8.3	9.7	1.2	−0.2	1.5	0.1	−0.1	0.0	6.8	4.1	0.5	0.3	−0.7	−1.3	0.5
26.5	0.1780	0.0160	0.0215	5.6	7.9	9.7	0.0	0.0	1.2	0.5	0.0	0.1	4.4	6.1	1.1	0.3	−1.1	−1.4	0.3
26.5	0.1780	0.0250	0.0171	7.0	6.8	9.8	0.0	−0.3	0.9	1.2	0.0	0.9	1.7	6.0	1.8	0.1	−0.7	−1.0	0.2
26.5	0.1780	0.0350	0.0181	9.9	7.6	12.5	0.0	−3.4	2.7	2.5	0.1	0.5	2.4	4.9	1.3	0.2	−1.1	−0.7	0.2
26.5	0.5620	0.0025	0.0339	3.5	10.2	10.8	5.1	−2.2	2.2	0.6	−1.1	−0.6	−4.3	5.6	1.4	0.3	−0.8	−2.3	3.0
26.5	0.5620	0.0085	0.0292	4.1	9.4	10.2	4.9	−0.7	1.4	0.7	0.0	−0.2	6.8	3.0	0.4	0.0	−0.5	−0.3	2.3
46.0	0.0178	0.0500	0.0687	12.2	7.3	14.2	−0.3	−0.1	1.8	−1.2	0.1	−0.6	1.5	5.8	3.3	0.5	−0.7	−0.2	0.6
46.0	0.0178	0.0750	0.0401	19.0	7.0	20.3	0.3	0.6	2.2	−1.1	0.0	−2.9	−1.5	4.1	3.2	0.4	−0.6	−1.9	0.1
46.0	0.0562	0.0160	0.0360	8.9	8.0	11.9	0.1	−0.2	2.0	−1.1	0.0	−0.7	4.1	6.1	1.5	0.5	−0.7	−0.8	0.6
46.0	0.0562	0.0250	0.0310	8.7	7.5	11.5	0.1	0.6	1.7	−1.2	0.0	−0.4	−1.2	6.9	1.0	0.2	−0.8	−0.6	0.1
46.0	0.0562	0.0350	0.0301	10.6	7.0	12.8	0.3	−0.8	1.5	−0.1	0.1	−1.0	3.4	5.3	2.1	0.2	−0.7	−1.0	0.1
46.0	0.0562	0.0500	0.0400	9.5	6.9	11.7	0.0	−1.0	2.0	−0.5	0.1	−1.9	−0.6	5.8	1.9	0.2	−1.1	−0.3	0.2

Q^2 [GeV^2]	β	$x_{I\!P}$	$x_{I\!P}\sigma_r^{D(3)}$	δ_{stat} [%]	δ_{sys} [%]	δ_{tot} [%]	δ_{had} [%]	δ_{ele} [%]	δ_θ [%]	δ_β [%]	$\delta_{x_{I\!P}}$ [%]	δ_t [%]	δ_{E_p} [%]	δ_{p_x} [%]	δ_{p_y} [%]	δ_{Q2} [%]	δ_{vtx} [%]	δ_{bgn} [%]	δ_{bcc} [%]
46.0	0.0562	0.0750	0.0420	16.1	6.7	17.4	0.0	−1.2	2.1	−0.7	0.1	−3.7	0.1	3.9	2.5	0.2	−0.6	−1.7	0.2
46.0	0.1780	0.0085	0.0219	8.2	9.2	12.3	0.2	−1.7	2.7	−0.6	0.0	0.0	6.0	5.3	1.0	0.3	−0.9	−3.0	0.5
46.0	0.1780	0.0160	0.0249	7.2	7.7	10.5	0.4	−0.5	1.1	−0.2	0.0	−0.8	4.3	5.8	0.9	0.2	−0.9	−1.5	0.2
46.0	0.1780	0.0250	0.0244	8.6	7.4	11.3	0.0	−0.4	1.5	−0.4	0.0	−0.1	3.8	5.8	1.0	0.1	−1.0	−1.3	0.2
46.0	0.1780	0.0350	0.0238	10.9	7.1	13.0	0.0	−0.2	2.6	0.2	0.2	0.0	1.7	5.8	2.6	0.1	−0.9	−0.4	0.2
46.0	0.1780	0.0500	0.0250	11.2	8.1	13.8	0.0	1.3	5.1	0.9	0.3	−3.2	1.1	3.6	3.1	0.1	−1.2	−0.4	0.3
46.0	0.1780	0.0750	0.0341	20.8	7.1	22.0	0.0	−2.4	0.2	1.6	0.1	−3.7	−1.2	3.6	2.7	−0.2	−1.0	−2.2	0.3
46.0	0.5620	0.0025	0.0400	5.5	10.8	12.1	5.0	−2.8	2.2	0.3	−0.9	0.2	−6.1	4.3	1.1	0.2	−0.7	−2.7	3.6
46.0	0.5620	0.0085	0.0301	5.6	9.6	11.2	5.6	−1.3	1.7	0.5	−0.1	−0.4	6.0	3.4	0.7	0.1	−0.5	−0.9	2.9
46.0	0.5620	0.0160	0.0242	8.7	8.4	12.1	0.0	−2.6	5.5	1.3	0.2	0.7	−1.9	3.9	0.4	0.1	−1.2	−2.1	2.8
46.0	0.5620	0.0250	0.0167	13.2	7.5	15.2	0.0	1.3	3.0	3.0	0.2	−1.3	−0.9	4.0	2.7	−0.9	−1.5	−0.7	2.7
80.0	0.0562	0.0350	0.0375	19.2	7.9	20.8	0.3	−2.1	2.8	−2.8	−0.1	0.6	1.8	5.2	2.0	1.7	−0.8	−2.2	0.1
80.0	0.0562	0.0500	0.0385	15.6	6.9	17.0	0.0	−1.1	2.7	−1.2	0.0	0.2	0.3	5.0	3.3	0.9	−0.8	0.0	0.1
80.0	0.0562	0.0750	0.0354	24.2	7.4	25.3	0.0	0.5	1.8	−0.7	0.1	−3.0	0.5	3.0	5.3	0.2	−0.8	−1.8	0.2
80.0	0.1780	0.0085	0.0396	14.9	8.6	17.2	−2.0	−1.5	2.2	−1.6	−0.1	−0.9	−0.8	5.8	1.1	0.4	−0.8	−4.8	1.0
80.0	0.1780	0.0160	0.0227	12.8	7.9	15.0	0.0	0.5	2.5	−0.4	0.0	0.2	5.2	5.1	0.9	0.3	−0.8	−1.3	0.2
80.0	0.1780	0.0250	0.0246	11.8	7.8	14.1	0.0	0.5	1.7	−0.9	0.1	0.2	0.7	6.8	2.3	0.5	−1.5	−1.4	0.2
80.0	0.1780	0.0350	0.0290	14.1	6.9	15.8	0.0	0.8	−0.3	−3.5	0.1	−0.2	4.1	4.2	0.3	0.2	−0.7	−0.7	0.2
80.0	0.1780	0.0500	0.0251	15.1	6.8	16.6	0.0	−1.5	0.9	−0.5	−0.1	−1.4	−0.2	3.9	4.5	0.4	−1.7	−1.2	0.3
80.0	0.1780	0.0750	0.0226	25.8	6.8	26.7	0.0	−1.5	1.3	0.8	0.1	−2.8	0.8	5.4	1.2	0.0	−0.6	−1.8	0.3
80.0	0.5620	0.0085	0.0266	9.8	10.4	14.3	4.7	−1.4	1.1	0.3	−0.2	0.3	5.0	6.1	1.1	0.3	−1.0	−3.1	2.9
80.0	0.5620	0.0160	0.0192	13.0	9.3	16.0	0.0	−5.2	0.3	0.5	0.2	−0.7	−2.9	4.8	0.0	0.2	−0.4	−4.5	2.8
80.0	0.5620	0.0250	0.0180	16.1	8.2	18.1	0.0	−5.5	2.8	1.2	0.2	−2.1	−0.8	2.3	2.5	0.4	−1.2	−1.5	2.7
80.0	0.5620	0.0350	0.0199	24.6	10.0	26.6	0.0	−4.7	0.6	1.8	0.1	0.4	−3.1	7.5	0.9	0.0	−0.9	−0.2	2.5
200.0	0.0562	0.0500	0.0285	27.4	6.2	28.1	0.0	1.4	1.6	−0.6	0.0	−1.0	0.8	3.7	2.9	0.3	−0.9	−2.6	1.6
200.0	0.0562	0.0750	0.0490	36.4	7.3	37.2	0.0	−0.2	0.6	0.1	0.1	−3.2	−1.3	5.4	3.0	−0.1	−0.7	−1.5	0.7
200.0	0.1780	0.0160	0.0260	19.6	8.4	21.3	−1.0	1.9	0.1	−0.4	0.1	0.5	5.3	4.7	2.2	0.5	−0.8	−2.3	1.7
200.0	0.1780	0.0250	0.0353	16.4	7.5	18.1	0.0	1.9	0.3	−0.5	0.1	0.1	6.0	3.8	1.3	−0.1	−0.6	−0.5	0.7
200.0	0.1780	0.0350	0.0290	22.1	6.9	23.1	0.2	−0.1	0.0	−0.2	0.0	1.0	−3.9	5.4	1.4	−0.1	−0.6	−0.6	0.2
200.0	0.1780	0.0500	0.0405	20.2	6.8	21.4	0.0	−2.0	0.7	−0.6	0.1	−0.6	1.1	4.6	4.2	−0.3	−0.7	−0.5	0.3
200.0	0.1780	0.0750	0.0359	34.5	7.0	35.2	0.0	−1.3	0.8	−1.3	0.0	−2.5	−1.0	4.0	4.3	−0.4	−0.8	−1.9	0.4
200.0	0.5620	0.0085	0.0210	18.6	10.1	21.2	3.3	−1.6	1.0	0.3	0.0	−0.5	3.1	7.7	1.2	0.1	−1.0	−2.6	3.1
200.0	0.5620	0.0160	0.0174	22.4	9.0	24.1	0.0	−2.2	−0.3	−0.2	0.0	0.6	−2.3	6.6	0.8	−0.6	−0.7	−4.2	2.7
200.0	0.5620	0.0250	0.0139	26.6	8.1	27.8	0.0	−6.0	2.1	0.7	0.2	−0.3	−0.7	3.6	0.7	−1.1	−0.8	−1.3	2.5
200.0	0.5620	0.0350	0.0275	33.1	9.9	34.6	0.0	−2.0	1.4	1.5	−0.1	−0.5	−3.5	7.8	3.1	−0.9	−0.9	−0.4	2.3
200.0	0.5620	0.0500	0.0261	28.7	6.9	29.5	0.0	−1.2	0.7	−0.3	0.2	0.7	0.3	6.0	1.9	−0.8	−0.4	0.0	2.1
200.0	0.5620	0.0750	0.0407	48.3	6.7	48.8	0.0	−0.9	0.4	1.7	0.0	−4.7	0.4	3.0	0.9	−1.3	−0.7	−1.8	1.7

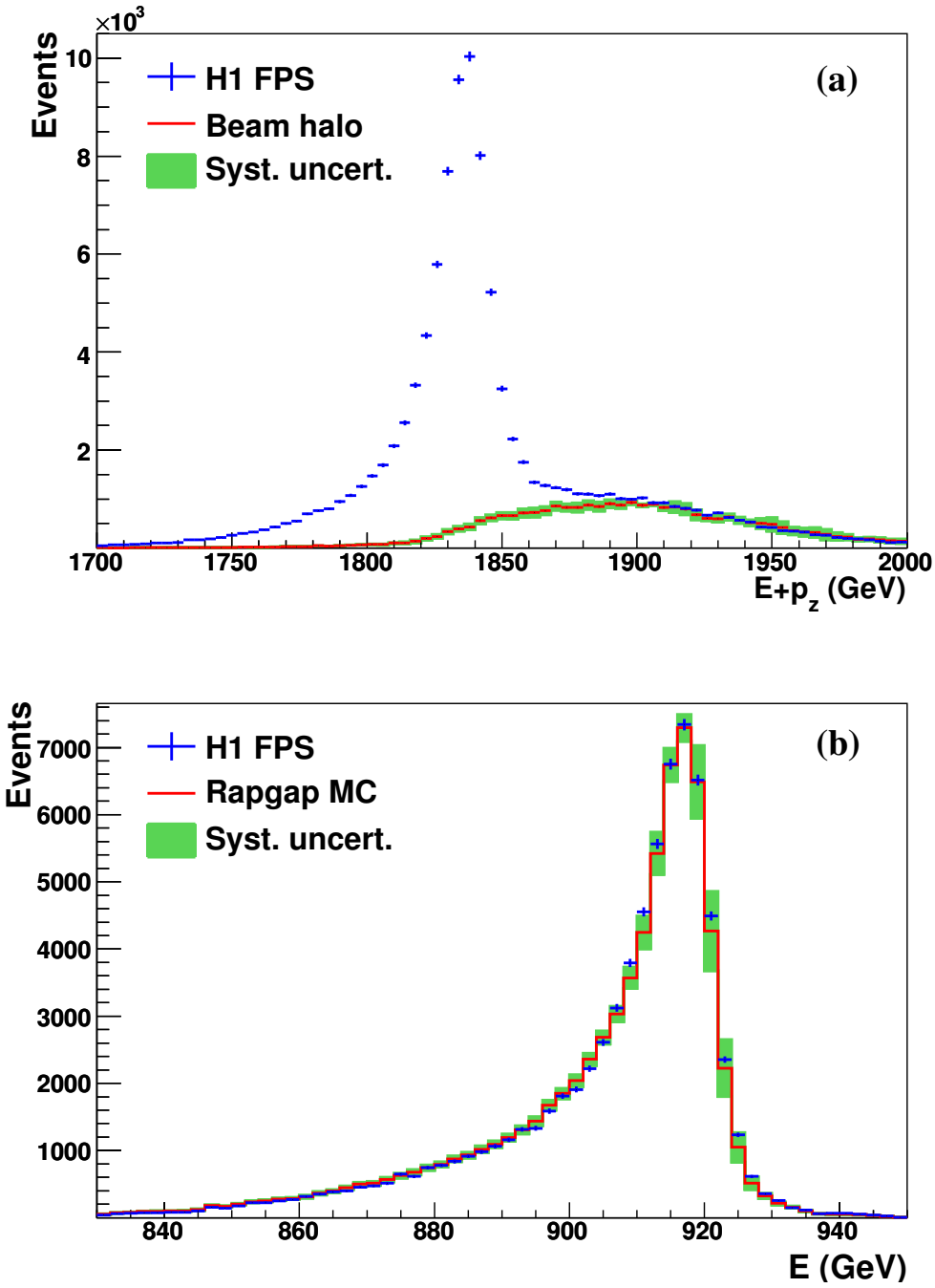

Figure 2: (a) The distribution of $E + p_z$ for FPS DIS events (histogram with error bars) and for random coincidences of DIS events reconstructed in the H1 central detector with beam-halo protons giving a signal in the FPS (histogram with shaded bands). The systematic uncertainties on the beam-halo background are presented as shaded bands around the beam-halo histogram. (b) The distribution of the leading proton energy reconstructed in the FPS (histogram with error bars). The beam-halo background is subtracted from the data. The RAPGAP Monte Carlo simulation is shown as a histogram with shaded bands indicating the experimental systematic uncertainties.

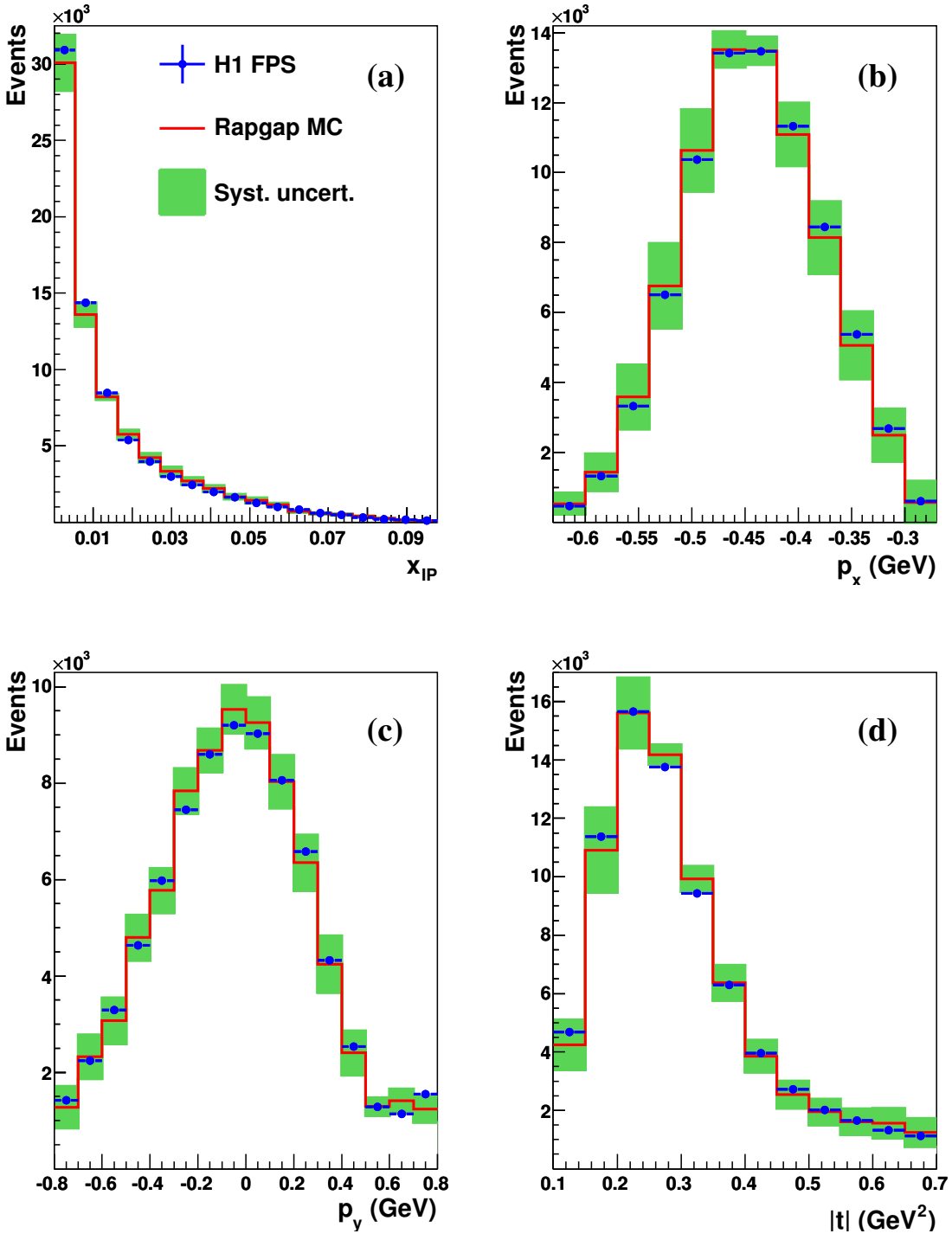

Figure 3: The distributions of the variables (a) $x_{I\!P}$, (b) p_x, (c) p_y and (d) $|t|$ reconstructed using the FPS (histogram with error bars). The beam-halo background is subtracted from the data. The RAPGAP Monte Carlo simulation is shown as a histogram. The experimental systematic uncertainties are presented as shaded bands around the Monte Carlo histogram.

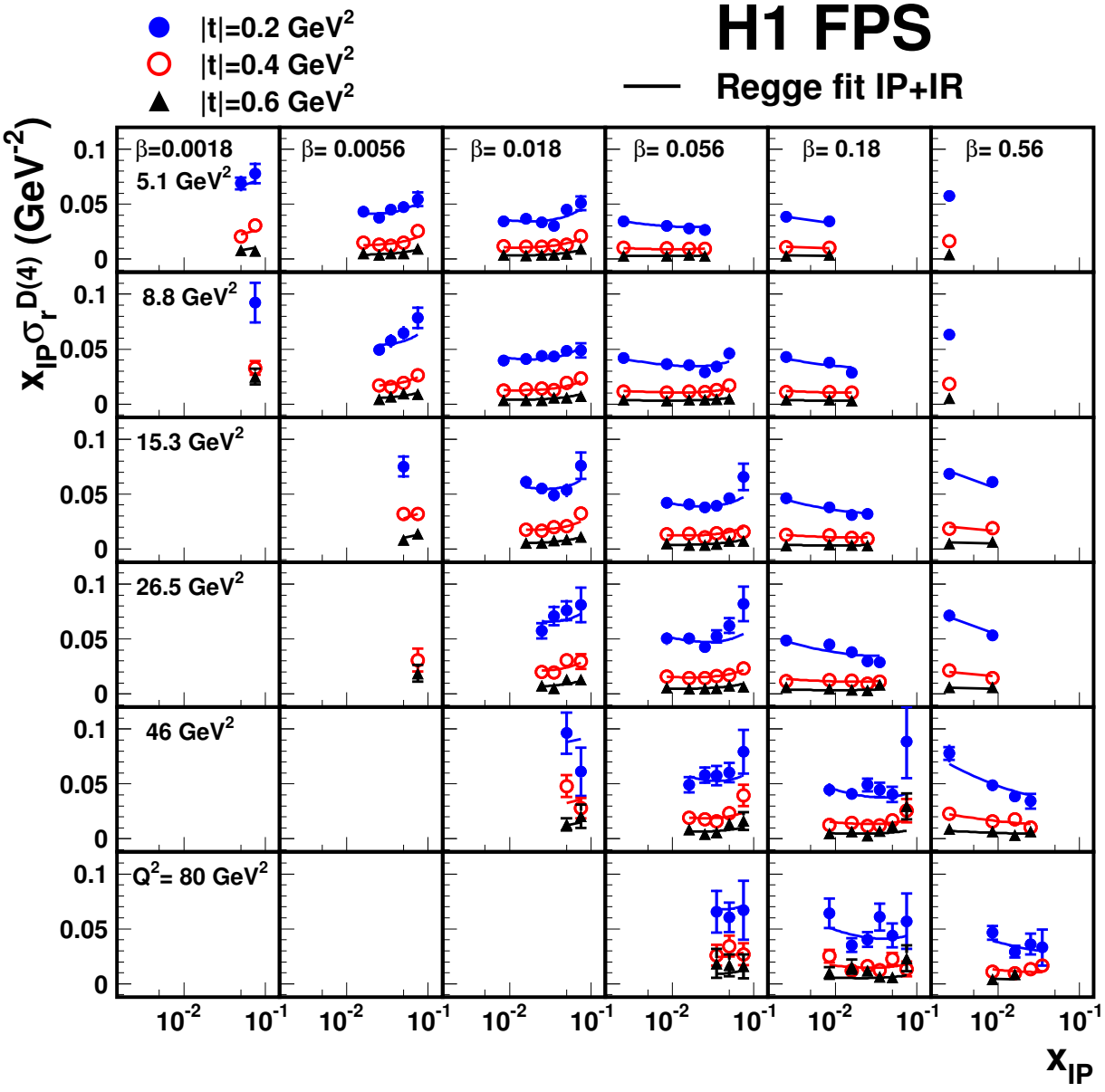

Figure 4: The reduced diffractive cross section $x_{I\!P}\,\sigma_r^{D(4)}(\beta, Q^2, x_{I\!P}, t)$ shown as a function of $x_{I\!P}$ for different values of t, β and Q^2. The error bars indicate the statistical and systematic errors added in quadrature. The overall normalisation uncertainty of 4.3% is not shown. The solid curves represent the results of the phenomenological Regge fit to the data, including both the pomeron ($I\!P$) and a sub-leading ($I\!R$) exchange.

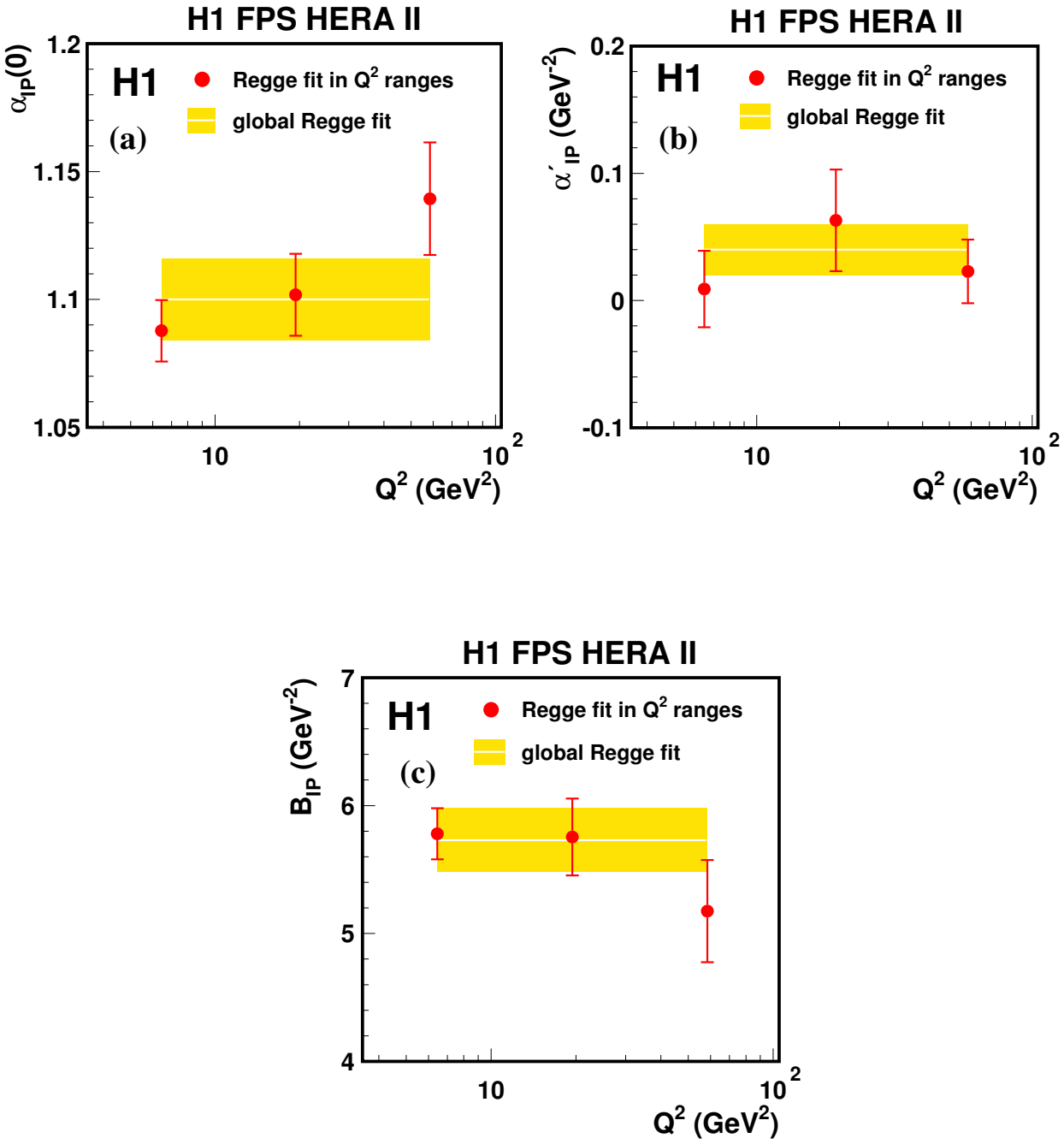

Figure 5: Results for (a) $\alpha_{I\!P}(0)$, (b) $\alpha'_{I\!P}$ and (c) $B_{I\!P}$ obtained from a modified version of the Regge fit performed in three different ranges of Q^2. The error bars correspond to the experimental uncertainties which are the statistical and uncorrelated systematic uncertainties added in quadrature. The white lines and shaded bands show the result and experimental uncertainty from the standard fit over the whole Q^2 range.

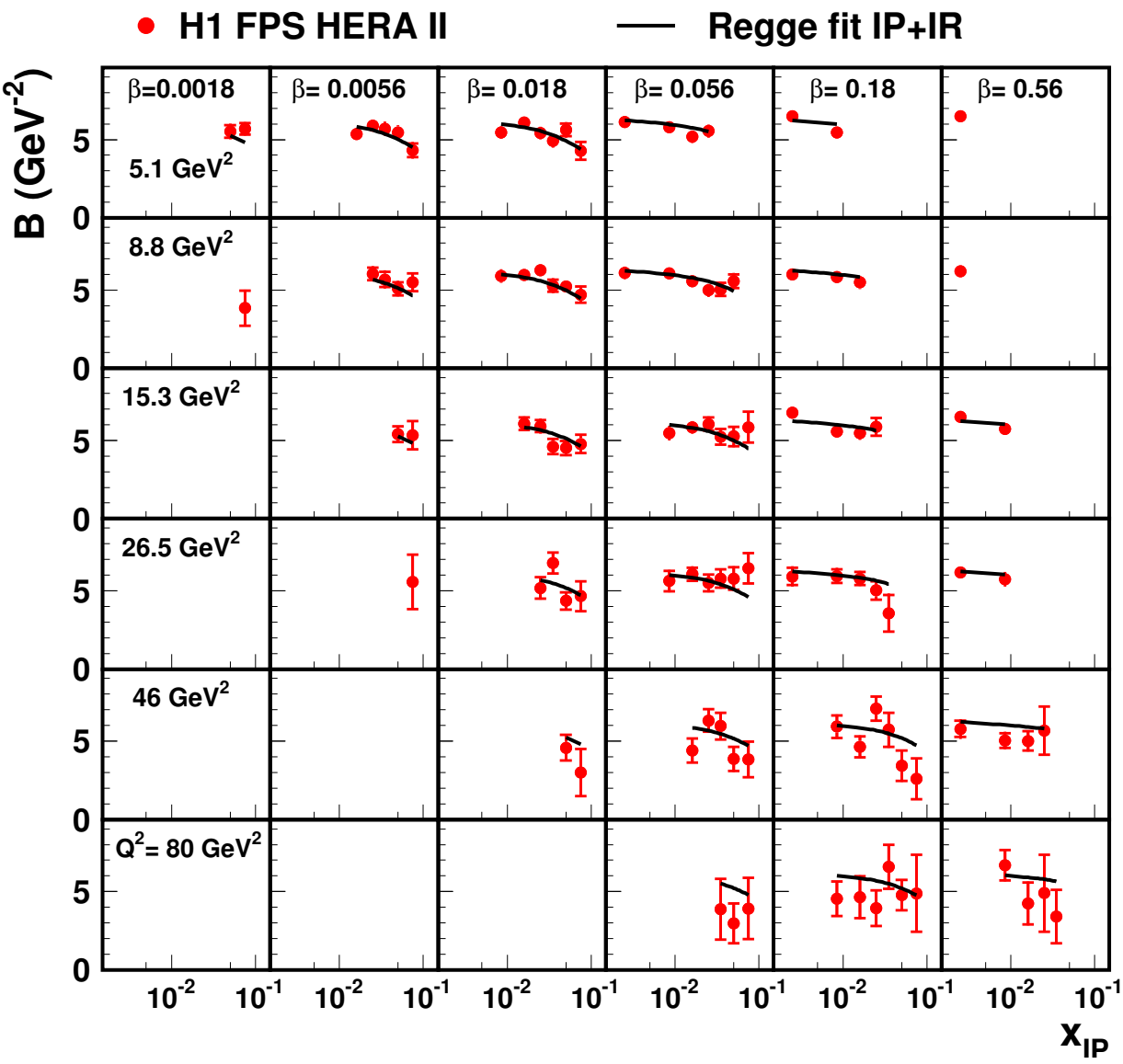

Figure 6: Results for the slope parameter B obtained from a fit of the form $\mathrm{d}\sigma/\mathrm{d}t \propto e^{Bt}$ shown as a function of $x_{I\!P}$ for different values of β and Q^2. The error bars indicate the statistical and systematic errors added in quadrature. The solid curves represent the results of the phenomenological Regge fit to $F_2^{D(4)}$ including both the pomeron ($I\!P$) and a sub-leading ($I\!R$) exchange.

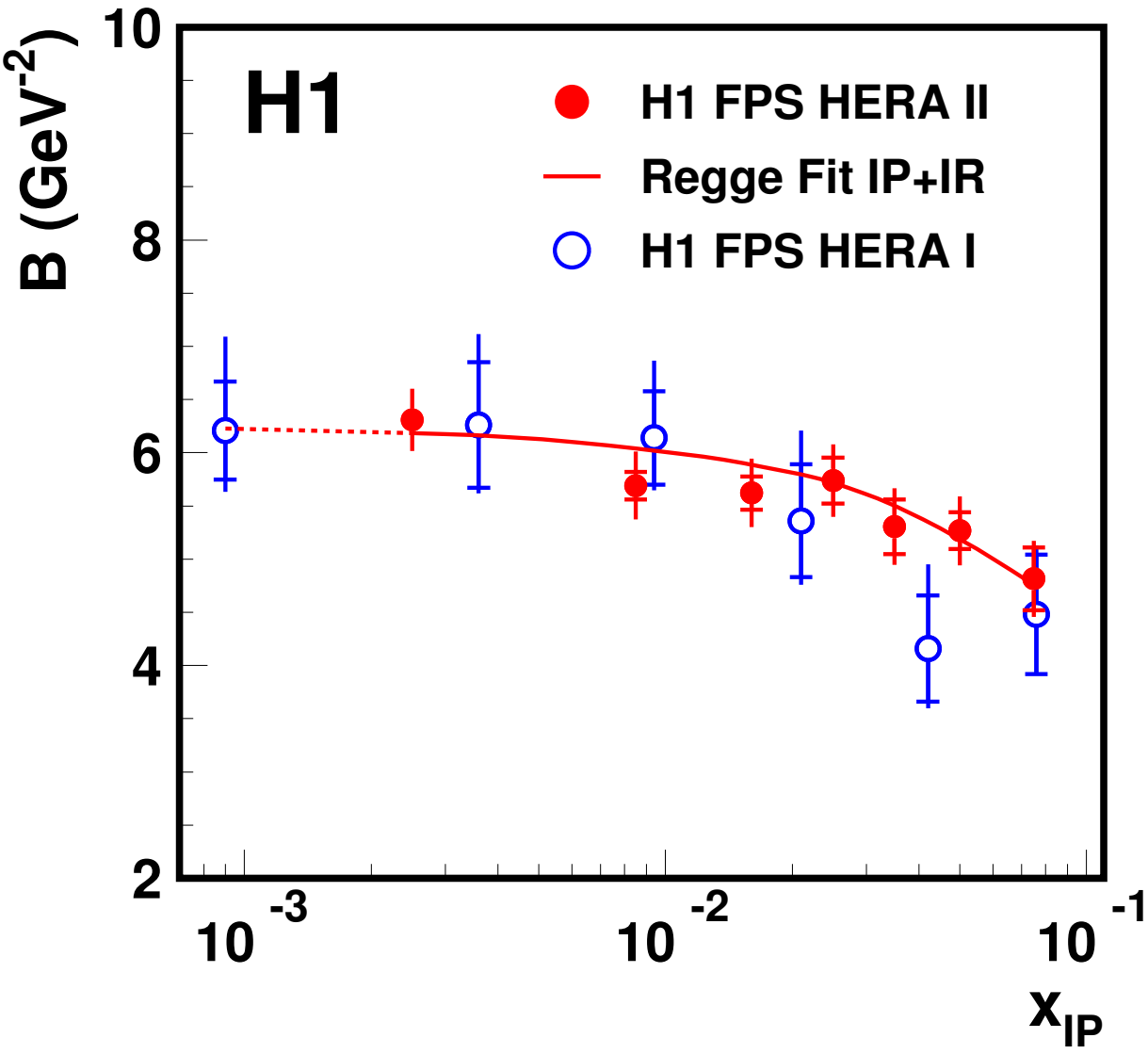

Figure 7: The slope parameter B obtained from a fit of the form $\mathrm{d}\sigma/\mathrm{d}t \propto e^{Bt}$ shown as a function of $x_{I\!P}$. The data are averaged over Q^2 and β. The inner error bars represent the statistical errors. The outer error bars indicate the statistical and systematic errors added in quadrature. The solid curve represents the results of the phenomenological Regge fit to the data, including both the pomeron ($I\!P$) and a sub-leading ($I\!R$) exchange. The dashed curve represents the prediction beyond the $x_{I\!P}$ range used in the fit. The previously published H1 FPS results [4] are also shown (open circles).

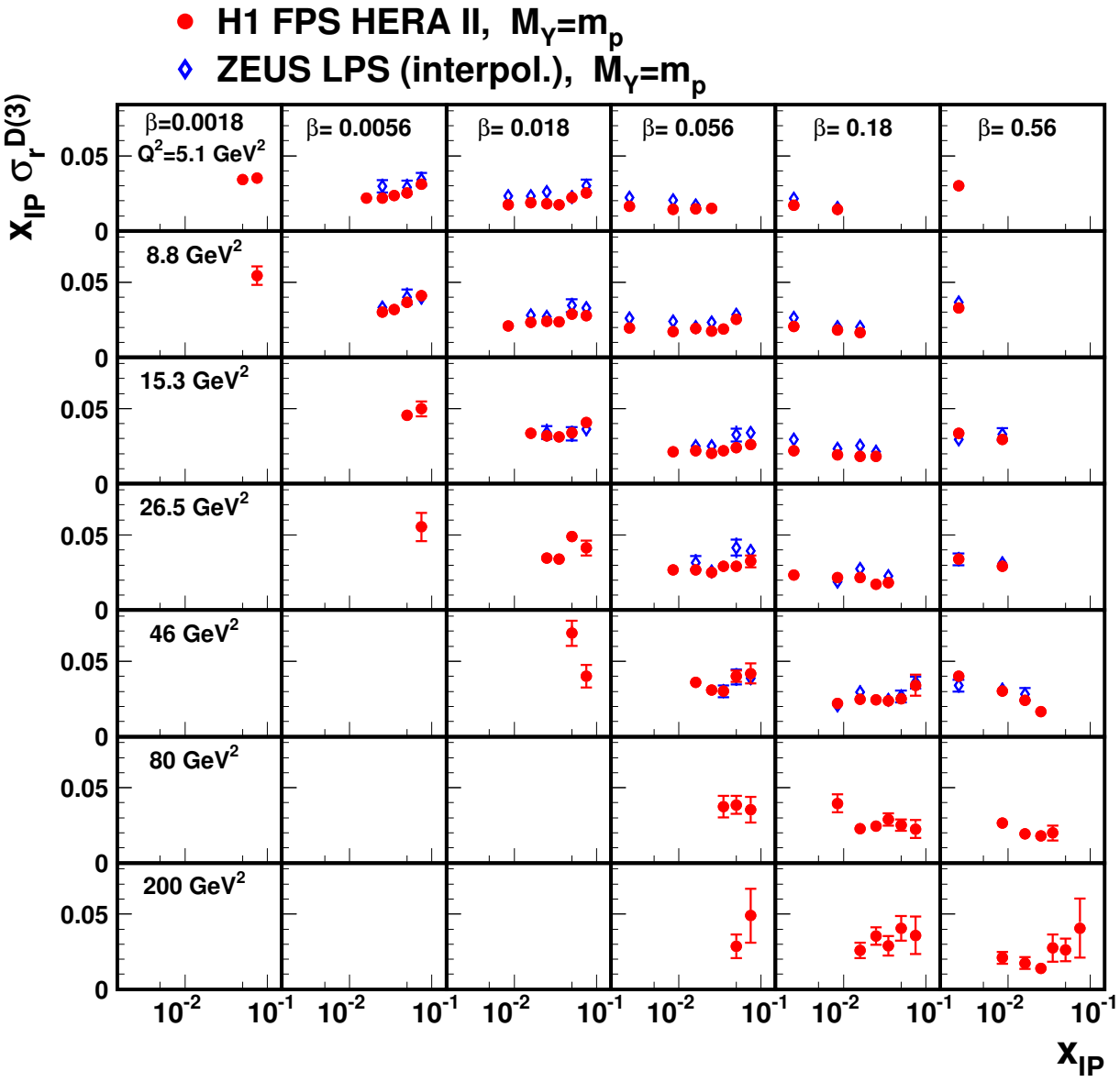

Figure 8: The reduced diffractive cross section $x_{I\!P}\,\sigma_r^{D(3)}(\beta, Q^2, x_{I\!P})$ for $|t| < 1$ GeV^2, shown as a function of $x_{I\!P}$ for different values of β and Q^2. The error bars indicate the statistical and systematic errors added in quadrature. The H1 FPS data are compared with the ZEUS LPS results [12] interpolated to the FPS $\beta, Q^2, x_{I\!P}$ values. The overall normalisation uncertainty of 6% on the H1 FPS data and the normalisation uncertainty of $^{+11}_{-7}$% on the ZEUS LPS data are not shown.

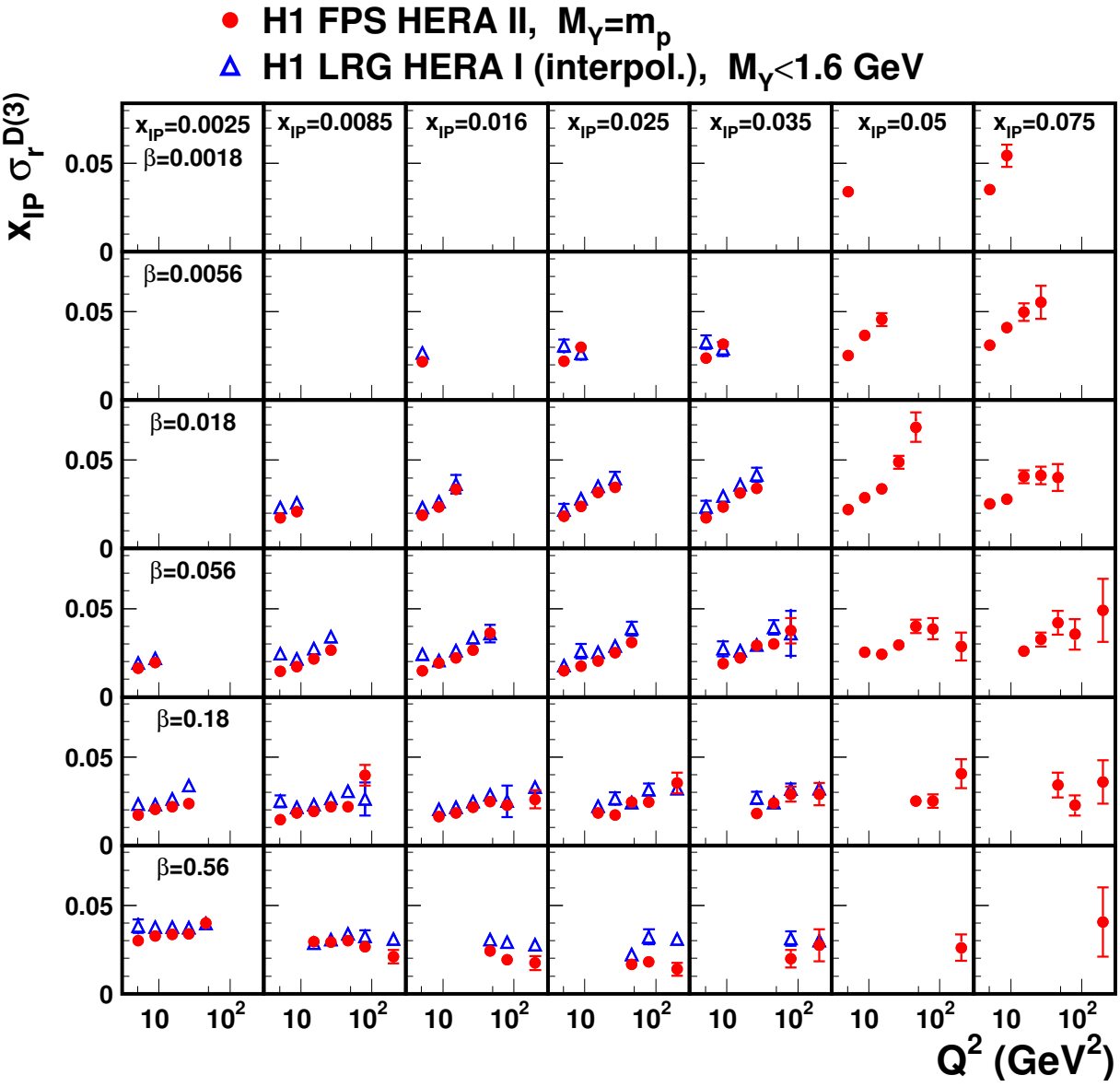

Figure 9: The reduced diffractive cross section $x_{I\!P}\,\sigma_r^{D(3)}(\beta, Q^2, x_{I\!P})$ for $|t| < 1$ GeV^2, shown as a function of Q^2 for different values of $x_{I\!P}$ and β. The error bars indicate the statistical and systematic errors added in quadrature. The H1 FPS data are compared with the H1 LRG results interpolated to the FPS $\beta, Q^2, x_{I\!P}$ values [5]. The overall normalisation uncertainty of 6% on the FPS data and the normalisation uncertainty of 6.2% on the LRG data are not shown.

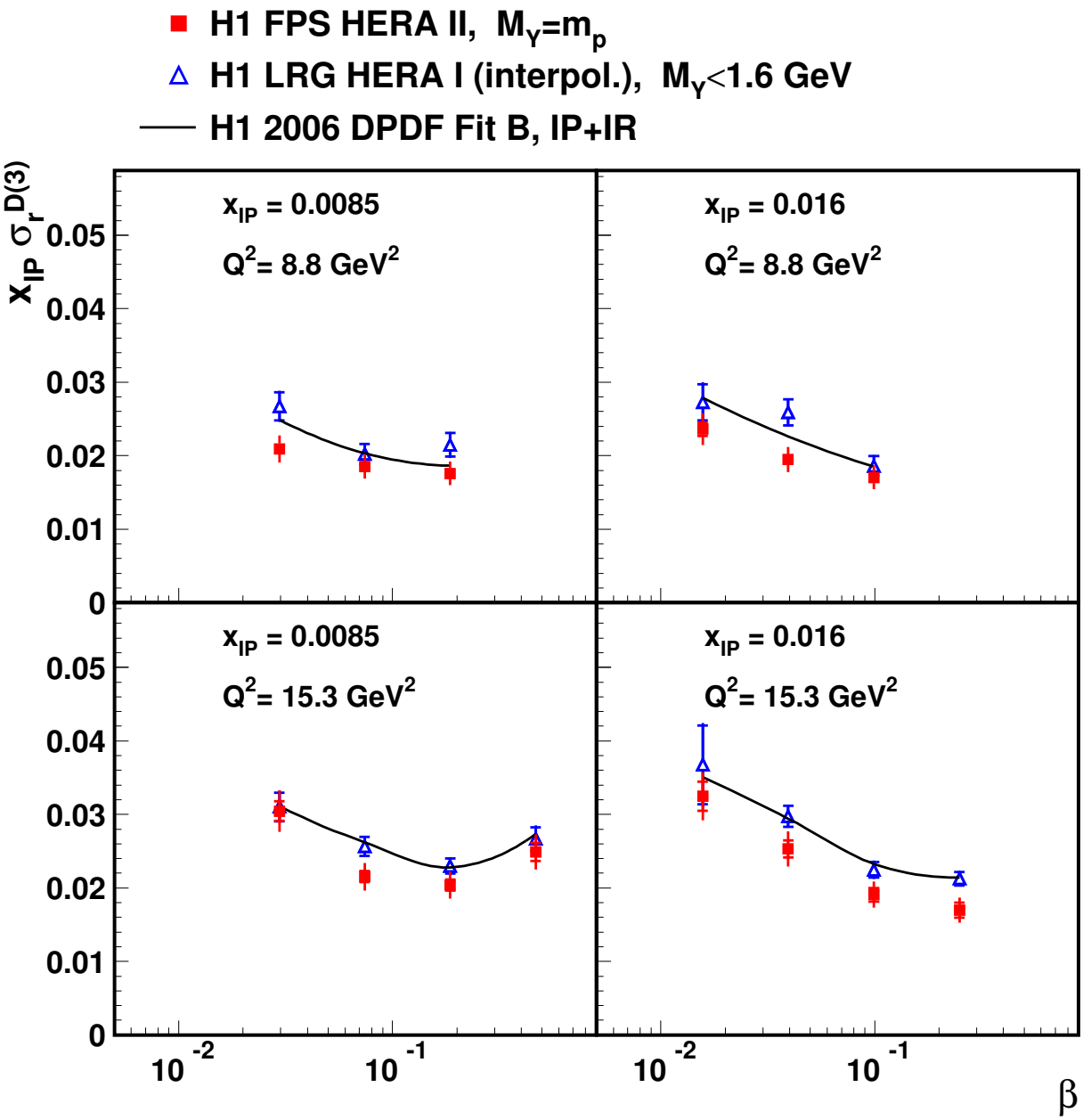

Figure 10: The reduced diffractive cross section $x_{I\!P}\,\sigma_r^{D(3)}(\beta, Q^2, x_{I\!P})$ for $|t| < 1$ GeV^2, shown as a function of β for selected values of $x_{I\!P}$ and Q^2. The inner error bars represent the statistical errors. The outer error bars indicate the statistical and systematic errors added in quadrature. The H1 FPS data are compared with the H1 LRG results [5] interpolated to the FPS $\beta, Q^2, x_{I\!P}$ values. The solid curves represent H1 2006 DPDF Fit B to the LRG data. The overall normalisation uncertainty of 6% on the FPS data and the normalisation uncertainty of 6.2% on the LRG data are not shown.

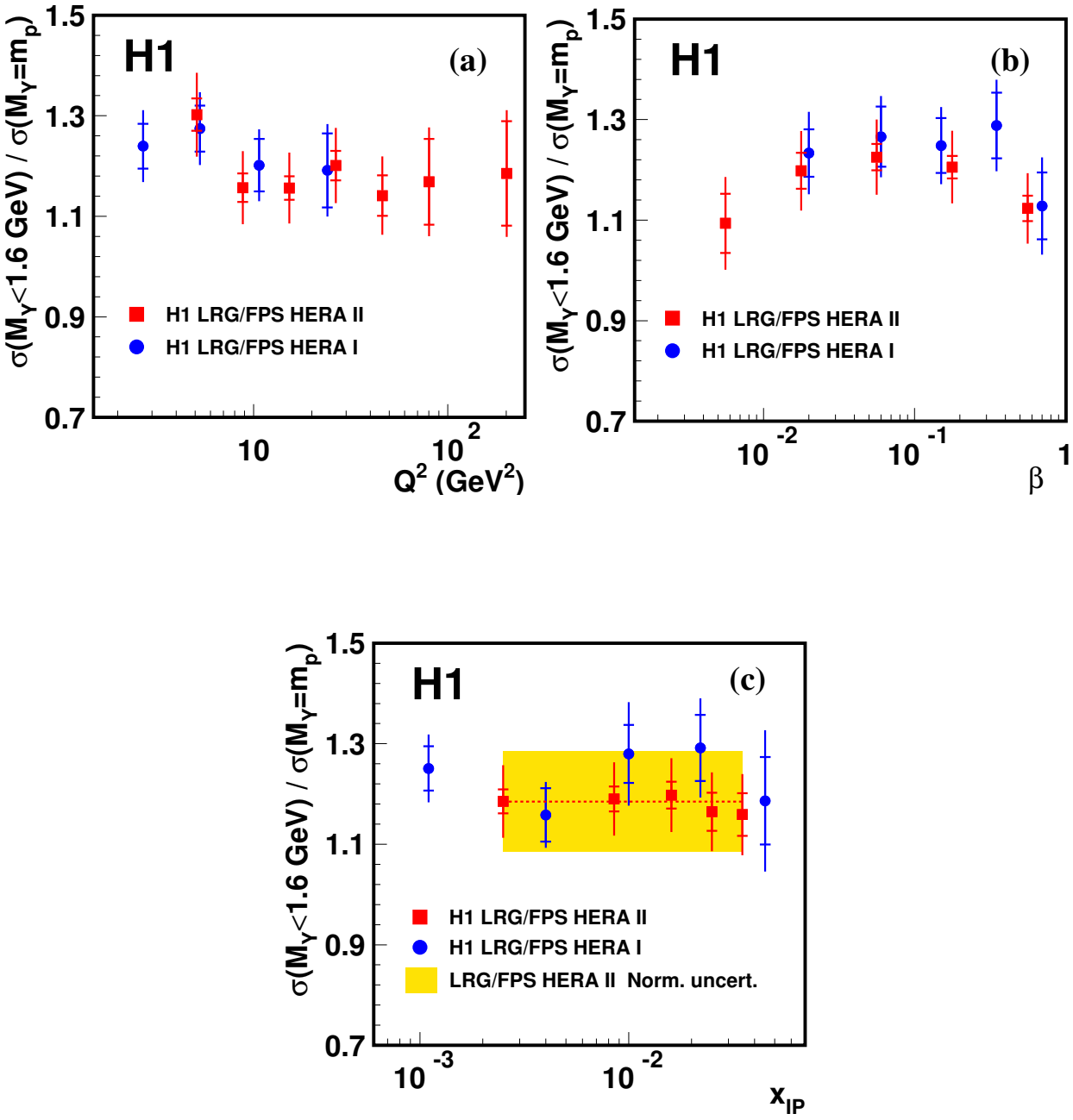

Figure 11: The ratio of the reduced diffractive cross section $\sigma_r^{D(3)}$ for $M_Y < 1.6$ GeV and $|t| < 1$ GeV^2 obtained using the H1 LRG data [5] to that for $M_Y = m_p$ and $|t| < 1$ GeV^2, obtained from the present and previously published FPS data [4]. The results are shown as a function of (a) Q^2, (b) β and (c) $x_{I\!P}$, after averaging over the other variables. The inner error bars represent the statistical errors. The outer error bars indicate the statistical and uncorrelated systematic errors added in quadrature. The combined normalisation uncertainty of 8.5% is shown as a band in figure (c). The dashed line in figure (c) represents the result of a fit to the data in the region shown assuming no dependence on $x_{I\!P}$.

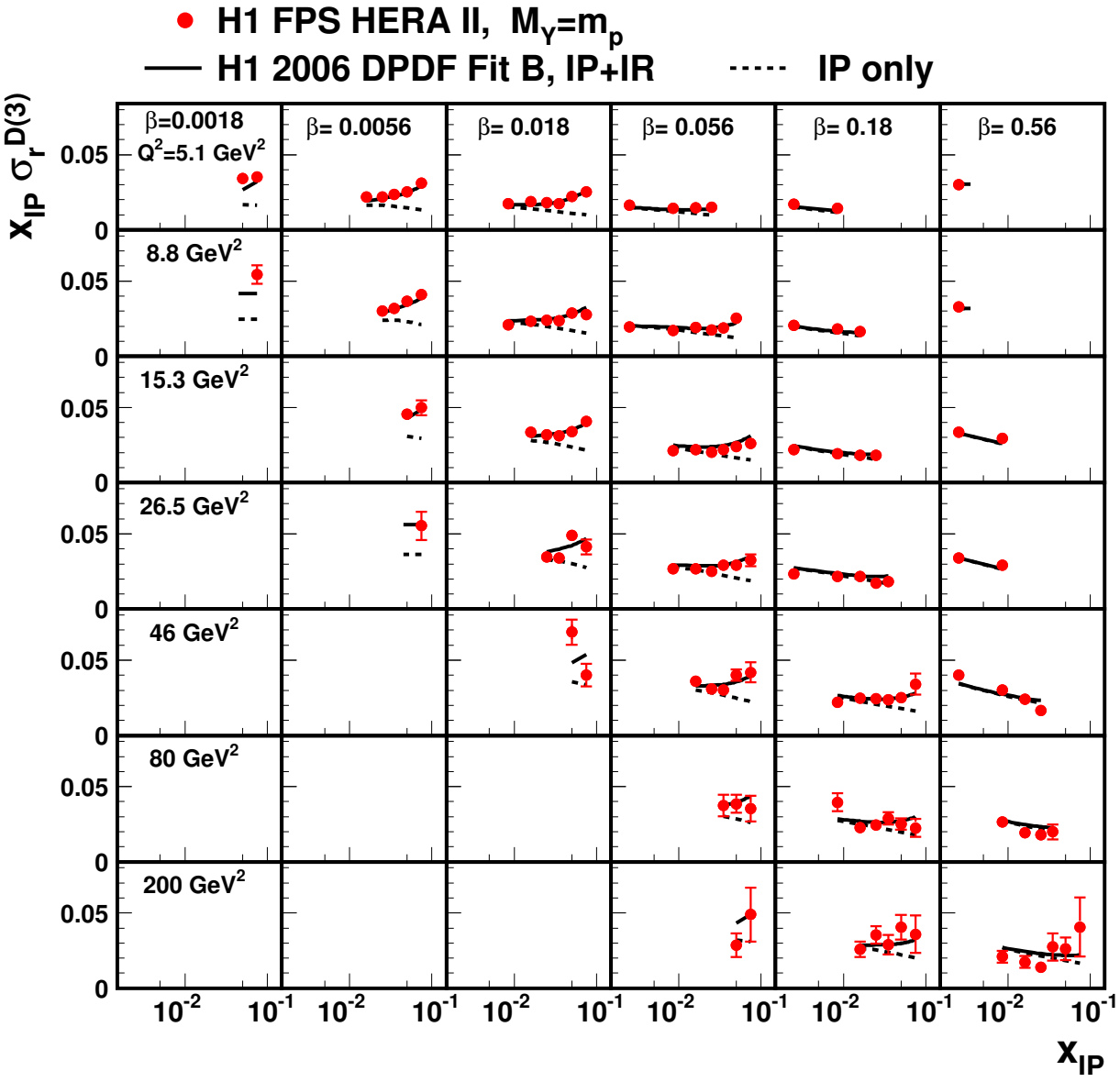

Figure 12: The reduced diffractive cross section $x_{I\!P}\,\sigma_r^{D(3)}(\beta, Q^2, x_{I\!P})$ for $|t| < 1$ GeV^2, shown as a function of $x_{I\!P}$ for different values of β and Q^2. The error bars indicate the statistical and systematic errors added in quadrature. The overall normalisation uncertainty of 6% is not shown. The solid curves represent the results of the H1 2006 DPDF Fit B to the LRG data [5] reduced by a global factor 1.20 to correct for the contributions of proton dissociation processes. The dashed curves indicate the contribution of pomeron exchange in this model.

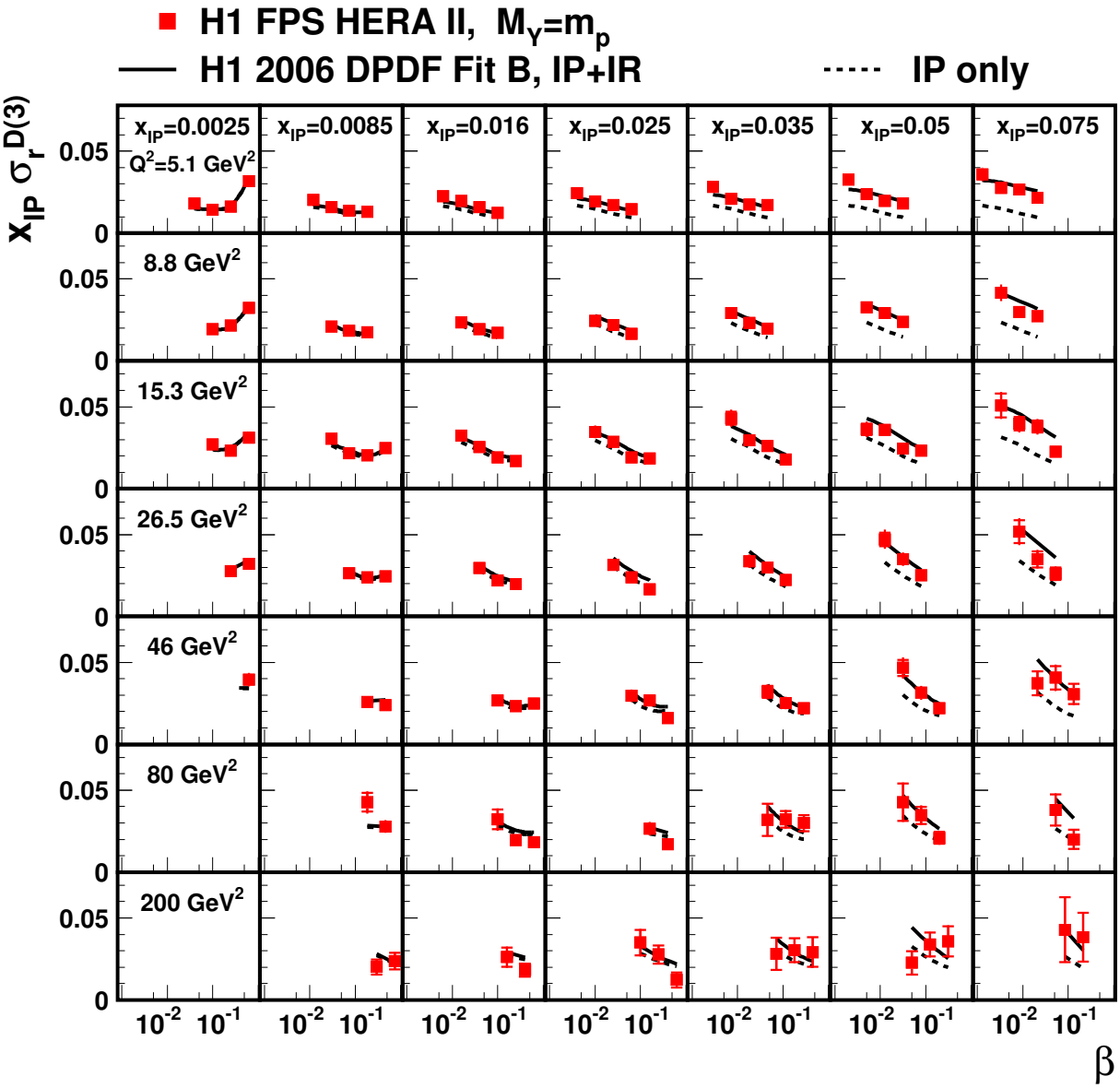

Figure 13: The reduced diffractive cross section $x_{I\!P}\,\sigma_r^{D(3)}(\beta, Q^2, x_{I\!P})$ for $|t| < 1$ GeV^2, shown as a function of β for different values of $x_{I\!P}$ and Q^2. The error bars indicate the statistical and systematic errors added in quadrature. The overall normalisation uncertainty of 6% is not shown. The solid curves represent the results of the H1 2006 DPDF Fit B to the LRG data [5] reduced by a global factor 1.20 to correct for the contributions of proton dissociation processes. The dashed curves indicate the contribution of pomeron exchange in this model.

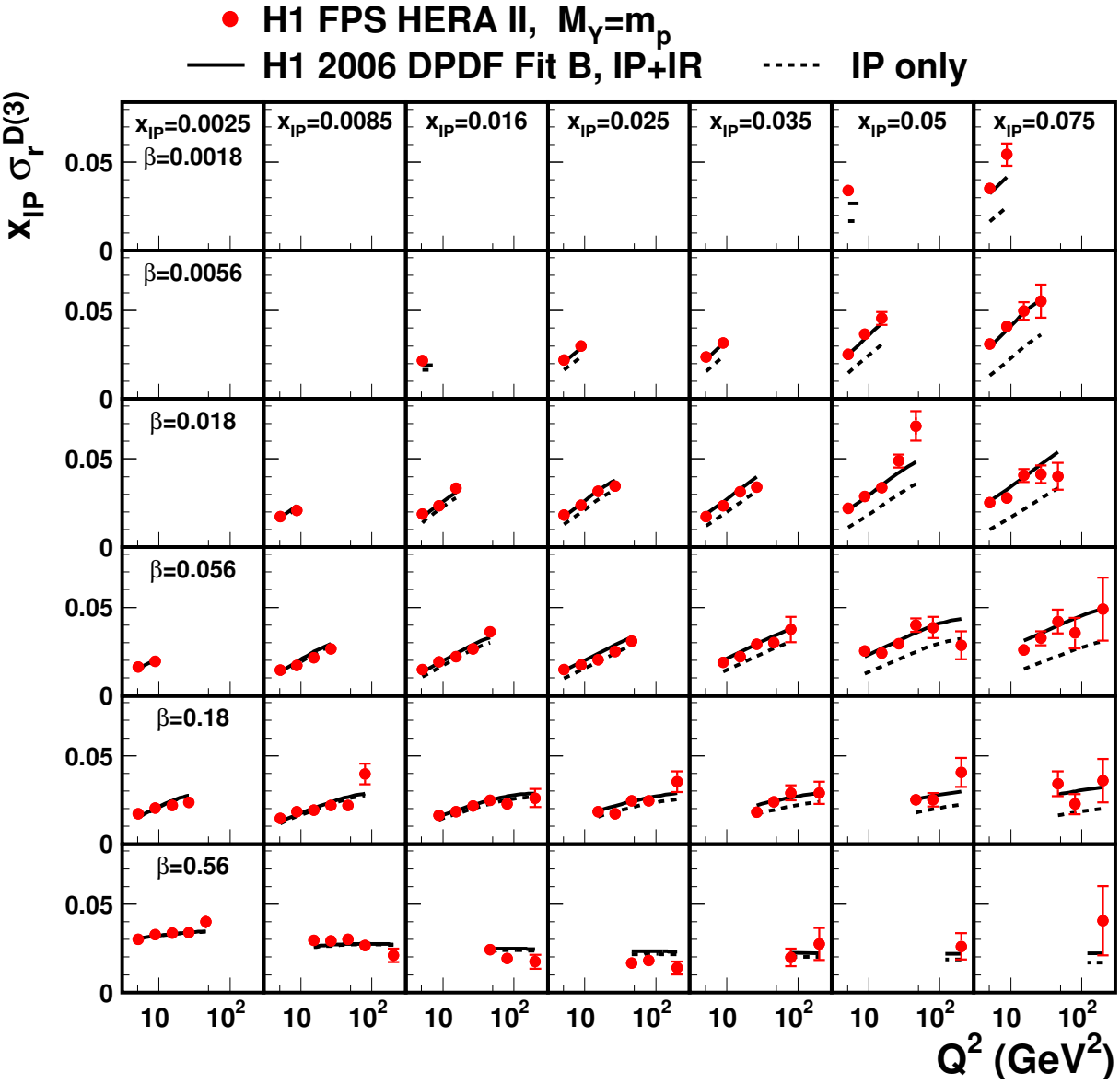

Figure 14: The reduced diffractive cross section $x_{I\!P}\,\sigma_r^{D(3)}(\beta, Q^2, x_{I\!P})$ for $|t| < 1$ GeV^2, shown as a function of Q^2 for different values of $x_{I\!P}$ and β. The error bars indicate the statistical and systematic errors added in quadrature. The overall normalisation uncertainty of 6% is not shown. The solid curves represent the results of the H1 2006 DPDF Fit B to the LRG data [5] reduced by a global factor 1.20 to correct for the contributions of proton dissociation processes. The dashed curves indicate the contribution of pomeron exchange in this model.

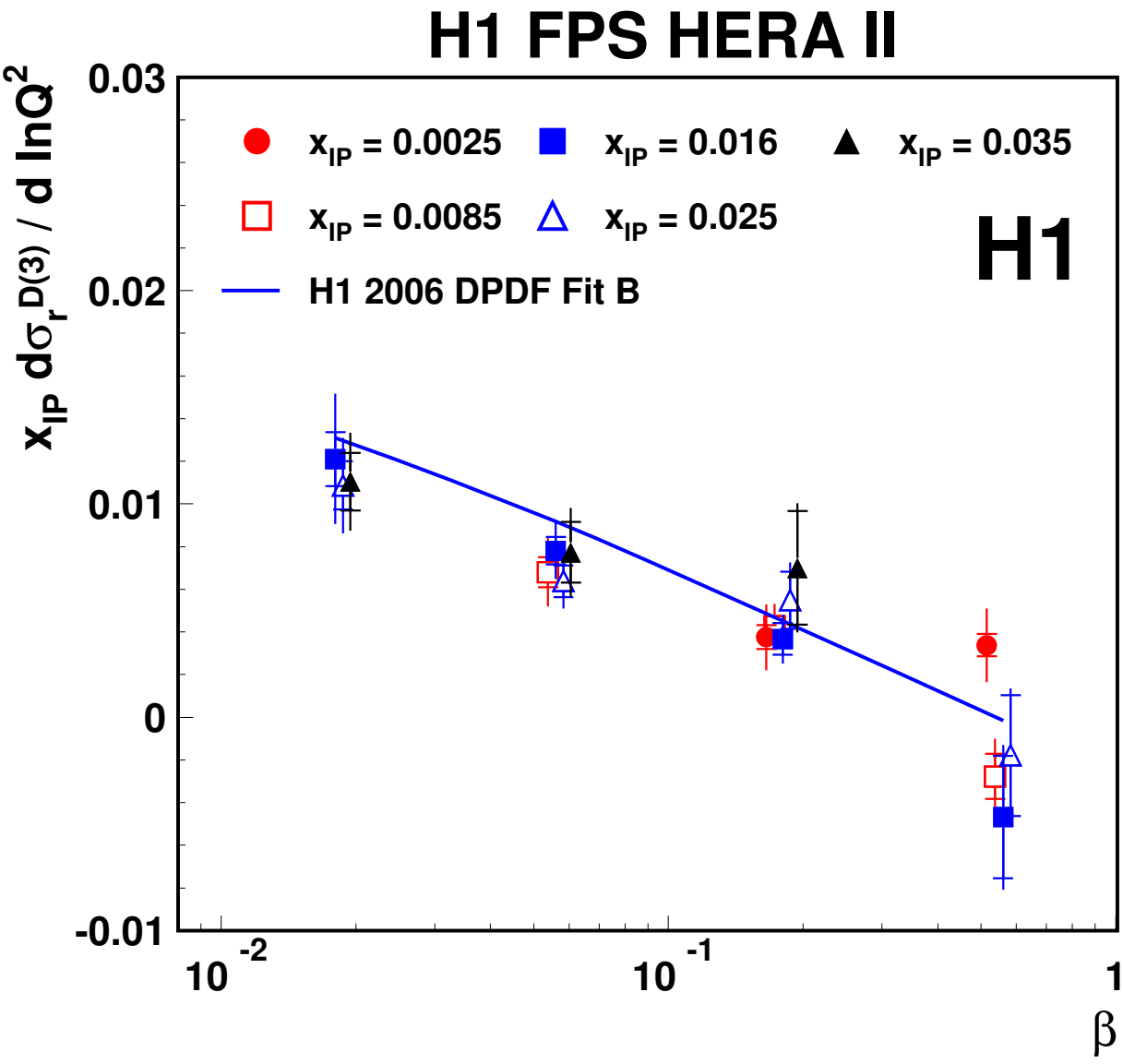

Figure 15: The logarithmic Q^2 derivative of the reduced diffractive cross section $x_{I\!P}\,\sigma_r^{D(3)}(\beta, Q^2, x_{I\!P})$ at different fixed values of $x_{I\!P}$ and β. The inner error bars represent the statistical errors. The outer error bars indicate the statistical and systematic errors added in quadrature. The solid curve represents the results of the H1 2006 DPDF Fit B [5] at $x_{I\!P} = 0.016$ reduced by a global factor 1.20 to correct for the contributions of proton dissociation processes.

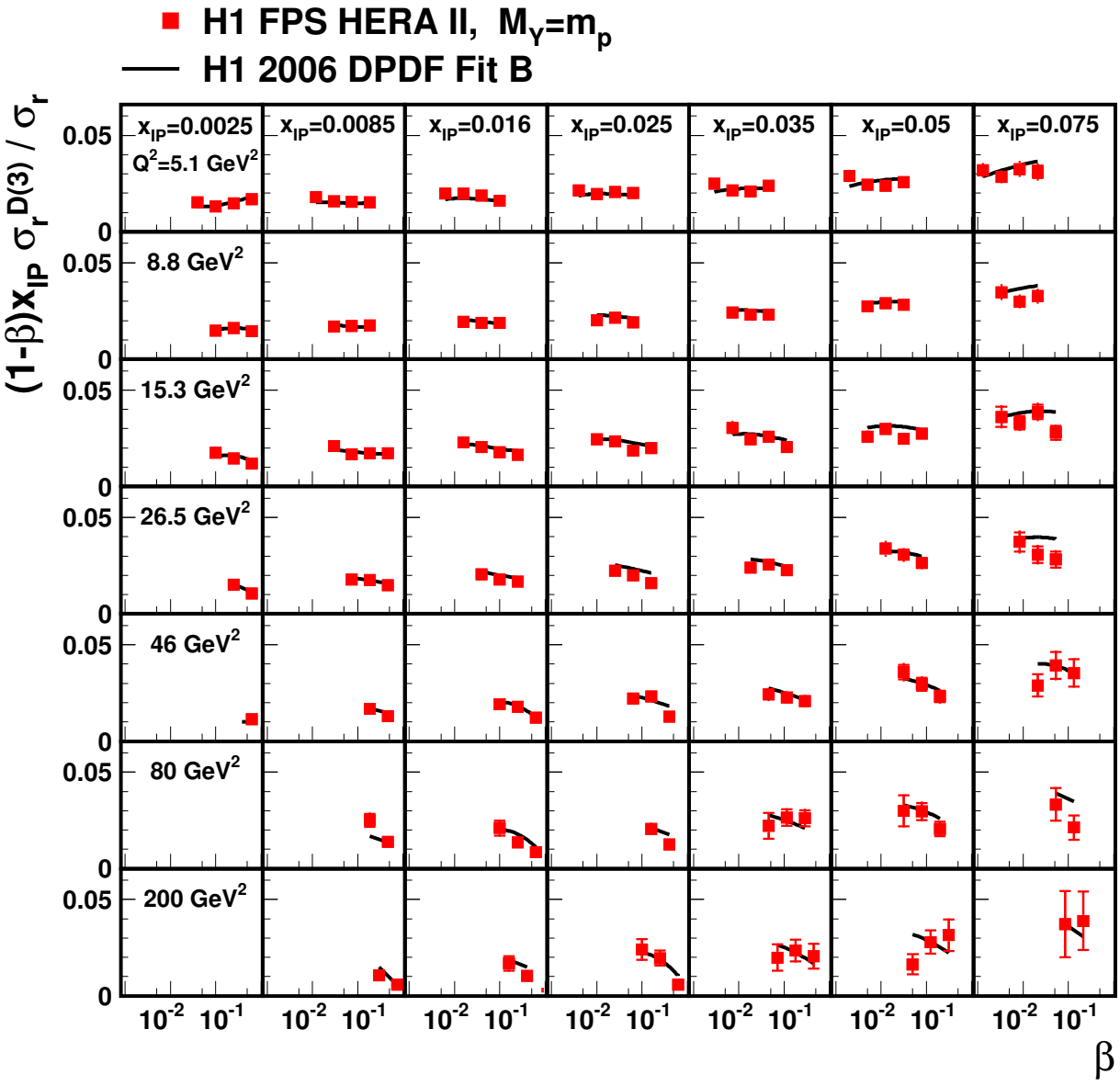

Figure 16: The ratio of the reduced diffractive cross section $\sigma_r^{D(3)}(\beta, Q^2, x_{I\!P})$ to the reduced inclusive cross section $\sigma_r(x = \beta x_{I\!P}, Q^2)$ obtained using the parameterisation H1PDF 2009, multiplied by $(1-\beta)x_{I\!P}$, shown as a function of β for different values of $x_{I\!P}$ and Q^2. The error bars indicate the statistical and systematic errors added in quadrature. The solid curves represent predictions obtained using the H1 2006 DPDF Fit B for the diffractive cross sections and H1PDF 2009 set for the inclusive cross sections. The results for the ratio derived from the PDF predictions are reduced by a global factor 1.20 to correct for the contribution of proton dissociation processes.

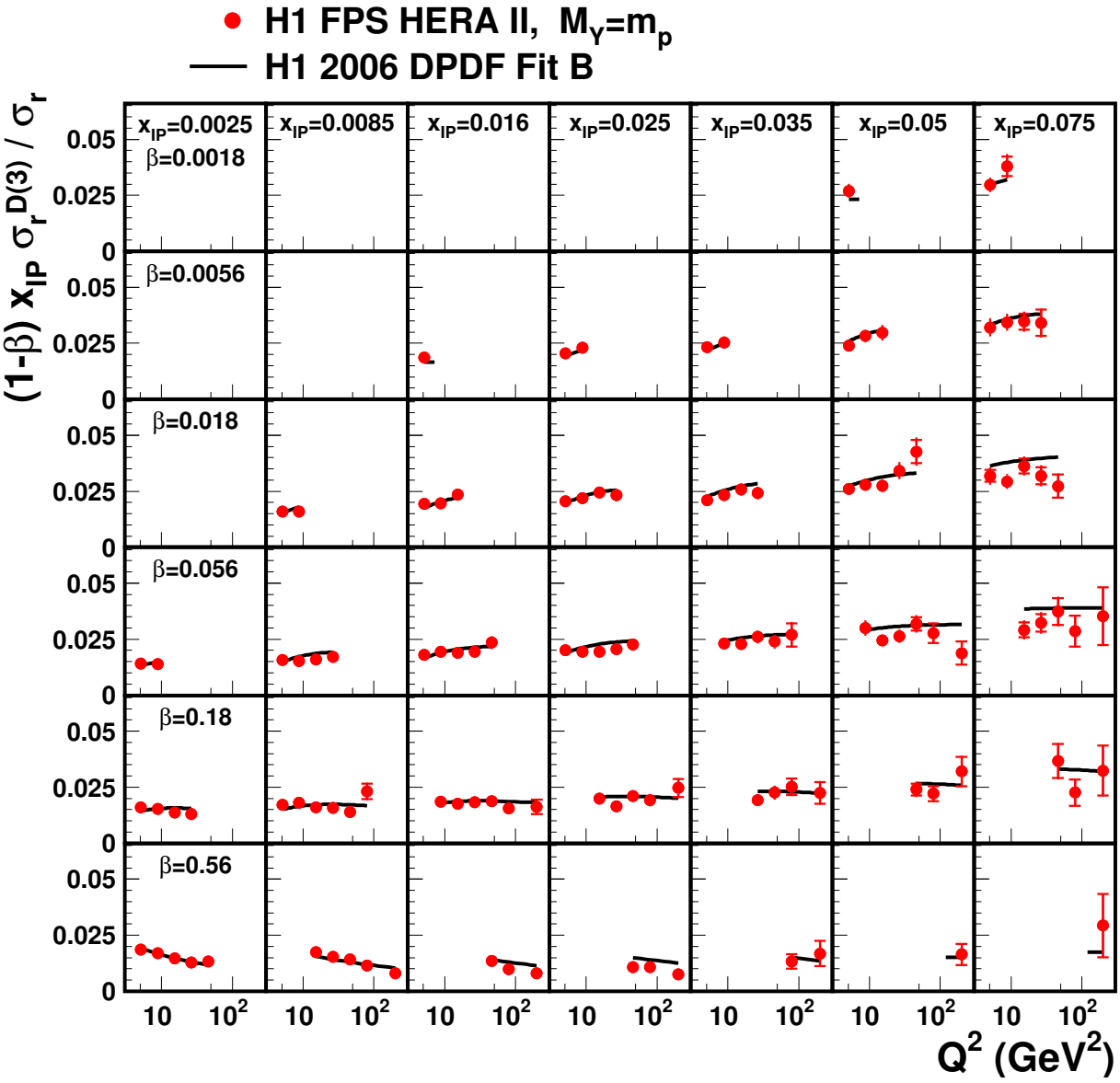

Figure 17: The ratio of the reduced diffractive cross section $\sigma_r^{D(3)}(\beta, Q^2, x_{I\!P})$ to the reduced inclusive cross section $\sigma_r(x = \beta x_{I\!P}, Q^2)$ obtained using the parameterisation H1PDF 2009, multiplied by $(1-\beta)x_{I\!P}$, shown as a function of Q^2 for different values of $x_{I\!P}$ and β. The error bars indicate the statistical and systematic errors added in quadrature. The solid curves represent predictions obtained using the H1 2006 DPDF Fit B for the diffractive cross sections and H1PDF 2009 set for the inclusive cross sections. The results for the ratio derived from the PDF predictions are reduced by a global factor 1.20 to correct for the contribution of proton dissociation processes.

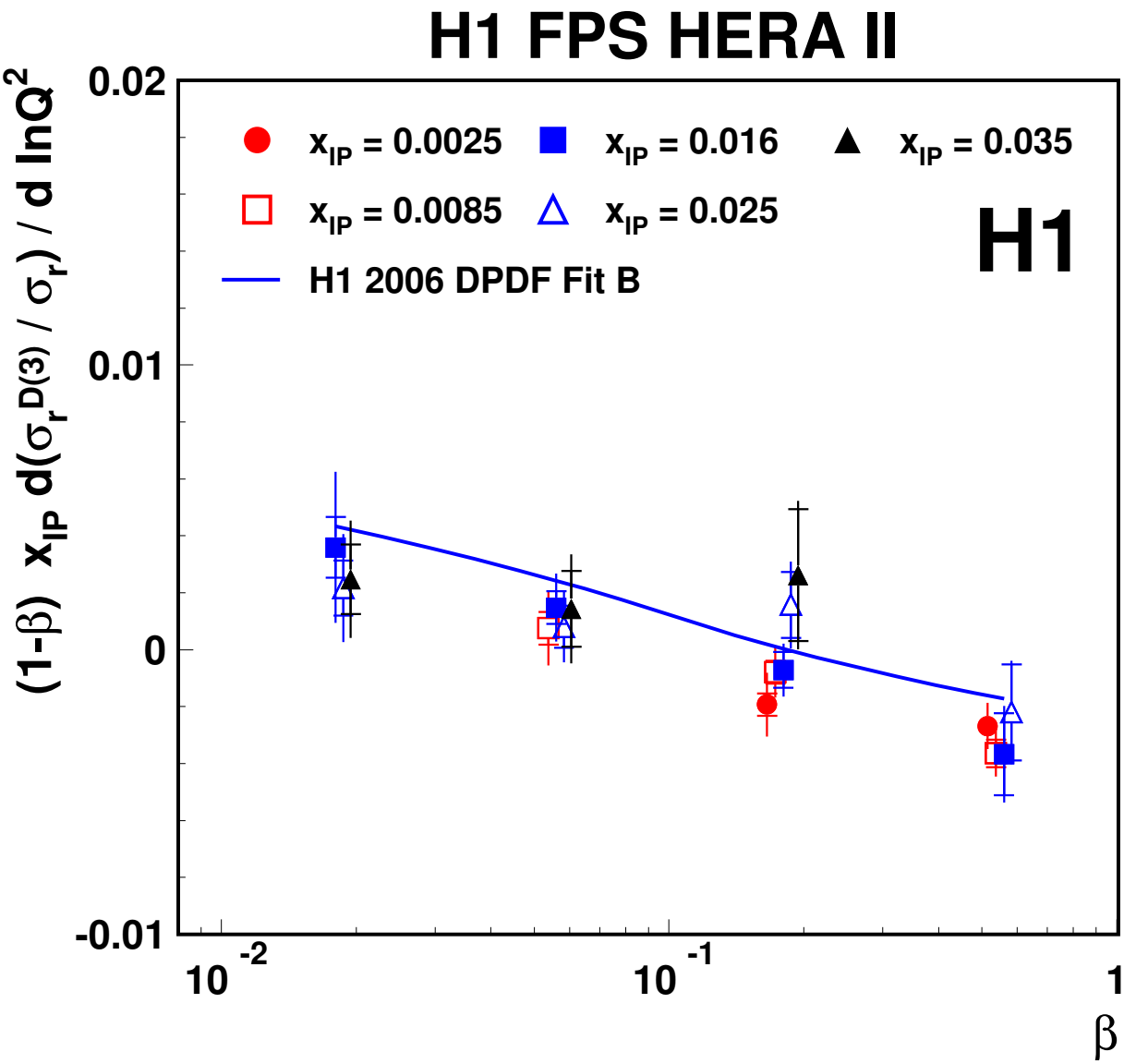

Figure 18: The logarithmic Q^2 derivative of the ratio of the reduced diffractive cross section $\sigma_r^{D(3)}(\beta, Q^2, x_{I\!P})$ to the reduced inclusive cross section $\sigma_r(x = \beta x_{I\!P}, Q^2)$ obtained using the parameterisation H1PDF 2009 multiplied by $(1 - \beta)\ x_{I\!P}$, shown at different fixed values of $x_{I\!P}$ and β. The inner error bars represent the statistical errors. The outer error bars indicate the statistical and systematic errors added in quadrature. The solid curves represent predictions at $x_{I\!P} = 0.016$ obtained using the H1 2006 DPDF Fit B for the diffractive cross sections and H1PDF 2009 set for the inclusive cross sections. The results for the ratio derived from the PDF predictions are reduced by a global factor 1.20 to correct for the contribution of proton dissociation processes.